Copyright Warning & Restrictions

The copyright law of the United States (Title 17, United States Code) governs the making of photocopies or other reproductions of copyrighted material.

Under certain conditions specified in the law, libraries and archives are authorized to furnish a photocopy or other reproduction. One of these specified conditions is that the photocopy or reproduction is not to be "used for any purpose other than private study, scholarship, or research." If a, user makes a request for, or later uses, a photocopy or reproduction for purposes in excess of "fair use" that user may be liable for copyright infringement,

This institution reserves the right to refuse to accept a copying order if, in its judgment, fulfillment of the order would involve violation of copyright law.

Please Note: The author retains the copyright while the New Jersey Institute of Technology reserves the right to distribute this thesis or dissertation

Printing note: If you do not wish to print this page, then select "Pages from: first page # to: last page #" on the print dialog screen

ABSTRACT

DATA MULTIPLEXING IN VECTOR ACOUSTIC COMMUNICATION: SYSTEM DESIGN AND EXPERIMENTS

by
Erjian Zhang

Acoustic particle velocity channels, which are vector components of the acoustic field, have been recently explored to achieve communication purposes underwater. Vector sensors and transducers that can utilize acoustic particle velocity channels have compact multichannel designs, which are perfect for compact size underwater platforms. In this dissertation, an underwater acoustic multiple-input multiple-output (MIMO) communication system featuring orthogonal frequency division multiplexing (OFDM) and frequency shift keying (FSK) modulation is discussed. By transmitting multiple independent data streams simultaneously over several channels within the same bandwidth, the proposed MIMO system increases the transmission rate. A variety of components of the system such as vector transducers and algorithms for synchronization, channel estimation, MIMO detection, channel coding, etc., are designed and implemented. Parameters of acoustic particle velocity channels and system performance are measured and studied via experimental data for various conditions and configurations, to understand the performance of the developed vector MIMO system.

On the other hand, wireless data communication and telemetry during drilling deep oil and gas wells are important enablers for safe and timely drilling operations. The transmission of information through drill strings and pipes using sound waves is a useful and practical approach. However, given the limited available bandwidth, transmission rates are typically smaller than what is needed. In this dissertation, a new method and system

are proposed to increase the transmission rate over the same bandwidth, by deploying more than one actuator. Upon using multiple actuators, several data streams can be transmitted simultaneously. This increases the data rate without the need for additional bandwidth. The experimental results of a testbed with two actuators are presented, where the transmission rate is doubled with no bandwidth increase. A strain sensor receiver and accelerometer receivers are used to separate and demodulate the two data streams. It is demonstrated that it is possible to recover the data in the new faster system benefiting from two actuators, while having about the same bit error probability performance as a one-actuator system. Various combinations of strain and acceleration sensors are considered at the receive side. Due to some properties of strain channels (e.g., smaller delay spreads and their less-frequency-selective behavior) presented in this dissertation, it appears that a strain sensor receiver and an accelerometer receiver together can offer a good performance when separating and demodulating the two actuators' data in the testbed. Overall, the experimental results from the proposed system suggest that upon using more than one actuator, it is feasible to increase the data rate over the limited bandwidth of pipes and drill strings.

DATA MULTIPLEXING IN VECTOR ACOUSTIC COMMUNICATION: SYSTEM DESIGN AND EXPERIMENTS

by
Erjian Zhang

A Dissertation
Submitted to the Faculty of
New Jersey Institute of Technology
in Partial Fulfillment of the Requirements for the Degree of
Doctor of Philosophy in Electrical Engineering

Helen and John C. Hartmann Department of
Electrical and Computer Engineering

August 2019

APPROVAL PAGE

DATA MULTIPLEXING IN VECTOR ACOUSTIC COMMUNICATION: SYSTEM DESIGN AND EXPERIMENTS

Erjian Zhang

Dr. Ali Abdi, Dissertation Advisor — Date
Professor of Electrical and Computer Engineering, NJIT

Dr. Alexander M. Haimovich, Committee Member — Date
Distinguished Professor of Electrical and Computer Engineering, NJIT

Dr. Joerg Kliewer, Committee Member — Date
Professor of Electrical and Computer Engineering, NJIT

Dr. Osvaldo Simeone, Committee Member — Date
Professor of Electrical and Computer Engineering, NJIT

Dr. Zoi-Heleni Michalopoulou, Committee Member — Date
Professor of Mathematics, NJIT

BIOGRAPHICAL SKETCH

Author: **Erjian Zhang**

Degree: Doctor of Philosophy

Date: August 2019

Undergraduate and Graduate Education:

- Doctor of Philosophy in Electrical Engineering,
  New Jersey Institute of Technology, Newark, NJ, 2019

- Master of Science in Electrical Engineering,
  New Jersey Institute of Technology, Newark, NJ, 2011

- Bachelor of Science in Electrical Engineering,
  Tongji University, Shanghai, P. R. China, 2009

Major: Electrical Engineering

Presentations and Publications:

E. Zhang and A. Abdi, "Experimental Results on Underwater Communication Using Vector Transducers," *Proceedings of Meetings on Acoustics,* vol. 23, no. 1, p. 070011, 2015.

E. Zhang and A. Abdi, "Underwater Communication Via Frequency Shift Keying in Particle Velocity Channels: Experimental Results," in *OCEANS*, Washington, D.C., 2015, pp. 1-4.

Y. Wang, E. Zhang, and A. Abdi, "A Multiple-Input Multiple-Output Orthogonal Frequency Division Multiplexing Underwater Communication System Using Vector Transducers," *The Journal of the Acoustical Society of America,* vol. 141, no. 5, pp. 3987-3987, 2017.

E. Zhang and A. Abdi, "Experimental Results on Synchronization With Chirp Signals Using a Vector Sensor Receiver," *The Journal of the Acoustical Society of America,* vol. 141, no. 5, pp. 3915-3915, 2017.

E. Zhang and A. Abdi, "A study of characteristics of underwater acoustic particle velocity channels measured by acoustic vector sensors," *The Journal of the Acoustical Society of America,* vol. 141, no. 5, pp. 3916-3916, 2017.

E. Zhang and A. Abdi, "Communication rate increase in drill strings of oil and gas wells using multiple actuators," *Sensors,* vol. 19, no. 6, p. 1337, 2019.

In memory of my grandfather,
I miss you.

To my parents,
without your love, I would be nothing.

To my family,
without your support, I would not have found my way to reach this point.

献给我的祖父，
我很想念你。

献给我的父母，
没有你们的爱，我将一无是处。

献给我的家人，
没有你们的支持与鼓励，我也不可能完成这篇论文。

ACKNOWLEDGMENT

Firstly, I would like to express my sincere gratitude to my advisor, Dr. Ali Abdi, for his patient guidance and excellent advice, warm encouragement, and consistent support throughout my Ph.D. journey. All I learned from you was invaluable to my study and research and will benefit me for my whole life. I will miss the time we spent on the field experiments and the late-night snack after a whole-day of hard work.

I am also grateful to Dr. Alexander M. Haimovich, Dr. Joerg Kliewer and Dr. Osvaldo Simeone from the Electrical and Computer Engineering Department and Dr. Zoi-Heleni Michalopoulou of the Mathematical Sciences Department of NJIT for serving on my dissertation committee and for their insight and continued support.

I want to thank my friends in the Elisha Yegal Bar-Ness Center for Wireless Information Processing (CWiP): Yu Liu, Nan Wu, Yuewen Wang, Annan Dong, Chen Yi, and all the others. I would also like to express profound gratitude to Ms. Angela Retino, Ms. Kathleen Bosco, Ms. Monteria Bass, Mr. Artur M. Pereira, and Mr. Hector Rivas from Electrical and Computer Engineering Department of NJIT for their enthusiastic assistance in every respect.

Last, and most notably, I would like to thank my family. Without their continuous support, encouragement, and love, this work would not have been possible.

TABLE OF CONTENTS

TABLE OF CONTENTS
(Continued)

Chapter **Page**

TABLE OF CONTENTS
(Continued)

Chapter **Page**

LIST OF TABLES

LIST OF FIGURES

LIST OF FIGURES
(Continued)

LIST OF FIGURES
(Continued)

Figure **Page**

LIST OF FIGURES
(Continued)

Figure **Page**

LIST OF FIGURES
(Continued)

Figure **Page**

CHAPTER 1

INTRODUCTION

Electromagnetic waves are the most common used media in terrestrial wireless communication systems. However, there are environments that electromagnetic waves suffer from high propagation attenuation. Underwater and oil/gas well applications are two examples where acoustic signals are the better candidate to achieve reliable wireless communication.

1.1 Overview of Underwater Acoustic Communication

1.1.1 Introduction of Underwater Acoustic Communication

The market of wireless underwater acoustic communication is anticipated to grow to about $3 billion in the next few years [1]. This market includes applications such as environmental monitoring, pollution monitoring, climate recording, hydrography and oceanography, with end users ranging from oil and gas to military and defense, homeland security, scientific research and development, and marine1. The underwater medium is a complex propagation environment [2]. Given the very limited underwater acoustic bandwidth, typically in the order of kHz, data rates of underwater communication systems are much smaller than terrestrial wireless communication systems. Upon transmitting multiple data streams over an available bandwidth, i.e., data multiplexing, data rate can be increased. Data multiplexing in wireless systems utilizing electromagnetic waves was first accomplished using multiple individual transmitters (multiple antennas) [3]. Using certain properties of electromagnetic waves, polarization multiplexing and orbital angular

momentum multiplexing were also devised for data rate increase in wireless terrestrial systems [4, 5]. Given the strong attenuation of electromagnetic waves in underwater environments, acoustic waves are proper carriers of information in underwater communication systems. In existing underwater systems, data are modulated on acoustic pressure, which is the scalar component of acoustic field, using one scalar transmitter. To increase data rate, multiple individual scalar transmitters were used to multiplex data for underwater communication [6]. However, given the voluminous size of a communication modem carrying several transmitters, many modern underwater platforms such as medium and small autonomous and unmanned underwater vehicles [7] do not have the option of communicating via multiple transmitters.

1.1.2 Introduction of Acoustic Particle Velocity Channel and Vector Transducers

Acoustic particle velocity is a vector quantity whose magnitude in each axis is spatial gradient of acoustic pressure in that direction [8]. Communication via acoustic particle velocity channels using vector transducers has been recently studied for underwater systems [9]. A compact vector transducer can measure or excite acoustic particle velocity and acoustic pressure, all co-located at a single point in space. In addition to the acoustic pressure channel [10, 11], acoustic particle velocity channels provide extra channels for communication [9, 12, 13]. To utilize these channels, vector transducers are used, which can transmit and receive both pressure and particle velocity signals [9, 13, 14].

Different characteristics of these channels such as capacity [15, 16], delay and Doppler spreads [17], instantaneous mutual information [18] and possible correlations [19] have been studied to date.

1.2 Acoustic Communication in Drill Strings of Oil and Gas Wells Application

When drilling to reach underground oil and gas reservoirs, drilling operators on the ground need to have information on parameters such as temperature, pressure, etc., at the bottom of wellbores. This is crucial for safe and timely drilling of wells. Such parameters are measured using some sensors downhole, and are communicated to surface platforms via a variety of techniques [20]. Mud pulses, electromagnetic waves and acoustics waves have been used for information transmission. For a review and comparison of different methods, interested readers can refer to [21]. Mud pulses data rate is usually few bits/sec only, whereas electromagnetic waves experience strong attenuation. Acoustic transmission of such information through drill strings is a viable and useful method. The limited available bandwidth [22], however, is a limiting factor on the achievable data rates.

1.3 Contributions

In this dissertation, a system for underwater acoustic communication is proposed and experimentally demonstrated that upon utilizing the unique physics of underwater acoustics, it is feasible to multiplex several data streams from a single transmitter. For example, by multiplexing two or three data streams, we double or triple the transmission rate over a given bandwidth, using only one transmitter. The key idea is to devise a method which benefits from the vector nature of the underwater acoustic field for data multiplexing and rate increase. In this chapter, we present a method and implement a system accordingly, to modulate multiple data streams on underwater acoustic particle velocity components, with particle velocity being the aforementioned vector field to explore. The fundamental difference between the introduced approach and other underwater acoustic communication

methods and systems is that they modulate data merely on the acoustic pressure, which is the scalar component of the acoustic field.

For drill strings of oil and gas wells applications, using multiple actuators is proposed, to transmit several data streams simultaneously over the same bandwidth, and then separate and demodulate them at the receive side. This allows for data rate increase and optimal utilization of the small available bandwidth. In fact, using two actuators on a drill string testbed, we have shown that data rate can doubled, by transmitting two data streams simultaneously, without increasing the bandwidth. While two piezoelectric actuators are used in this dissertation's experiments, one can use magnetostrictive actuators [22-24] as well.

1.4 Organization

This dissertation is organized as following:

In Chapter 2, a 2×1 multiple-input single-output (MISO) underwater system is introduced, where two independent data streams are sent thru two particle velocity channels. Experimental results are presented and analyzed, to explore the performance of the proposed vector transmitter and compare it to an array of two scalar transmitters.

Chapter 3 presents underwater experimental results on two vector acoustic communication systems: A 3×1 multiple-input single-output (MISO) system and a 1×3 single-input multiple-output (SIMO) system. The MISO system utilizes the three x-velocity, y-velocity and pressure channels to transmit three independent data streams, so, tripling the transmission rate. On the other hand, the SIMO system benefits from data reception via the three x-velocity, y-velocity and pressure channels, to improve link quality.

In both systems, the bit duration is chosen to be long enough so that there is no inter-symbol interference (ISI) to mitigate. Experimental feasibility of a 3×1 vector MISO system using a vector transducer transmitter is demonstrated first. Later, experimental data of a 1×3 vector SIMO system having a vector transducer receiver is discussed, to understand its improved performance compared to a 1×3 fully scalar conventional SIMO system which has three spatially-separated scalar receivers, i.e., regular hydrophones.

To further increase the data rate, a method to modulate a third data stream on the same vector transmitter is explored in Chapter 4. The implemented system utilizes OFDM with zero-forcing (ZF), minimum mean square error (MMSE) and Maximum Likelihood (ML) detection. Carrier frequency offset (CFO) and channel responses are estimated using null and pilot tones, respectively. The preliminary results are shown in this chapter. To test the system robustness against Doppler effect, the transmitter is manually moved back and forth during the experiments, to mimic the drifting in realistic environment.

The details on OFDM implementation and how tripling data rate is done can be found in Chapter 5. The performance of both FSK and OFDM underwater acoustic system are tested in real ocean environment. Results of both systems are presented and discussed.

In Chapter 6, using multiple actuators is proposed for applications in drill strings of oil and gas wells, to transmit several data streams simultaneously over the same bandwidth, and then separate and demodulate them at the receive side. The experimental testbed is explained. Channel measurements and communication test results are presented as well.

Finally, the conclusion and remarks are given in Chapter 7. Thoughts on the future research and the possible study directions are provided also.

CHAPTER 2

UNDERWATER COMMUNICATION USING VECTOR TRANSMITTER

To explore the feasibility of using vector transmitter for underwater communication, FSK modulation is the first to consider due to its simplicity, so that the focus can be concentrated more on understanding the properties of particle velocity channels and vector transducers.

In this chapter, a 2×1 multiple-input single-output (MISO) underwater system is introduced, where two independent data streams are sent thru two particle velocity channels. Moreover, physically, there is only one vector transmitter being used.

2.1 Transmission of Two Data Streams Using A Two-Channel Vector Transmitter

The top view of a 2×1 MISO acoustic vector system is shown in Figure 2.1. There is one vector projector [9] with four scalar elements at the transmit side, labeled by A, B, C and D, with spacing L_{Tx}, and a scalar sensor (hydrophone) at the receive side. The four channels in Figure 2.1 are labeled as h_A, h_B, h_C and h_D. When L_{Tx} is small, elements A and B operate as a dipole in x-direction, and elements C and D operate as a y-oriented dipole. The pressure-equivalent particle velocity channels are given by [9, 25]

$$\begin{aligned} h^x &= \left(jkL_{Tx} \right)^{-1} \left(h_A - h_B \right), \\ h^y &= \left(jkL_{Tx} \right)^{-1} \left(h_C - h_D \right), \end{aligned} \tag{2.1}$$

where $j = \sqrt{-1}$, $k = 2\pi / \lambda$ is the wavenumber, $\lambda = c / f_0$ is the wavelength, c is the speed of sound and f_0 is the carrier frequency. More details of the pressure-equivalent particle velocity channels can be found in Chapter 5.

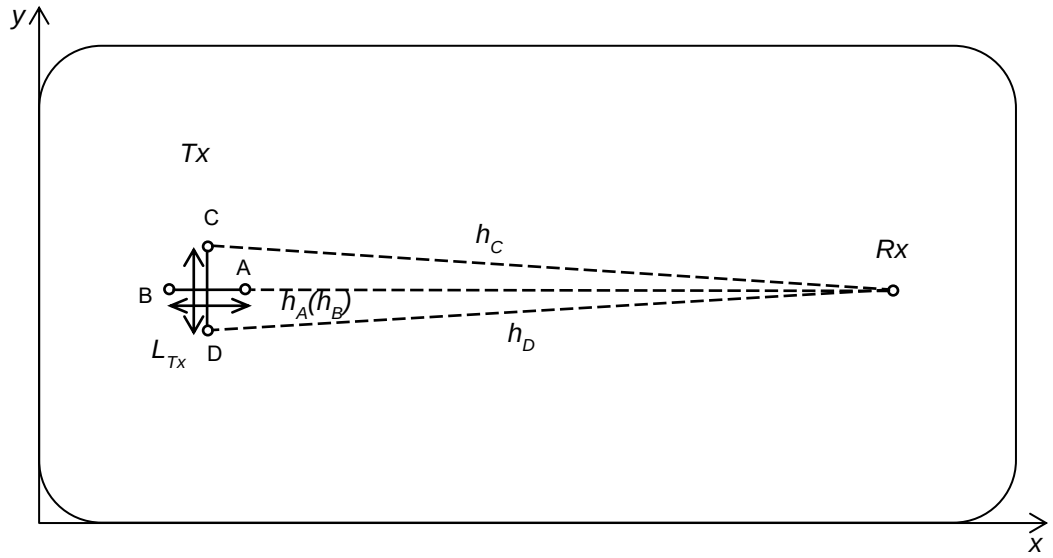

Figure 2.1 Top view of the proposed 2×1 MISO underwater acoustic communication system. The transmitter *Tx* is a vector projector and the receiver *Rx* is a scalar sensor.

Upon transmitting two signals thru the above two particle velocity channels, the received signal can be written as

$$r = \begin{bmatrix} h^x & h^y \end{bmatrix} \begin{bmatrix} s_1 \\ s_2 \end{bmatrix} + n. \tag{2.2}$$

Here s_1 and s_2 are two independent FSK modulated signals and n is the acoustic pressure ambient noise. Note that bit duration T_b is chosen to be long enough, so that the channels in (2.2) can be considered as frequency-flat, causing no inter-symbol interference (ISI).

The block diagram of the receiver is shown in Figure 2.2, which includes two non-coherent binary FSK (BFSK) demodulators, to recover the signals s_1 and s_2.

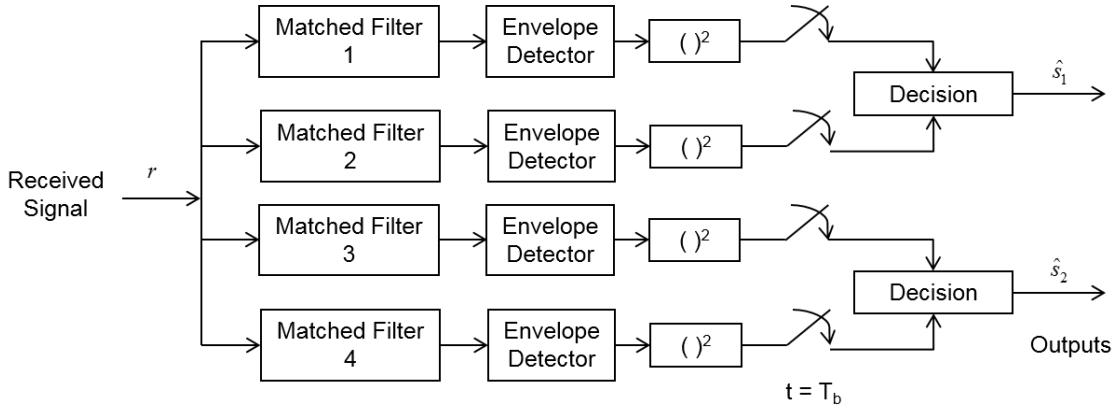

Figure 2.2 Block diagram of two non-coherent BFSK demodulators [26] at the receive side of the 2×1 MISO underwater acoustic communication system.

2.2 Initial Experimental Results

2.2.1 Experiment Setup

In the experiments, BFSK modulated signals are generated by MATLAB® and then applied to one vector projector or two scalar projectors using a D/A converter controlled by MATLAB® Data Acquisition Toolbox™. Received signals are captured by one scalar hydrophone connected to an A/D converter controlled by MATLAB® Data Acquisition Toolbox™. The carrier frequency is chosen to be $f_0 = 20.2$ kHz. The bit duration is set at $T_b = 0.1$ s, to ensure that in one of the experiment setups, lab water tank, we have $T_b \gg \tau_{\text{rms}}$, where τ_{rms} is rms multipath delay spread of the tank [27]. The frequency spacing Δf is chosen to be 100 Hz, to keep BFSK frequencies orthogonal. The vector projector with four elements acts as two dipoles, to transmit two independent data streams, simultaneously.

2.2.2 Lab Test Results

The MISO system with one vector projector and one scalar sensor receiver is first tested in the lab water tank, as shown in Figure 2.3b. As shown in Figure 2.3a, a fully scalar MISO

system is also considered for comparison, which consists of two scalar projectors and one scalar sensor receiver. The transmitters and receiver in both systems are separated by about 1m in the same lab water tank. Each transmission in the experiments is 5 minutes long for each MISO system.

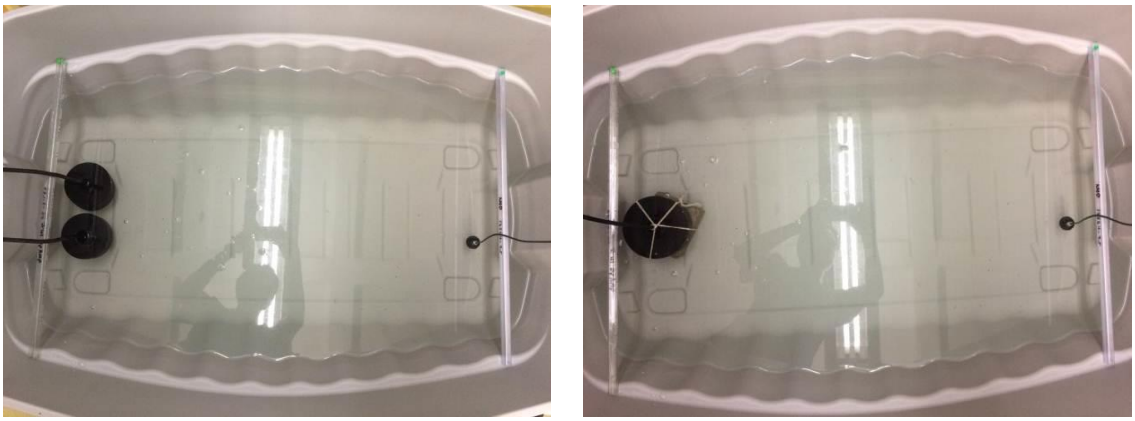

a **b**

Figure 2.3 Two MISO systems in the lab water tank. **a**: Two scalar projectors and one scalar receiver; **b**: One vector projector and one scalar receiver.

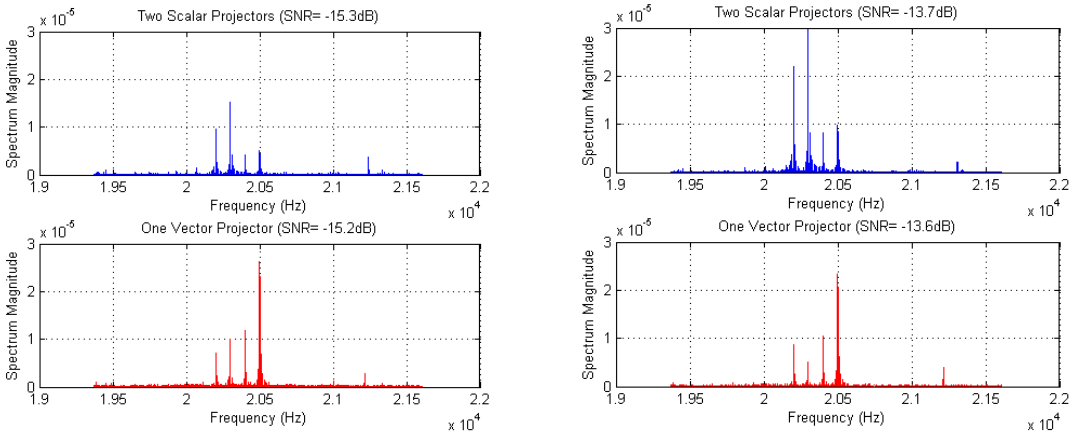

(a) SNR is about -15dB (b) SNR is about -13dB

Figure 2.4 Spectra of the received signals for both MISO systems, measured in the lab.

Bit error rates (BERs) of the MISO systems are shown in Table 2.1. With similar received signal-to-noise ratios (SNRs), the vector system shows zero or very close to zero

BER. The smaller size of the vector projector compared to the two scalar projectors together is another advantage of the proposed vector system. To better understand the BER results, the spectra of the received signals are shown in Figure 2.4.

Unbalanced power distribution is observed in both systems. After inspecting the received signals and the demodulated bits, one can observe that all errors occurred at frequencies which had lower spectral magnitudes. This means that Figure 2.4 explains the BER results in Table 2.1.

Table 2.1 Experimental BER Performance of the MISO Systems in the Lab

Transmitting System	SNR (dB)	BER
Two scalar projectors	-15.3	0.02
One vector projector	-15.2	<0.001
Two scalar projectors	-13.7	<0.001
One vector projector	-13.6	0.006

2.2.3 Pool Test Results

The same MISO system with one vector projector and one scalar sensor receiver is also tested in a large pool, where the transmitter and receiver are placed at the same depth, about 15 m far apart. The fully scalar MISO system with two scalar projectors and one scalar sensor receiver is also deployed in the pool, for comparison purposes. Other parameters remain the same as those considered in the lab experiments. BER results and received signal spectra of both MISO systems in the pool are shown in Table 2.2 and Figure 2.5, respectively.

With the same received SNR, the vector system exhibits a lower BER, which may be attributed to the frequency content of the received signals shown in Figure 2.5. The last

frequency in the fully scalar system spectrum, the top panel of Figure 2.5, has a very small magnitude, which causes many errors. In addition to lower BER, the compact size of the transmitter is another benefit of the vector system.

Table 2.2 Experimental BER Performance of the MISO Systems in the Pool

Transmitting System	SNR (dB)	BER
Two scalar projectors	-9.6	0.028
One vector projector	-9.7	<0.001

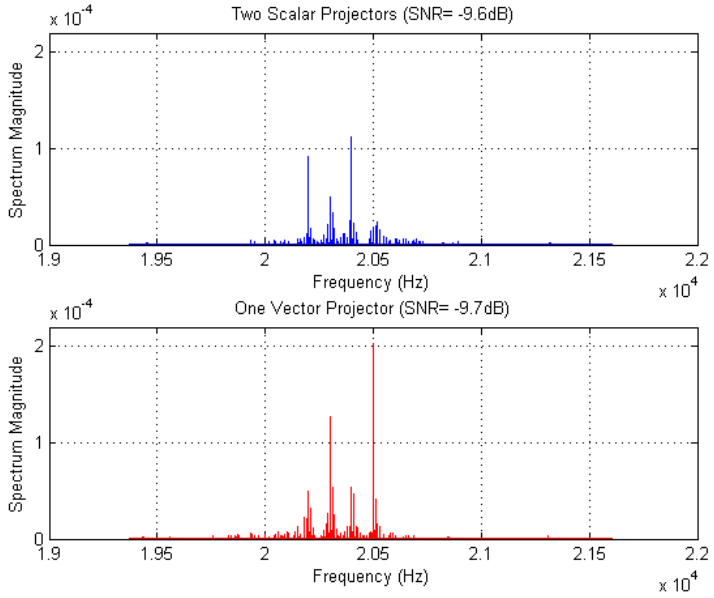

Figure 2.5 Spectra of the received signals for both MISO systems, measured in the pool.

2.3 Conclusion

In this chapter, the simultaneous underwater transmission of two independent data streams using a two-channel acoustic vector transducer is considered, where two independent FSK signals are sent thru two orthogonal particle velocity channels. Lab and pool experiments demonstrate that the proposed vector system offers zero or very low bit error rate,

compared to a fully scalar system with two individual scalar transmitters. The compact size of the vector transmitter is another advantage which makes it particularly suitable for small underwater vehicles and platforms.

CHAPTER 3

UNDERWATER COMMUNICATION USING VECTOR RECEIVER

In this chapter, underwater experimental results on two vector acoustic communication systems are presented: A 3×1 multiple-input single-output (MISO) system and a 1×3 single-input multiple-output (SIMO) system. The MISO system utilizes the three x-velocity, y-velocity and pressure channels to transmit three independent data streams, so, tripling the transmission rate. On the other hand, the feasibility of utilizing a vector receiver in underwater communication system is explored. The SIMO system benefits from data reception via the three x-velocity, y-velocity and pressure channels, to improve link quality. In both systems, the bit duration is chosen to be long enough so that there is no inter-symbol interference (ISI) to mitigate.

The rest of the chapter is organized as follows. In Section 3.1, experimental feasibility of a 3×1 vector MISO system using a vector transducer transmitter is demonstrated. Experimental data of a 1×3 vector SIMO system having a vector transducer receiver is discussed in Section 3.2, to understand its improved performance compared to a 1×3 fully scalar conventional SIMO system which has three spatially separated scalar receivers, i.e., regular hydrophones. Concluding remarks are provided in Section 3.3.

3.1 The 3×1 MISO System with a Three-Channel Vector Transmitter and One Scalar Receiver

The feasibility of a 3×1 MISO system using a vector transmitter is presented in this section via underwater experiments. The MISO system modulates three independent binary FSK

(BFSK) signals on the three x-velocity, y-velocity and pressure channels, to triple the transmission rate.

3.1.1 Experimental Setup

Experiments are performed in a large pool. Transmitters and receiver are about 13 meters apart. Our vector transmitter includes the same ring transducer [28] with four segments which used in Chapter 2 to modulate the *x* and *y* components of acoustic particle velocity, plus a co-located scalar transducer to modulate the acoustic pressure, as shown in Figure 3.1. They are about 30 cm deep in water. The vector transmitter can be considered as two orthogonal dipoles that modulate two independent BFSK signals s_1 and s_2 on *x*-velocity and *y*-velocity channels, plus modulating the third BFSK signal s_3 on the co-located pressure channel. This means that three independent data streams are transmitted simultaneously by a three-channel vector transmitter, to triple the data rate. A single scalar hydrophone is used as the receiver.

Figure 3.1 Vector transmitter of the MISO system includes a ring transducer (left) with four segments which acts as two orthogonal dipoles for two independent data streams, plus a nearly co-located scalar transducer (right) for the third data stream. The transducers are at the same depth and there is no spacing between them.

The MISO system equation can be written as

$$r = \begin{bmatrix} h_x & h_y & h \end{bmatrix} \begin{bmatrix} s_1 \\ s_2 \\ s_3 \end{bmatrix} + n. \tag{3.1}$$

Here r is the received signal, h_x and h_y are the particle velocity channel coefficients in x and y directions, respectively, h is the pressure channel coefficient, s_1, s_2 and s_3 are three independent BFSK modulated signals, and n represents noise at the receiver.

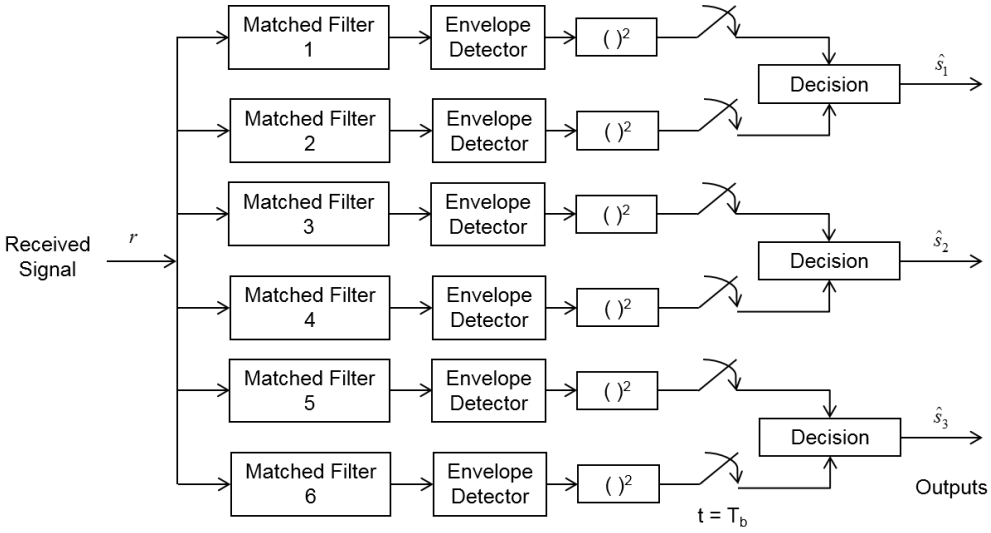

Figure 3.2 Block diagram of a non-coherent BFSK demodulator for three independent data streams.

The resonance frequency for the ring transducer is 20.41 kHz when used as two dipoles. Since BFSK is used for signal modulation, two frequencies are assigned to represent 0's and 1's for each data stream. These frequencies are 20.2, 20.3, 20.4, 20.5, 20.6 and 20.7 kHz for simultaneous transmission of three independent data streams. Sampling rate at both the transmit and receive sides are fixed at 100k samples/sec. To avoid ISI, bit duration T_b is set to 0.1 sec., to be much longer than the delay spread caused by multipath propagation. In each experiment, 6000 bits are split into three equal-length data

streams and transmitted simultaneously. The receiver records not only the signal transmission, but also the noise before and after the transmission. Block diagram of the non-coherent BFSK demodulator [26] that used for three data streams is shown in Figure 3.2.

3.1.2 Experimental Results

Table 3.1 presents the bit error rate (BER) of the MISO system for different transmit signal amplitudes. Here the amplitude means the amplitude of the BFSK sine waveform applied to each transmitter. As expected, BER decreases as the signal amplitude is increased.

Table 3.1 BER Performance of the MISO System for Different Transmitting Amplitudes

Signal Amplitude (V)	BER
0.6	0.1338
1	0.0042
2	<0.0001

Figure 3.3 shows the corresponding spectra of the received signal r in Equation (3.1), for different transmit signal amplitudes. These spectra also show that the amplitudes at FSK frequencies increase when the same signal amplitude at the transmitter side over two particle velocity and one pressure channels is increased.

The table and the spectra both demonstrate the feasibility of using a compact multichannel vector transmitter to simultaneously modulate co-located particle velocity and pressure channels, to increase the transmission rate, instead of using an array of multiple spatially separated scalar transmitters.

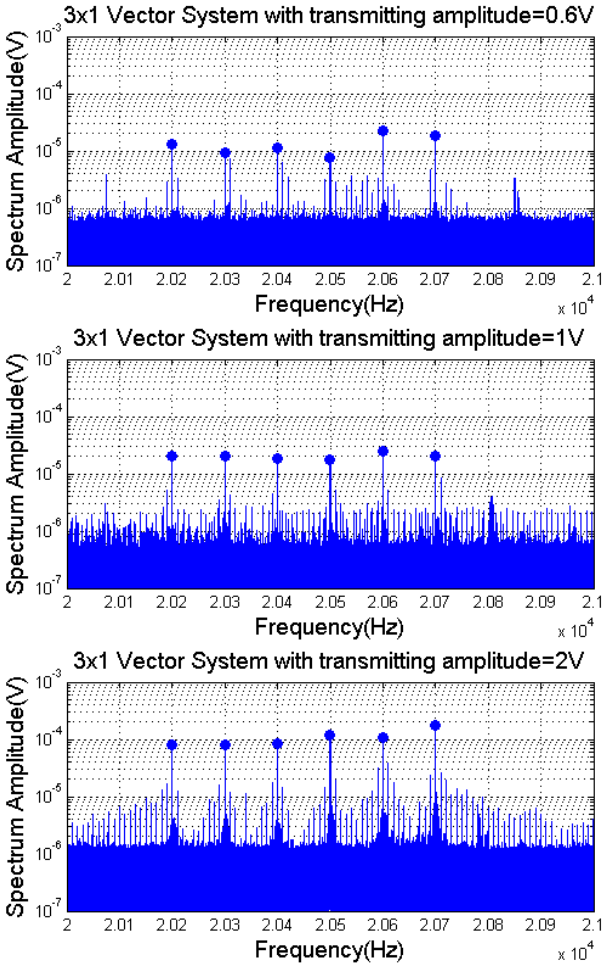

Figure 3.3 Spectra of the received signal r in (1) for the 3×1 MISO vector system, for transmit signal amplitudes 0.6 V, 1 V and 2 V, respectively.

3.2 The 1×3 SIMO System with One Scalar Transmitter and A Three-Channel Vector Receiver

The advantages of a 1×3 SIMO system using a vector receiver is presented in this section via underwater experiments, compared to a 1×3 fully scalar conventional SIMO system which has three spatially separated scalar receivers, i.e., regular hydrophones. The SIMO vector system benefits from data reception via the three *x*-velocity, *y*-velocity and pressure channels, to improve link quality. Another advantage is the small size of the receiver, as it measures three co-located channels.

3.2.1 Experimental Setup

Locations of the SIMO transmitter and receivers are shown in Figure 3.4, where the transmitter and receivers are about 15 meters apart. The SIMO system equations can be written as

$$\begin{bmatrix} r \\ r_x \\ r_y \end{bmatrix} = \begin{bmatrix} h \\ h_x \\ h_y \end{bmatrix} s + \begin{bmatrix} n \\ n_x \\ n_y \end{bmatrix}. \tag{3.2}$$

Here r, r_x and r_y are the received pressure, *x*-velocity and *y*-velocity signals, respectively, h is the pressure channel coefficient, h_x and h_y are the particle velocity channel coefficients in *x* and *y* directions, respectively, s is the BFSK modulated signal, n is the pressure noise, and n_x and n_y represent particle velocity noises in *x* and *y* directions, respectively.

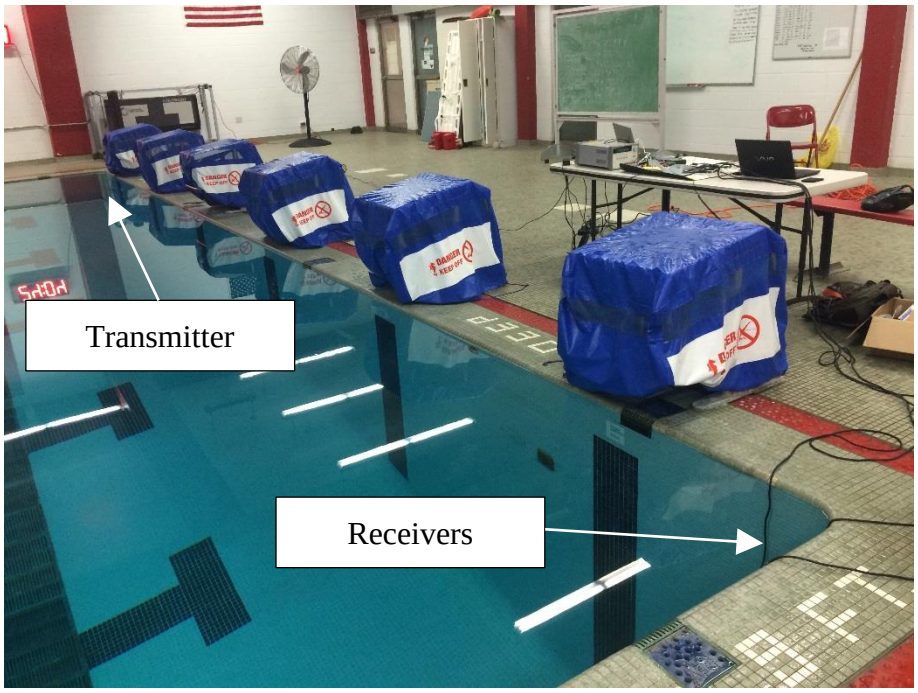

Figure 3.4 Locations of the transmitter and the receivers in the pool.

The frequencies 20.2 kHz and 20.3 kHz are used to represent 0's and 1's, respectively, in the BFSK signal. Sampling rate at both the transmit and receive sides are fixed at 100k samples/sec., and bit duration $T_b = 0.1\,\text{s}$.

The block diagram of the multichannel receiver is shown in Figure 3.5, which is a non-coherent BFSK demodulator with equal gain combining [26, 29]. The receiver combines the measured particle velocity and pressure signals.

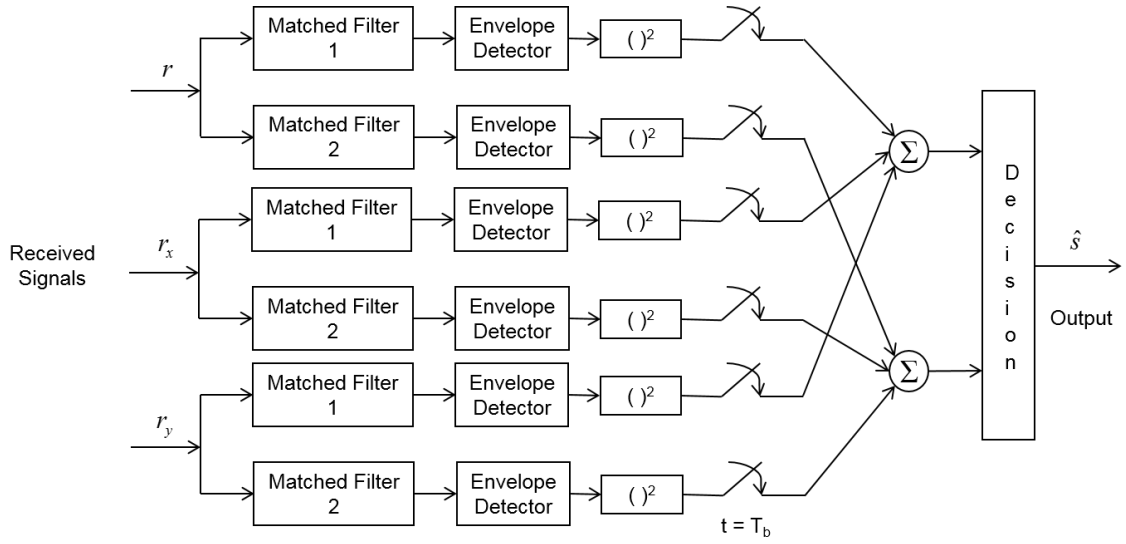

Figure 3.5 Block diagram of a non-coherent BFSK demodulator with a three-channel equal gain combiner.

3.2.2 Experimental Results

Noise characteristics of a vector communication receiver are discussed in [12], including smaller particle velocity noise powers. To investigate this matter using experimental data, in Figure 3.6, measured noise powers are presented in all channels of the 1×3 SIMO vector system, as well as a benchmark 1×3 fully scalar conventional SIMO system which has three spatially separated scalar receivers, i.e., hydrophones. One can observe that in the vector system, the two velocity noise powers are much smaller than the pressure noise

power (Figure 3.6, top panel). Additionally, pressure noise powers in the fully scalar system are all high (Figure 3.6, bottom panel). Different noise level for the 3rd pressure channel of the scalar system, CH3 in Figure 3.6, bottom panel, could be because the first two scalar receivers in the scalar system, CH1 and CH2, are exactly the same, whereas the 3rd scalar receiver is different. Therefore, the receive voltage response (RVR) of the 3rd scalar receiver might be different from the first two scalar receivers.

The transmit signal amplitude in both vector and scalar systems is set to be 0.6 V. Since velocity and pressure channels can have different signal and noise powers, to study the received signal-to-noise ratio (SNR) in each system as a measure of link quality, the received average SNR per channel is defined as follows [12]

$$\rho = \left(\Omega_h / \Omega_n + \Omega_h^x / \Omega_n^x + \Omega_h^y / \Omega_n^y \right) \Big/ 3 \tag{3.3}$$

where Ω_h, Ω_h^x and Ω_h^y are the signal powers in the pressure, *x*-velocity and *y*-velocity channels, respectively, and Ω_n, Ω_n^x and Ω_n^y are the corresponding noise powers. To measure SNR in each channel, multiple signal transmissions are made, and each is 75 sec. long. Figure 3.7 shows multiple measurements of individual SNRs, i.e., $10\log_{10}(\Omega_h / \Omega_n)$, $10\log_{10}(\Omega_h^x / \Omega_n^x)$ and $10\log_{10}(\Omega_h^y / \Omega_n^y)$ as well as the average SNR per channel $10\log_{10}(\rho)$, for both systems.

One can observe in Figure 3.7, top panel, that in the vector system, the two velocity SNRs in CH2 and CH3 are about 10 dB higher than the pressure SNR in CH1. Additionally, comparison of the two systems in Figure 3.7 reveals that the average SNR ρ of the vector system is about 10 dB higher than the average SNR of the fully scalar conventional system.

One can also observe in Figure 3.7 that for repeated similar transmissions, measured SNRs in velocity channels are more stable, compared to SNRs in pressure channels which exhibit higher variance. This might be related to the directional beam pattern of acoustic dipoles [30] which generate velocity signals in our vector receiver system, whereas scalar sensors in the fully scalar receiver system which generate pressure signals have omni-directional beam patterns.

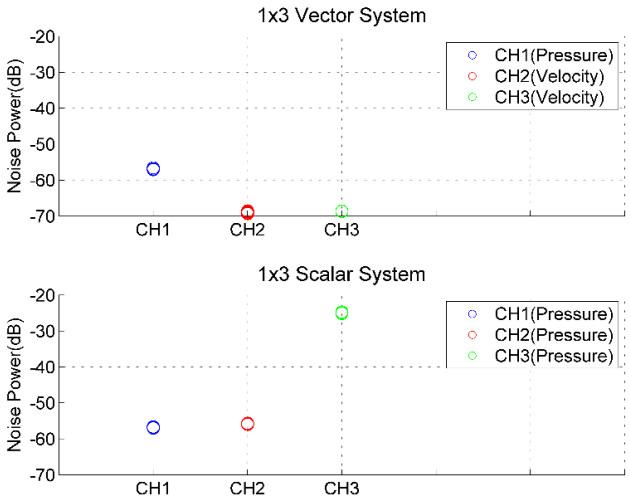

Figure 3.6 Measured noise powers in all channels of the 1×3 SIMO vector system (top), as well as measured noise powers in all channels of the benchmark 1×3 SIMO fully scalar conventional system (bottom).

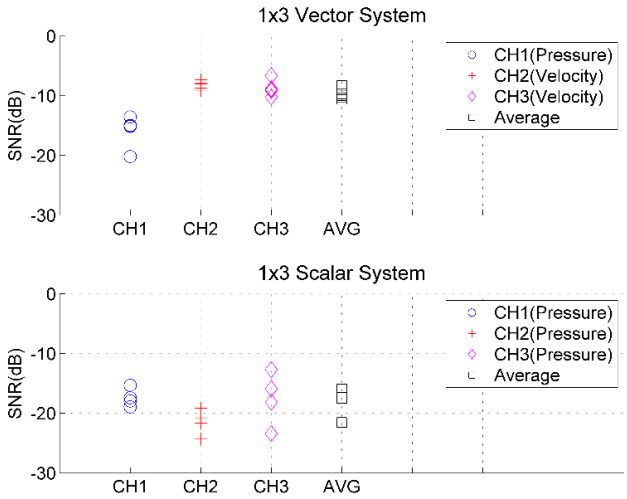

Figure 3.7 Measured individual and average received SNRs for the 1×3 SIMO vector system (top) and the benchmark 1×3 SIMO fully scalar conventional system (bottom).

3.3 Conclusions

In this chapter, feasibility and advantages of underwater communication using acoustic vector transducers are studied via experiments. These transducers utilize acoustic particle velocity channels. It is demonstrated that using a multichannel compact vector transducer transmitter, multiple independent data streams can be simultaneously transmitted, to increase the transmission rate and achieve high speed communication. It is also shown that upon using a multichannel compact vector transducer communication receiver, significant SNR improvement can be obtained, compared to a conventional communication receive array, composed of spatially separated scalar sensors. Small size of vector transducers makes them particularly suitable for small platforms and underwater sensor networks with small transceivers.

CHAPTER 4

A MULTIPLE-INPUT MULTIPLE-OUTPUT ORTHOGONAL FREQUENCY DIVISION MULTIPLEXING UNDERWATER COMMUNICATION SYSTEM USING VECTOR TRANSDUCERS

The feasibility of utilizing the vector transmitter and receivers in underwater communication are demonstrated in Chapters 2 and 3. To fully take the advantage of data multiplexing, and further increase the data rate of the system, orthogonal frequency division multiplexing (OFDM) modulation technique is considered in this chapter.

In previous chapters, two data streams modulated on one vector transmitter is demonstrated. To further increase the data rate, a method to modulate a third data stream on the same vector transmitter is also explored. The implemented system utilizes OFDM with zero-forcing (ZF), minimum mean square error (MMSE) and Maximum Likelihood (ML) detection. Carrier frequency offset (CFO) and channel responses are estimated using null and pilot tones, respectively. The preliminary results are shown in this chapter. The details on OFDM implementation and how tripling data rate is done can be found in Chapter 5. To test the system robustness against Doppler effect, the transmitter is manually moved back and forth during the experiments, to mimic the drifting in realistic environment.

4.1 OFDM System Parameters and Experimental Setup

Tests for the OFDM system are conducted in both water tank and pool. The signal source is one multi-mode ring transducer working as vector transmitter, which can transmit two or three data streams simultaneously, shown in Figure 4.1. Same system parameters are used in both environment and listed in Table 4.1. Two sets of receivers are used. Receiver

set A includes four hydrophones, two Omni transducers and one spherical transducer. All four hydrophones and two Omni transducers are used as scalar receivers, and the spherical transducer is used as a three-channel vector transducer, which leads to nine total receiving channels. Receiver set B includes eight well-matched scalar hydrophones. All different types of the receiver are shown in Figure 4.2. OFDM Signals are transmitted multiple times in both environments and every transmission contains 50 OFDM blocks with preamble and postamble, as shown in Figure 4.3.

Table 4.1 System Parameters for The Experiments

Center frequency	f_c = 20.4 kHz
Bandwidth	B = 8 kHz
Subcarrier spacing	Δf = 7.8 Hz
OFDM block duration	T = 128 ms
Sampling frequency	f_s = 200k samples/sec
Modulation type	QPSK
Bandwidth efficiency	α = 0.37, 0.73, 1.10
Data rate	R = 5.86, 8.78 kbps
Number of subcarriers	K = 1024
Number of pilot tones	K_d = 256
Number of null subcarriers	K_n = 96
Time guard interval	T_g = 25 ms

Figure 4.1 Multi-mode Ring Transducer.

Figure 4.2 All types of the receivers used in the experiments. From left to right are a scalar hydrophone, an omni scaler transducer and a spherical vector transducer.

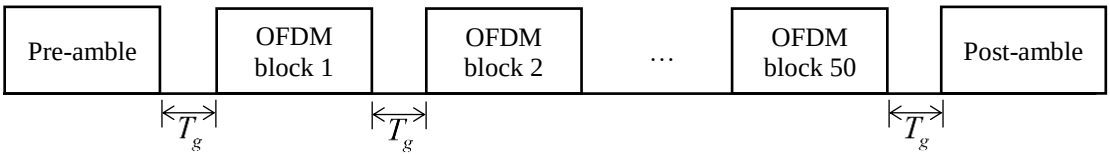

Figure 4.3 Structure of the transmitted OFDM signals.

4.2 Performance Results of Receiver Set A

4.2.1 BER Performance with Two or Three Data Streams in Water Tank

In water tank, the transmitter and receivers are about 1 m apart, as shown in Figure 4.4 for receiver set A and Figure 4.5 for receiver set B. The water depth in the tank is approximately 20 cm. Due to the space limitation, multiple receivers are placed on the horizontal plane at the same depth as the transmitter in the water tank. Signal power is unit for each data stream when generated and later be properly scaled up to keep the transmitting voltage amplitude at 0.5 V at the output of the DAC for three data streams cases and directly applied to the transmitter. The same scaling factor would be used in two data streams cases

to ensure the same signal power for each data stream across all scenarios. When transmitters and receivers are static in the tank, the water tank has low noise and almost no doppler, which makes the result under this scenario can be used as a benchmark to test the OFDM system. Bit error rate (BER) and corresponding Signal-to-noise ratio (SNR) will be reported. For each receiver, the signal power of one OFDM block is calculated by using the amplitude of the pilot carriers for each data stream, and the noise power is calculated based on the amplitude of the null carriers [31]. Signal and noise power are averaged over 50 OFDM blocks for each transmission and averaged again over all the receivers to mitigate the difference among the receivers. Therefore, one SNR will be reported for each data stream each transmission. All the performance reported in this chapter has been verified by doing multiple transmission and can be reproduced.

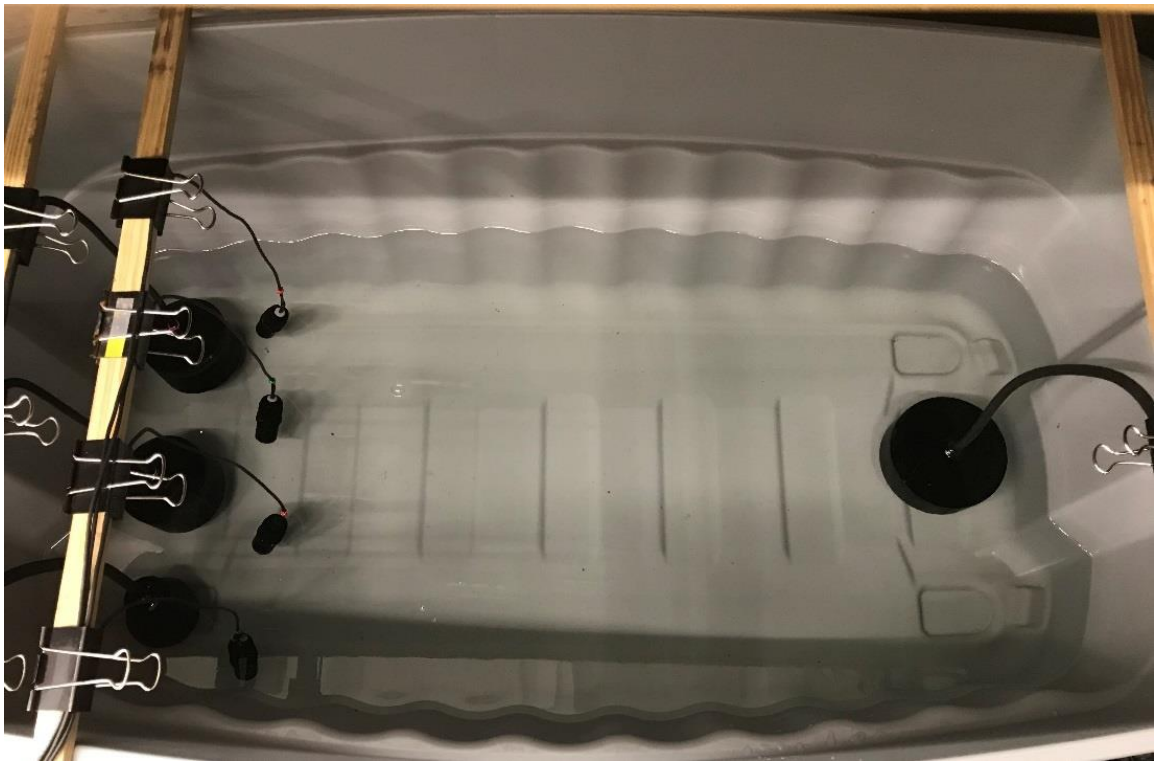

Figure 4.4 The water tank used for experiments, with ring transducer on the right and receiver set A on the left.

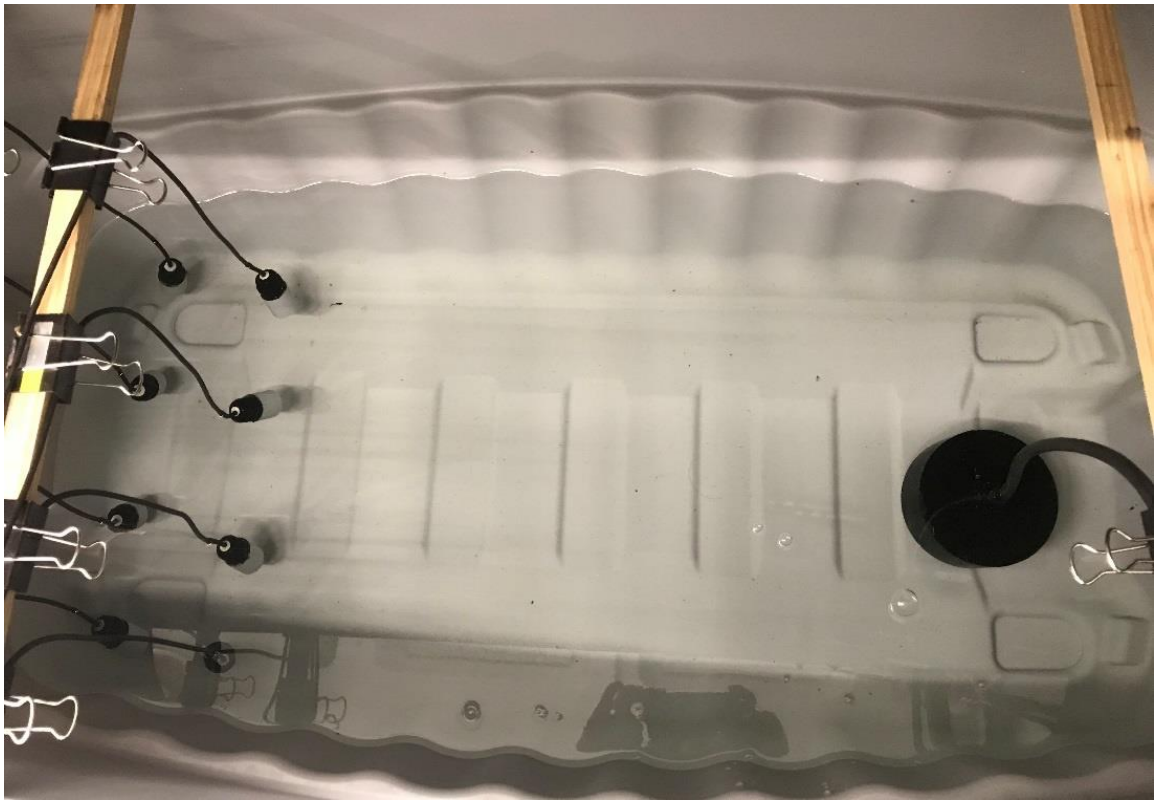

Figure 4.5 The water tank used for experiments, with ring transducer on the right and receiver set B on the left.

Table 4.2 BER Performance of Two or Three Data Streams in Water Tank with Receiver Set A

Rx set A		Static in Water Tank				Manually Drifting in Water Tank			
		SNR (dB)	BER			SNR (dB)	BER		
			ZF	MMSE	ML		ZF	MMSE	ML
2x9	DS1	25.09	<0.0001	<0.0001	<0.0001	10.75	0.0030	<0.0001	<0.0001
	DS2	26.19	<0.0001	<0.0001	<0.0001	11.53	0.0022	<0.0001	<0.0001
3x9	DS1	24.38	0.1811	0.0267	<0.0001	9.38	0.4313	0.0133	0.0003
	DS2	25.50	0.1140	0.0206	<0.0001	10.18	0.4296	0.0074	0.0002
	DS3	24.91	0.4460	0.0113	<0.0001	9.74	0.4902	0.0069	0.0064

The summary of SNR and BER performance are shown in Table 4.2. The BER after decoding are shown in the table. Both receiver sets are tested for two data streams and three data streams scenarios. BERs for individual OFDM blocks in one transmission are shown in Figure 4.6 and Figure 4.7. Figure 4.8 shows a typical CFO estimation in tank using the

method introduced previously. Since the transmitter and receiver are static in the tank, CFO searching are done within [-1, 1] range with 0.1 Hz step size, and the estimation results are almost a constant over the entire transmission, and the reason for the non-zero estimation is caused by the asynchronized transmitter and receiver clock source.

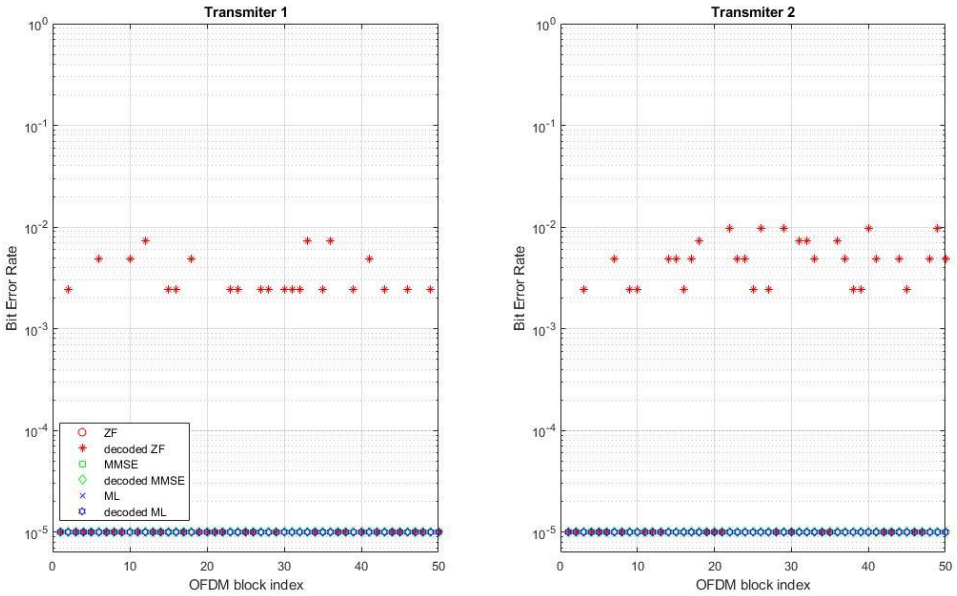

Figure 4.6 Bit error rates of individual blocks for 2I9O-OFDM, in water tank.

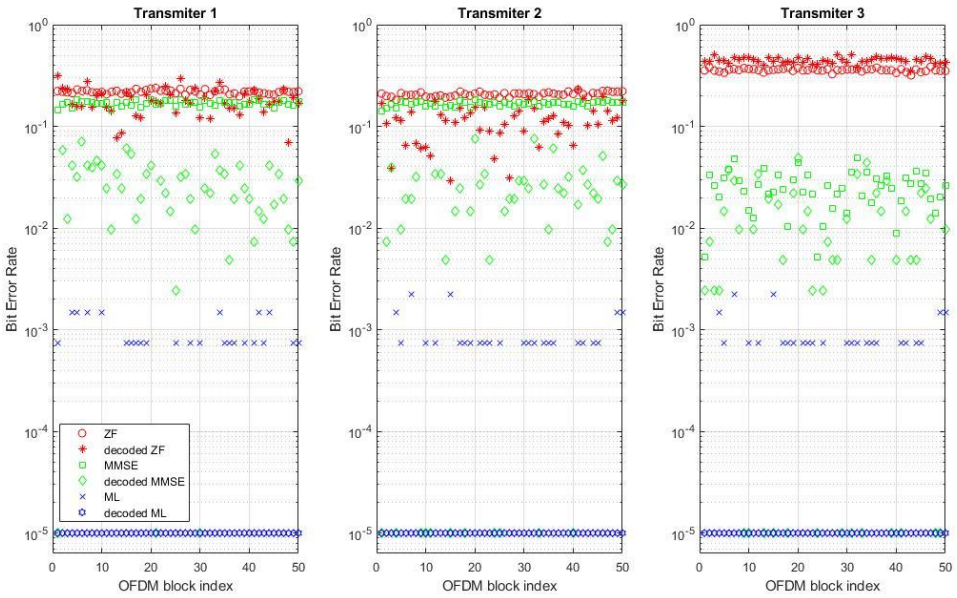

Figure 4.7 Bit error rates of individual blocks for 3I9O-OFDM, in water tank.

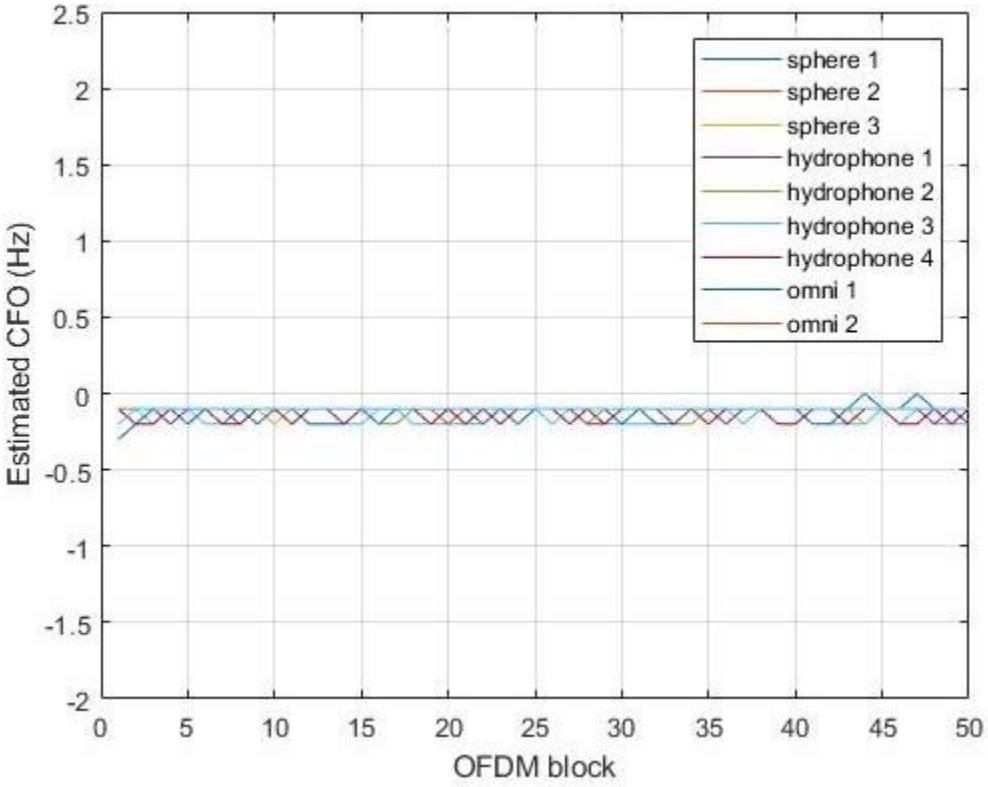

Figure 4.8 CFO estimation of one trial for 3I9O-OFDM, in water tank, corresponding to Figure 4.7.

To simulate the water drifting happens in the real environment, some tests are done while the transmitter is moving in the direction towards the receiver back and forth slowly. The result summary with drifting is shown in Table 4.3. The corresponding BERs for individual OFDM blocks in one transmission are shown in Figures 4.9 and 4.10. With the movement of the transmitter, the CFO searching range is extended to [-4, 4] to ensure the correct CFO could be captured during the process. The step size remains 0.1 Hz.

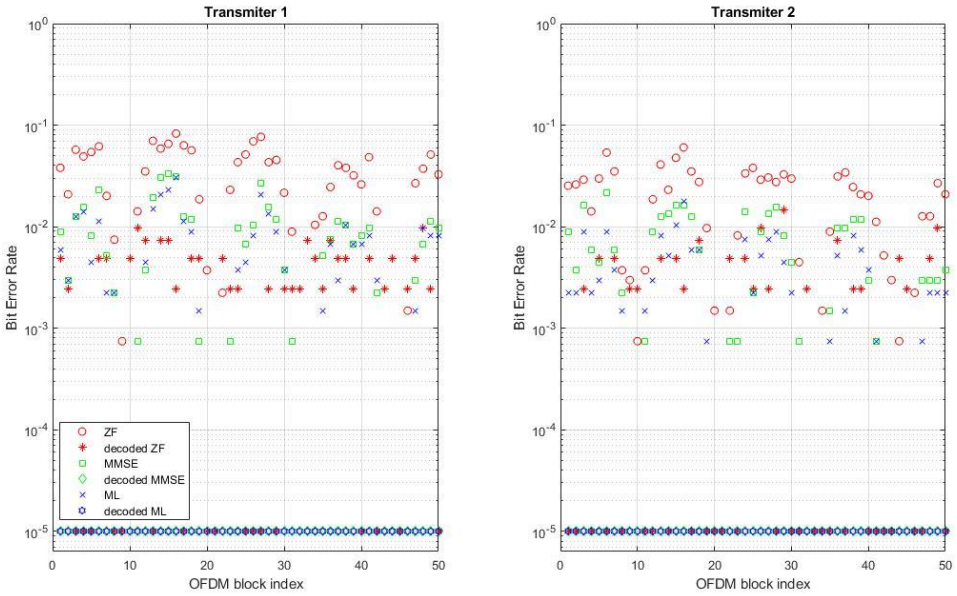

Figure 4.9 Bit error rates of individual blocks for 2I9O-OFDM, in water tank with manual drifting.

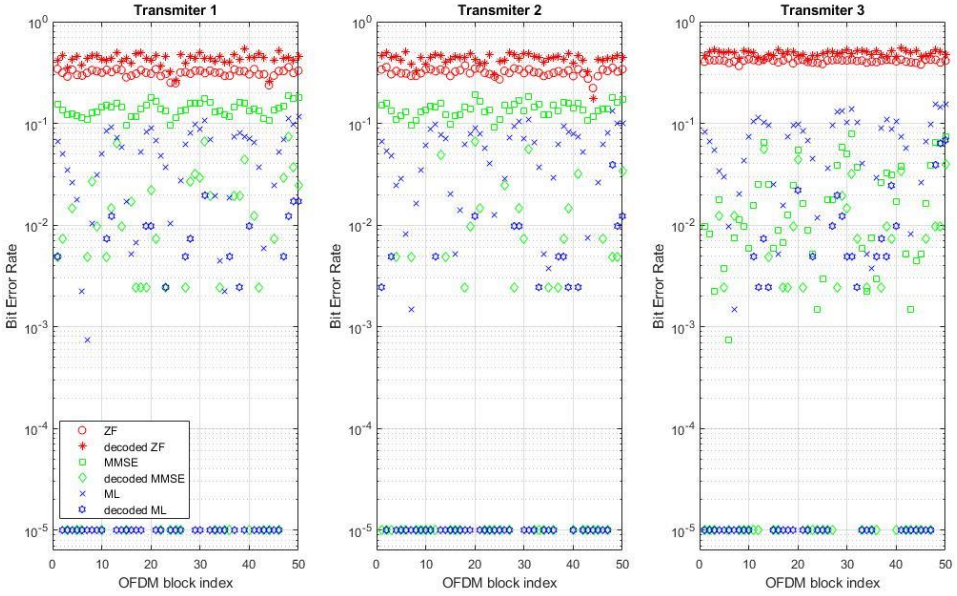

Figure 4.10 Bit error rates of individual blocks for 3I9O-OFDM, in water tank with manual drifting.

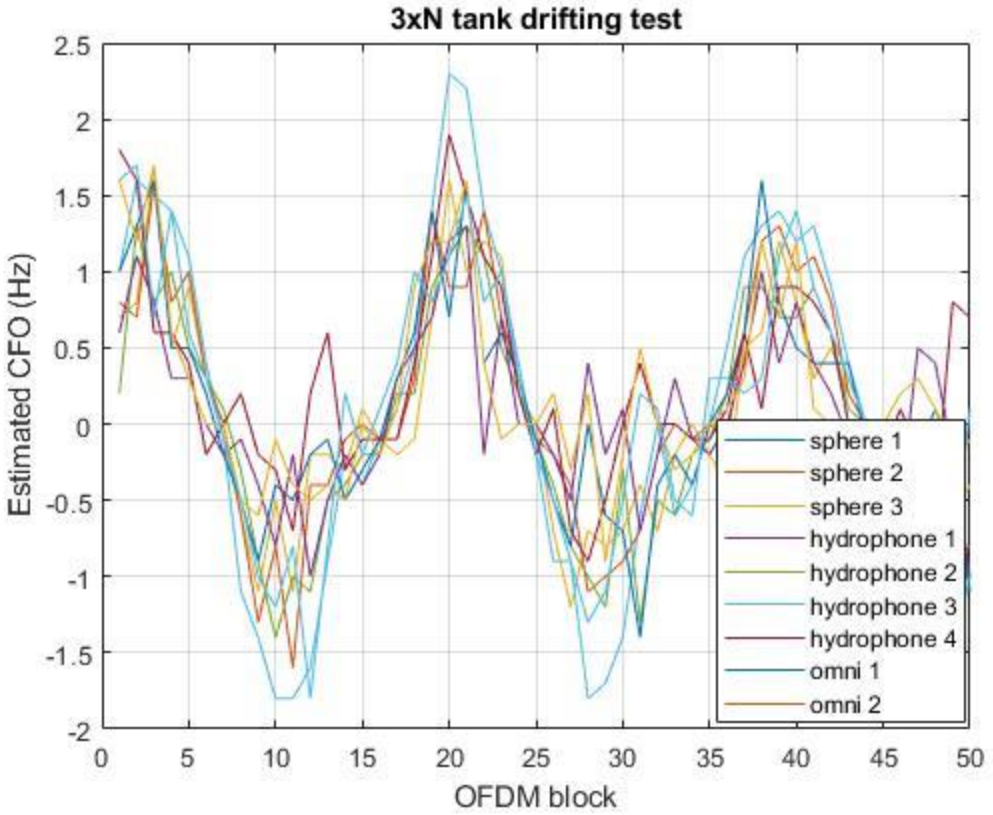

Figure 4.11 CFO estimation of one transmission for 3I9O-OFDM, in water tank with manual drifting, corresponding to Figure 4.10.

4.2.2 BER Performance with Two or Three Data Streams in Pool

Tests in this subsection are done in the pool in a similar way compare to those are done in the tank. Instead of placing all the receivers on a horizontal plane, both receiver set are mounted vertically. Receiver set A is illustrated in Figure 4.12. Hydrophones of receiver set B are equally spaced with 7.5 cm between elements. The transmitter and receivers are about 5 m apart, as shown in Figure 4.13. The transmitter is placed 1 m deep in the pool and the center of the receiver array is at about the same depth. Same scaling method used in water tank is utilized to keep the signal power of each data stream the same for a fair comparison. Transmitting voltage amplitude is kept at 0.5 V at the output of the DAC, which after the PA & MN can be amplified to about 121 V and applied to the transducer.

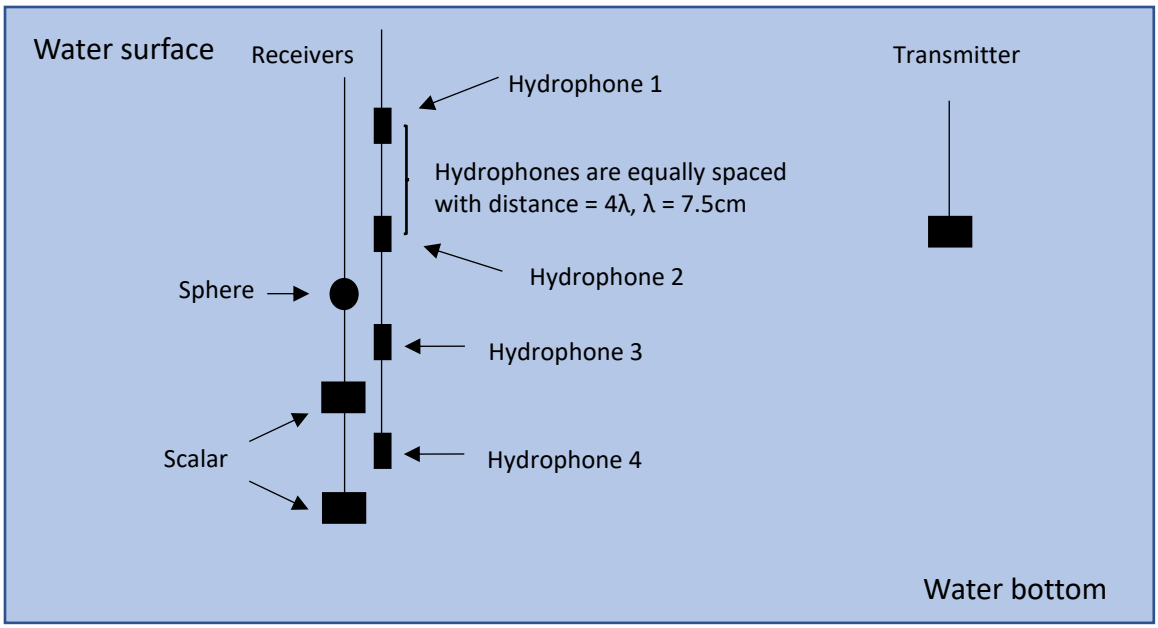

Figure 4.12 Illusion of receiver set A in pool.

The summary of SNR and BER performance are shown in Table 4.3. The BER after decoding are shown in the table like the water tank results. Both receiver sets are tested for two data streams and three data streams scenarios in the pool as well. BERs for individual OFDM blocks in one transmission are shown in Figures 4.14 and 4.15. Figure 4.16 shows a typical CFO estimation in tank using the method introduced previously.

Figure 4.13 Experimental setup in pool.

Table 4.3 BER Performance of Two or Three Data Streams in Pool Using Receiver Set A

Rx set A		Static in Pool				Manually Drifting in Pool			
		SNR (dB)	BER			SNR (dB)	BER		
			ZF	MMSE	ML		ZF	MMSE	ML
2x9	DS1	14.91	0.1205	<0.0001	<0.0001	10.75	0.0030	<0.0001	<0.0001
	DS2	13.73	<0.0001	<0.0001	<0.0001	11.53	0.0022	<0.0001	<0.0001
3x9	DS1	14.95	0.3048	0.0223	0.0009	9.38	0.4313	0.0133	0.0003
	DS2	11.97	0.2363	0.0131	0.0020	10.18	0.4296	0.0074	0.0002
	DS3	13.42	0.4820	0.0224	0.0029	9.74	0.4902	0.0069	0.0064

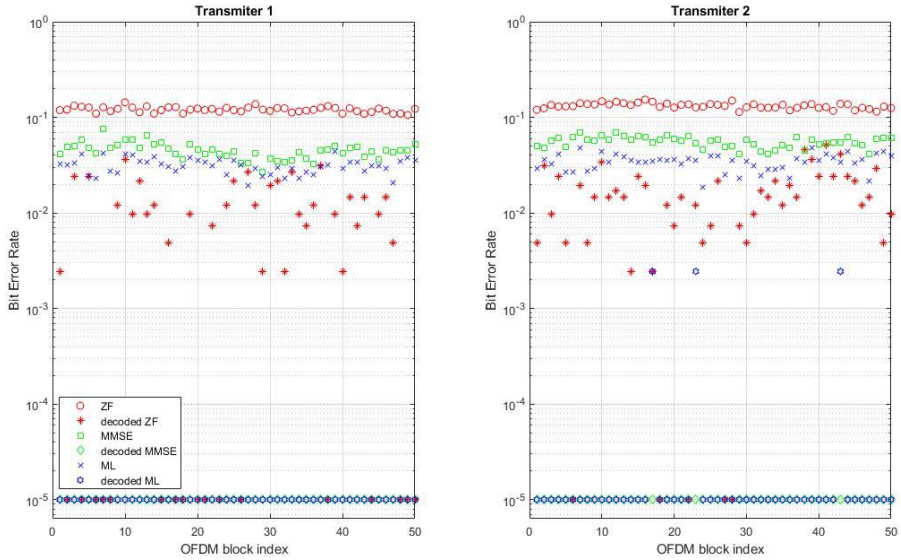

Figure 4.14 Bit error rates of individual blocks for 2I9O-OFDM, in pool.

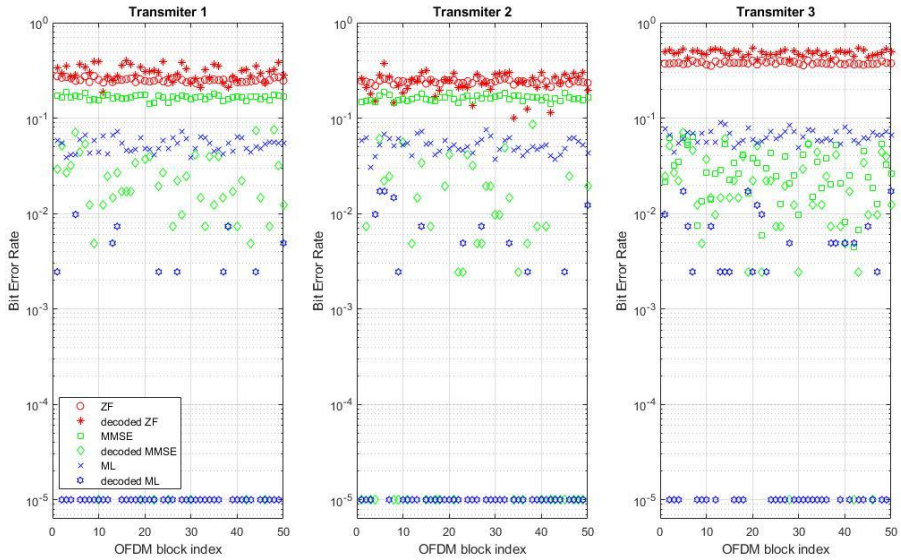

Figure 4.15 Bit error rates of individual blocks for 3I9O-OFDM, in pool.

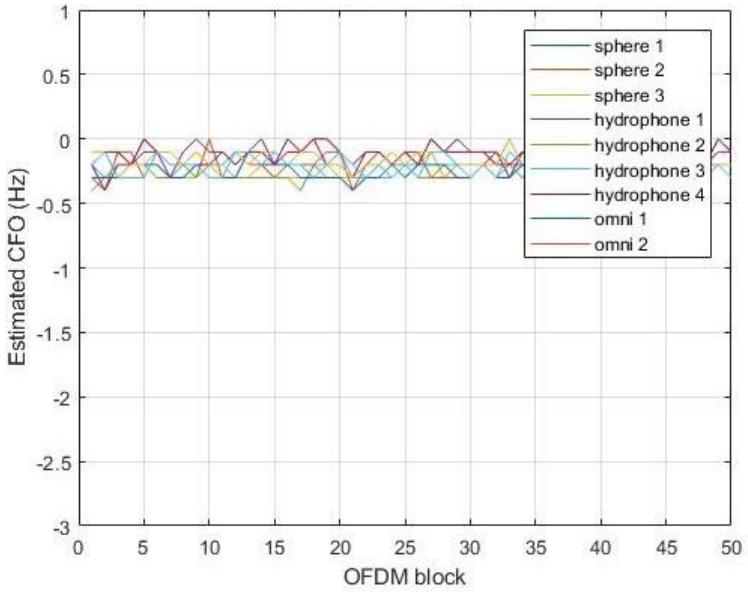

Figure 4.16 CFO estimation of one transmission for 3I9O-OFDM, in pool, corresponding to Figure 4.15.

To test the CFO estimation function, similar drifting compare to the tanks tests has been added in the pool. The movement of the transmitter in the pool has a larger range compare to the tank drifting test due to the nature of a larger pool and longer transmitter/receiver distance.

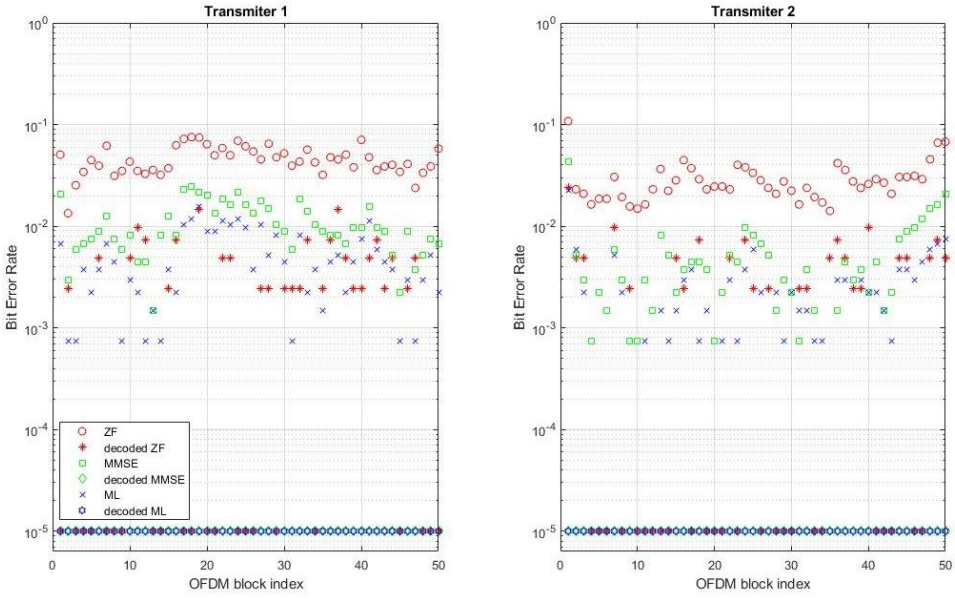

Figure 4.17 Bit error rates of individual blocks for 2I8O-OFDM, in pool with manual drifting.

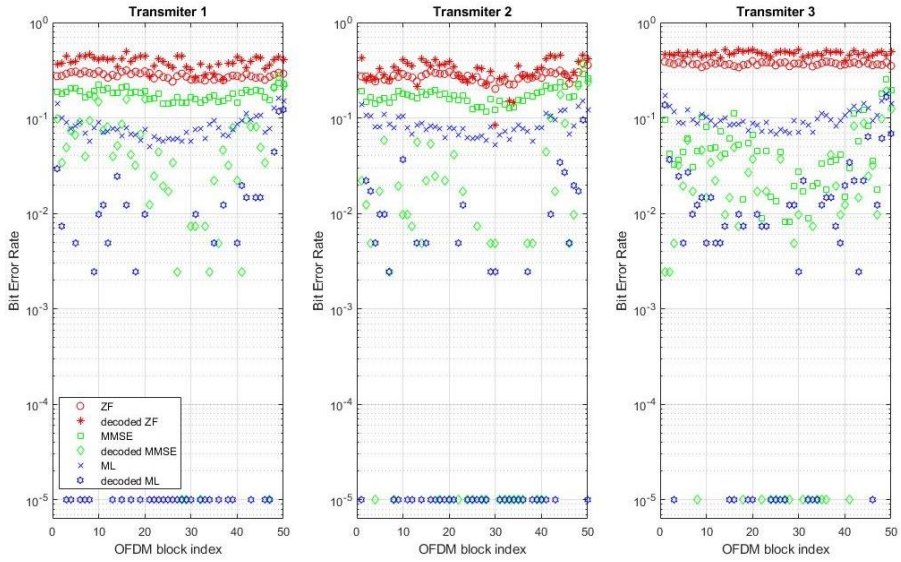

Figure 4.18 Bit error rates of individual blocks for 3I8O-OFDM, in pool with manual drifting.

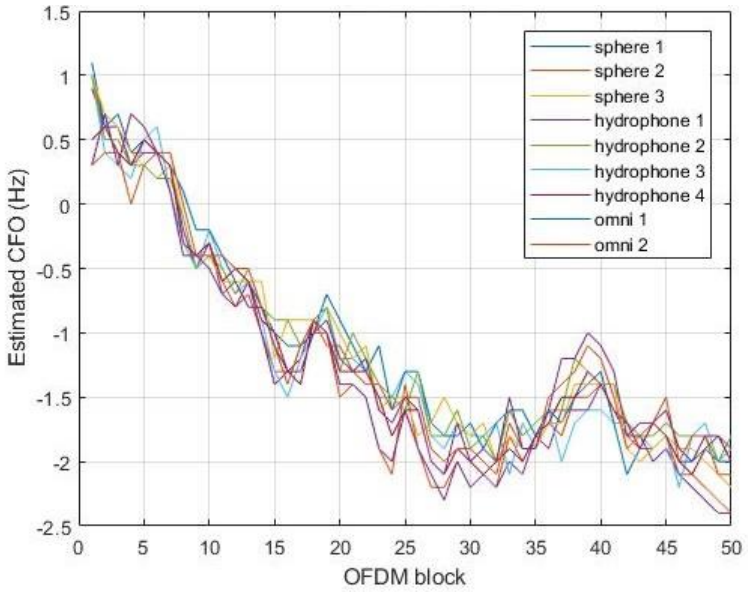

Figure 4.19 CFO estimation of one transmission for 3I9O-OFDM, in pool with manual drifting, corresponding to Figure 4.18.

4.3 Performance Results of Receiver Set B

Similar Tests are done in both water tank and pool by placing receiver set B (eight scalar hydrophones) with receiver set A, where the transmitter setup remains same. The distance between the transmitter and the receivers is kept the same.

4.3.1 BER Performance with Two or Three Data Streams in Water Tank

The summary of SNR and BER performance with receiver set B in water tank is shown in Table 4.4. The BERs for individual OFDM blocks in one transmission are shown in Figures 4.20 and 4.21. Figure 4.22 shows a typical CFO estimation in pool when transmitter and receivers are static.

Table 4.4 BER Performance of Two or Three Data Streams in Water Tank with Receiver Set B

Rx Set B		Static in Water Tank				Manually Drifting in Water Tank			
		SNR (dB)	BER			SNR (dB)	BER		
			ZF	MMSE	ML		ZF	MMSE	ML
2x8	DS1	15.04	0.0019	<0.0001	<0.0001	8.32	0.0024	<0.0001	<0.0001
	DS2	15.44	0.0027	<0.0001	<0.0001	8.12	0.0029	<0.0001	<0.0001
3x8	DS1	15.84	0.0372	0.0002	<0.0001	6.58	0.3118	0.0277	0.0157
	DS2	15.62	0.0128	0.0001	<0.0001	6.70	0.2782	0.0177	0.0148
	DS3	15.32	0.4352	0.0002	<0.0001	6.58	0.4764	0.0160	0.0614

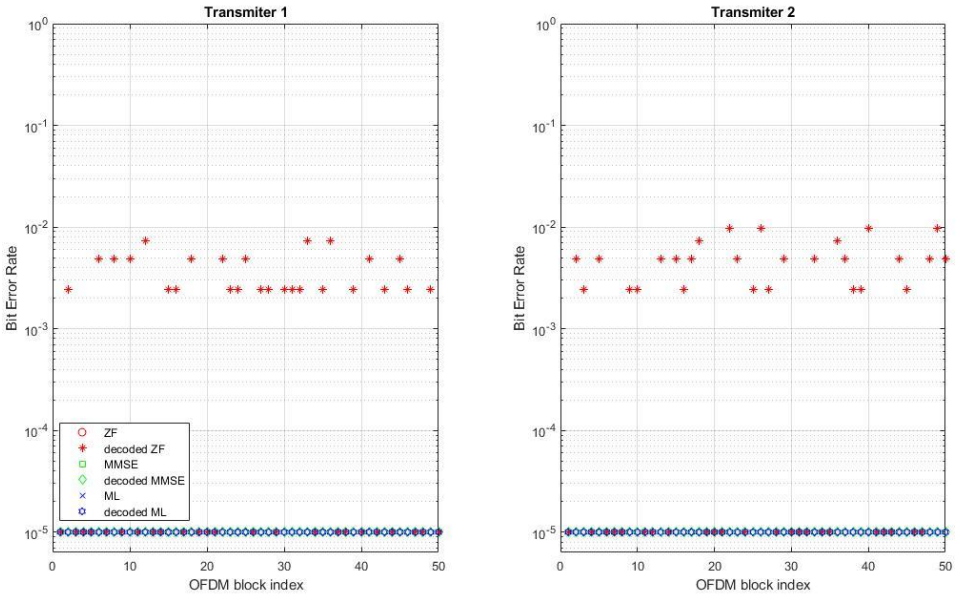

Figure 4.20 Bit error rates of individual blocks for 2I8O-OFDM, in water tank.

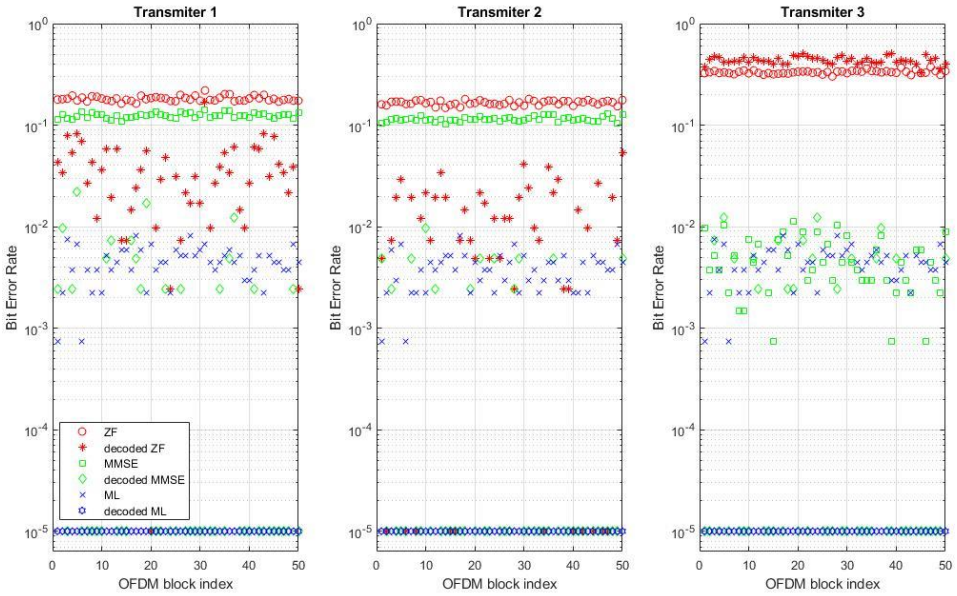

Figure 4.21 Bit error rates of individual blocks for 3I8O-OFDM, in water tank.

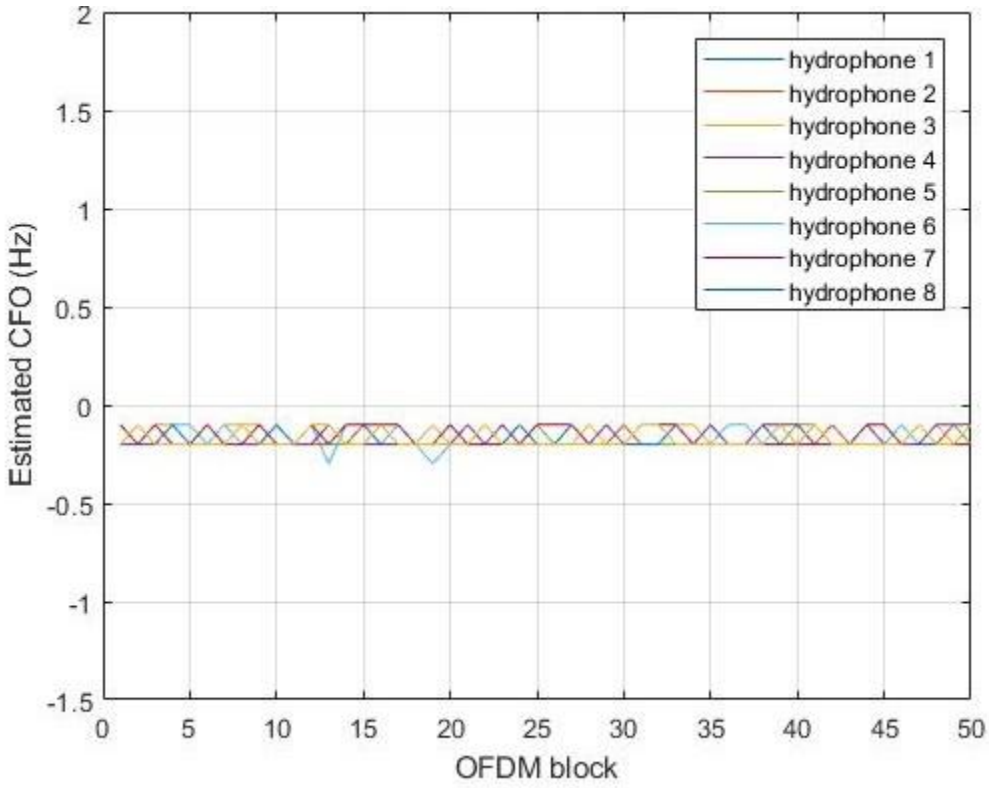

Figure 4.22 CFO estimation of one trial for 3I8O-OFDM, in water tank, corresponding to Figure 4.21.

With adding drifting, the result for receiver set B in water is shown in Figures 4.23 and 4.24. Figure 4.25 shows a typical CFO estimation in pool with drifting.

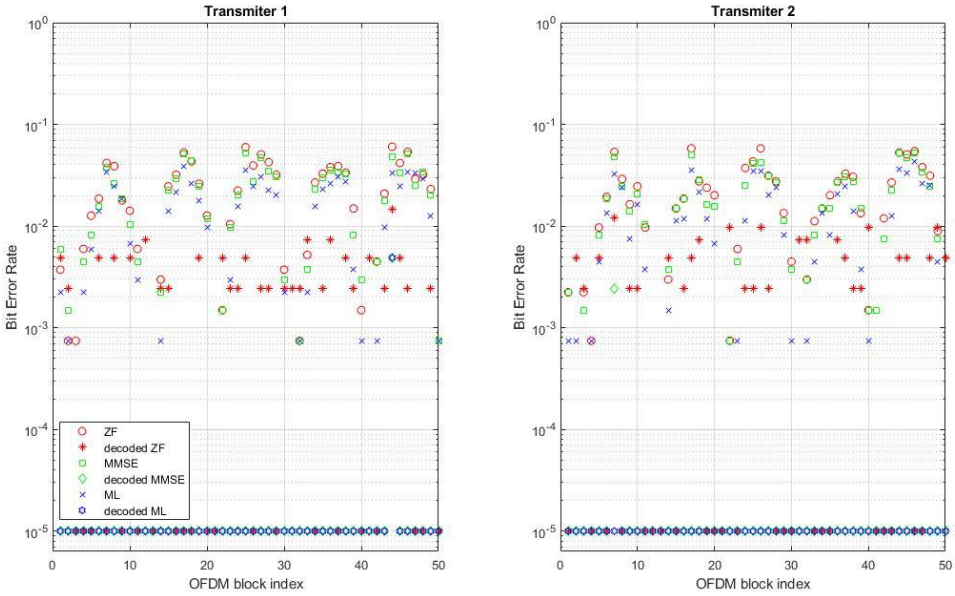

Figure 4.23 Bit error rates of individual blocks for 2I8O-OFDM, in water tank with manual drifting.

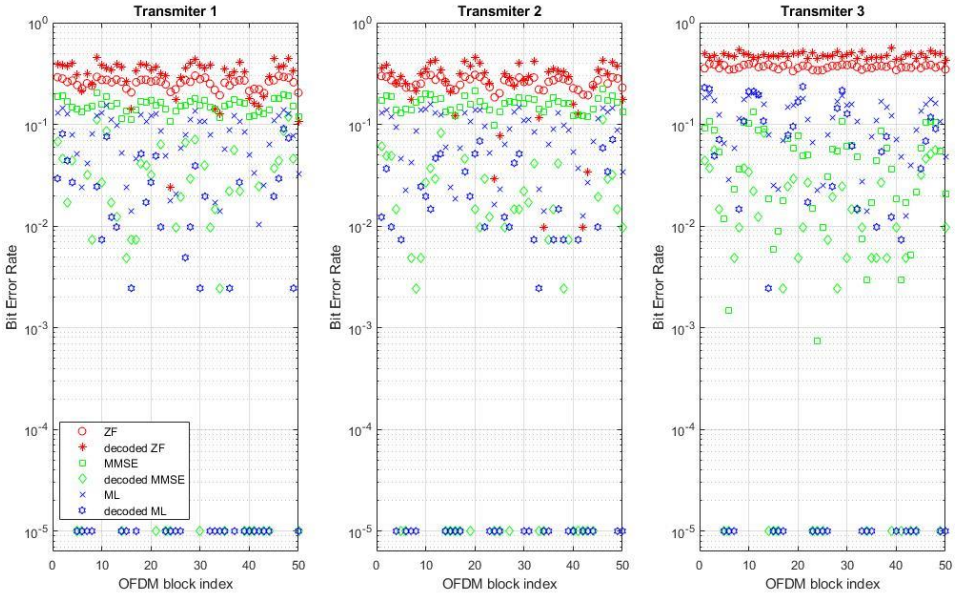

Figure 4.24 Bit error rates of individual blocks for 3I8O-OFDM, in water tank with manual drifting.

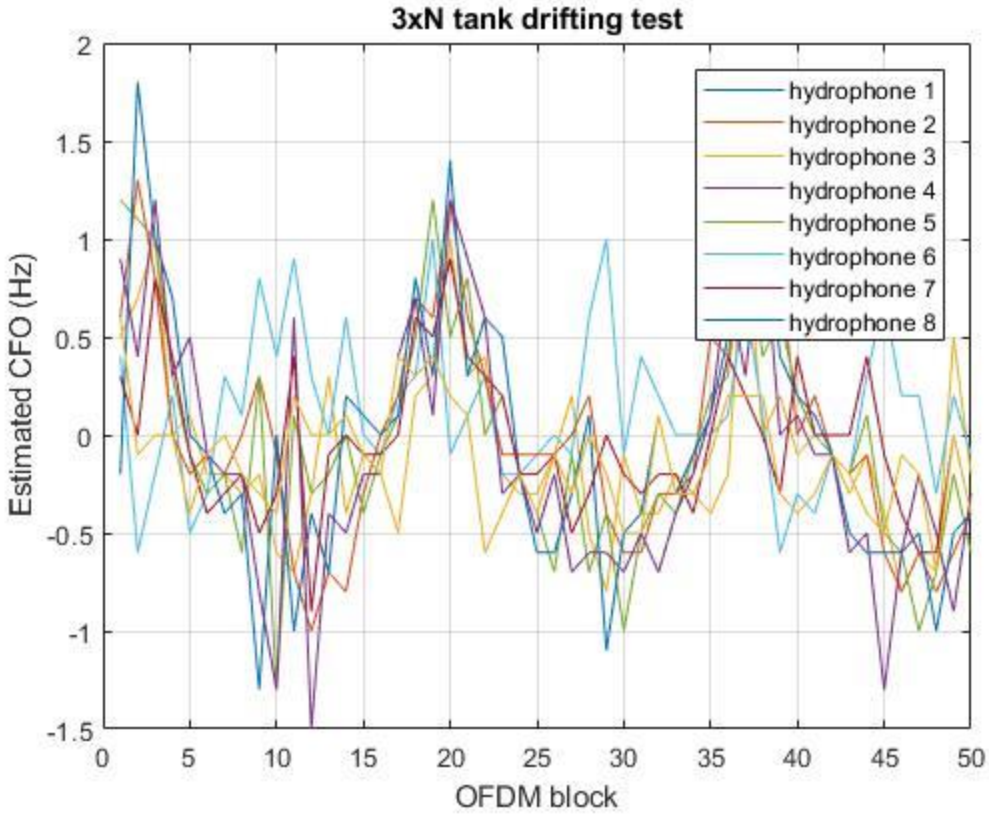

Figure 4.25 CFO estimation of one trial for 3I8O-OFDM, in water tank with manual drifting, corresponding to Figure 4.24.

4.3.2 BER Performance with Two or Three Data Streams in Pool

The pool result summary is shown in Table 4.5. The BERs for individual OFDM blocks in one transmission are shown in Figures 4.26 and 4.27. Figure 4.28 shows a typical CFO estimation in pool when transmitter and receivers are static.

Table 4.5 BER Performance of Two or Three Data Streams in Pool with Receiver Set B

Rx set B		Static in Pool				Manually Drifting in Pool			
		SNR (dB)	BER			SNR (dB)	BER		
			ZF	MMSE	ML		ZF	MMSE	ML
2x8	DS1	16.70	0.0020	<0.0001	<0.0001	11.93	0.0025	0.0001	<0.0001
	DS2	16.59	0.0027	<0.0001	<0.0001	12.39	0.0045	0.0005	0.0001
3x8	DS1	11.65	0.1213	0.0827	0.0260	8.59	0.2130	0.1515	0.1117
	DS2	13.78	0.0428	0.0192	0.0094	9.43	0.1608	0.0954	0.0748
	DS3	11.55	0.4617	0.0337	0.0640	9.70	0.4410	0.0766	0.1467

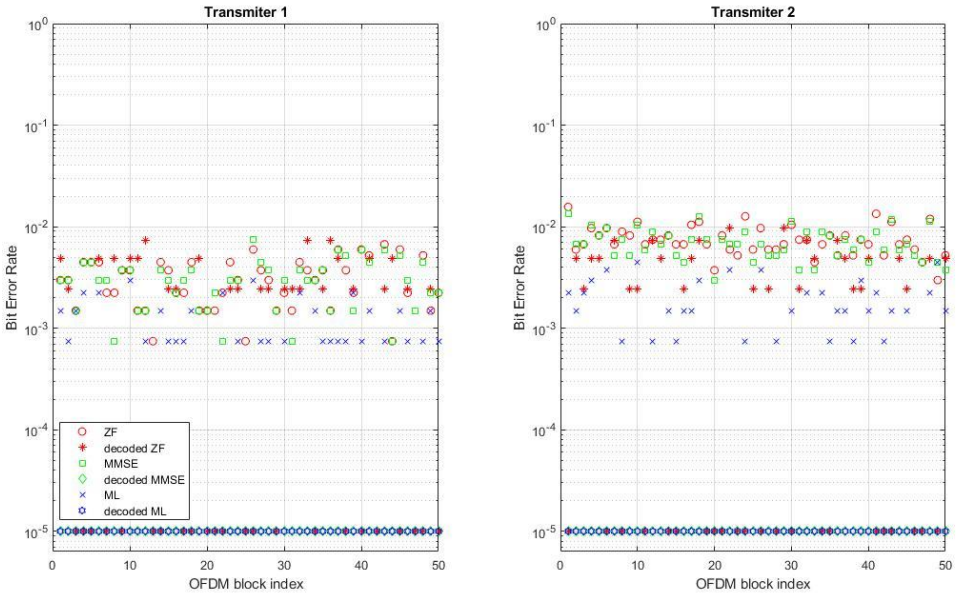

Figure 4.26 Bit error rates of individual blocks for 2I8O-OFDM, in pool.

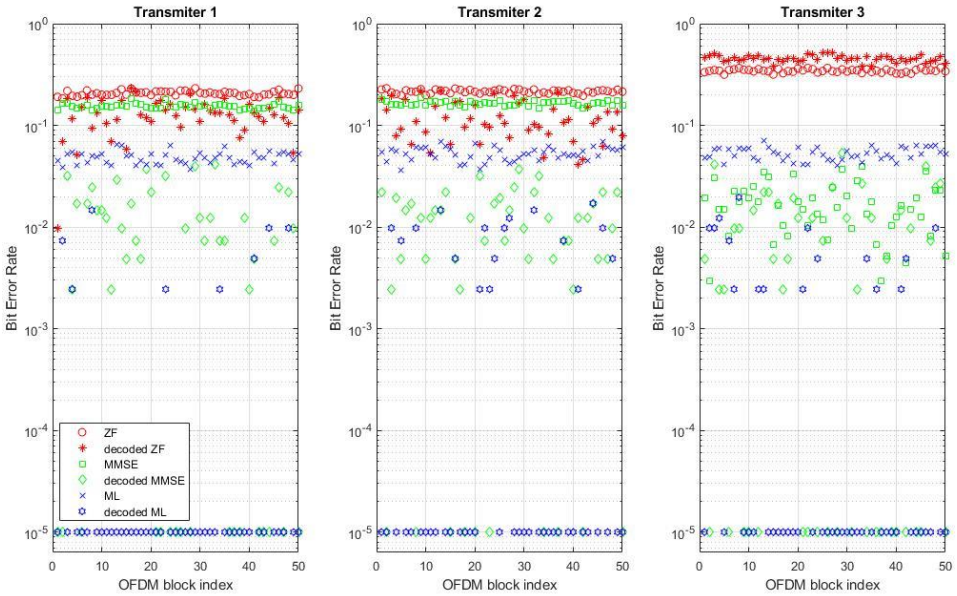

Figure 4.27 Bit error rates of individual blocks for 3I8O-OFDM, in pool.

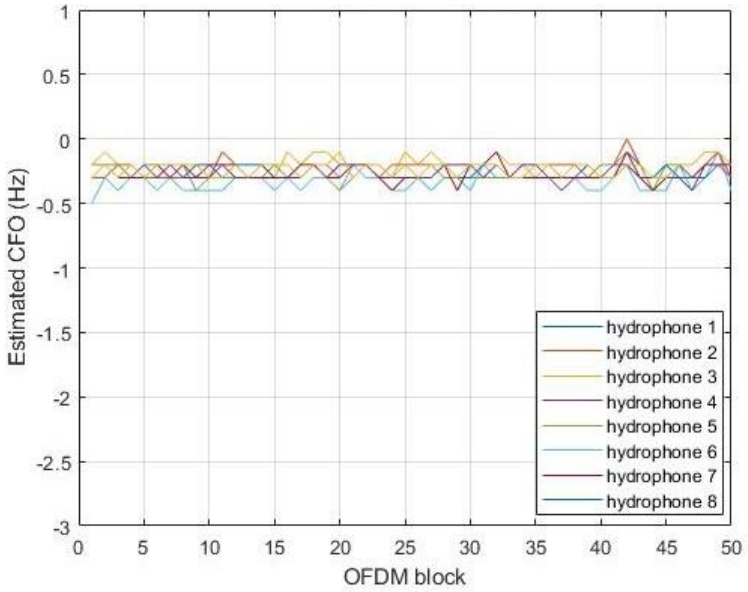

Figure 4.28 CFO estimation of one trial for 3I8O-OFDM, in pool, corresponding to Figure 4.27.

The results in the pool with manual drifting are shown in Figures 4.28 and 4.29. The CFO estimation corresponding to Figure 4.29 are shown in Figure 4.30.

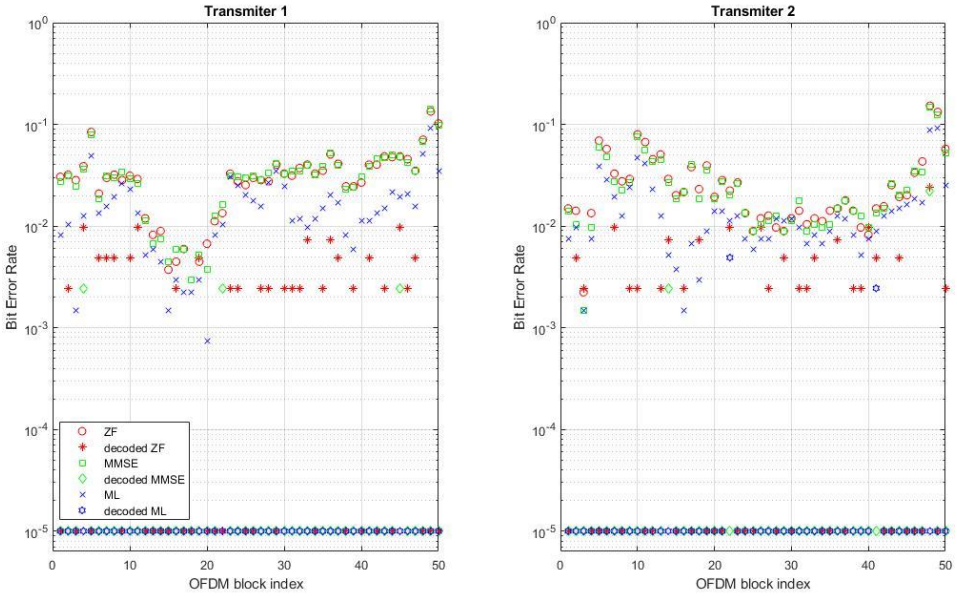

Figure 4.29 Bit error rates of individual blocks for 2I8O-OFDM, in pool with manual drifting.

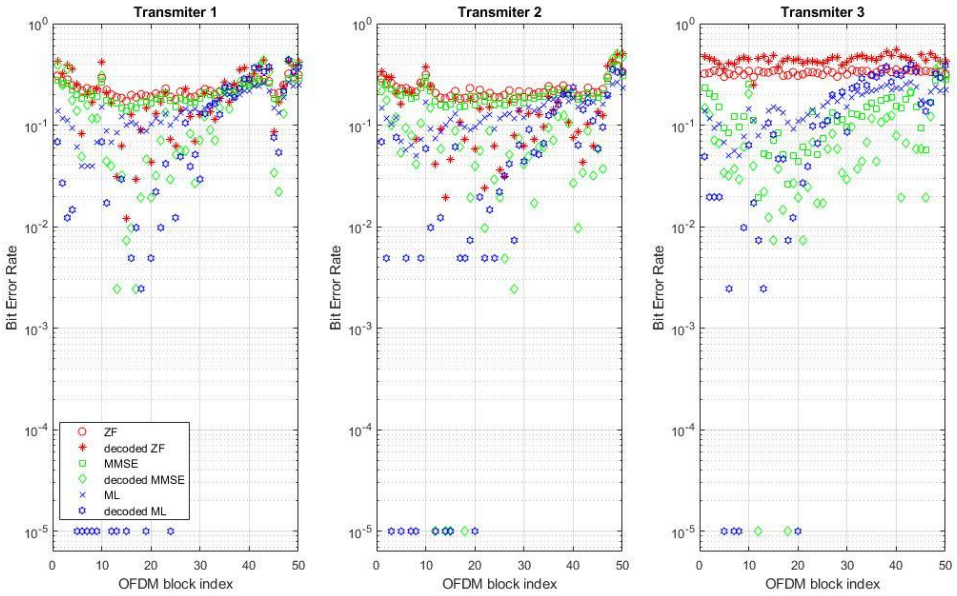

Figure 4.30 Bit error rates of individual blocks for 3I8O-OFDM, in pool with manual drifting.

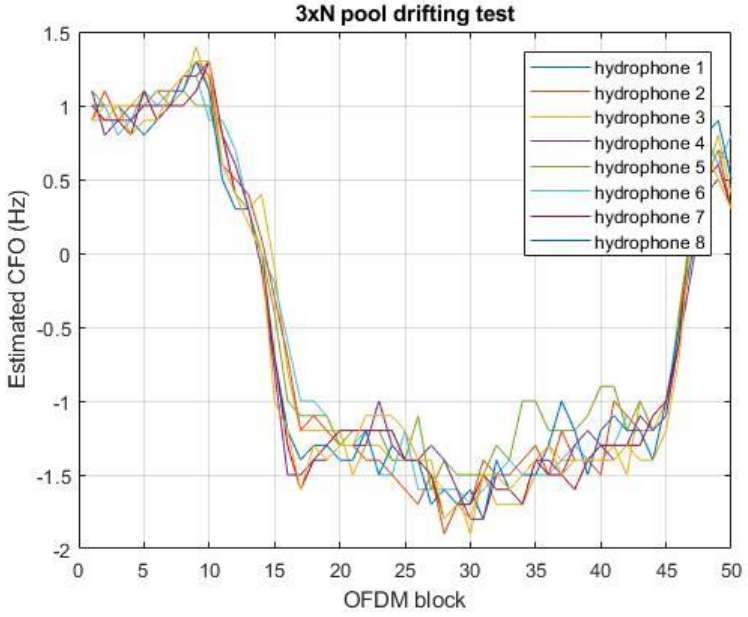

Figure 4.31 CFO estimation of one trial for 3I8O-OFDM, in pool with manual drifting, corresponding to Figure 4.30.

4.4 Conclusions and Summary

In this chapter, an OFDM underwater communication system is implemented by using vector transmitter and receiver. With a reasonable SNR, the implemented system can achieve solid BER performance with doubling or even tripling the data rate by just using one single vector transmitter. Even with an artificial drifting added, the system shows a decent tolerance against Doppler effect.

When even higher data rate is required for certain application, one can use two vector transmitters simultaneously to quadruple the data rate. Here a preliminary result is given. With four data streams transmitted by two vector ring transducer and received by receiver set A mentioned previously, one can achieve the BER performance listed in Table 4.6 in both water tank and pool, with 4kHz bandwidth. The estimated CFO of the pool result ranges from -2.5 Hz to 1.7 Hz. Without proper power amplifier at the time of the experiments, the tests are conducted where transmitters and receivers are just 1m apart, to achieve reasonable SNR. Furthermore, the results listed are obtained by using ML detection method. With the number of data streams increased, one may need a greater number of receiving channels to separate the data streams properly without increase the computational complicity. Here, a multi-channel vector transmitter can be a good candidate to increase the receiving channels without increasing the number of physical devices.

Table 4.6 BER Performance of Four Data Streams in Water tank and Pool with Receiver Set A

Rx set A		Static in Water Tank		Manually Drifting in Pool	
		SNR (dB)	BER ML	SNR (dB)	BER ML
4x8	DS1	19.93	<0.0001	16.70	<0.0001
	DS2	20.58	<0.0001	15.05	<0.0001
	DS3	15.39	<0.0001	15.76	0.0010
	DS4	16.12	<0.0001	14.96	0.0049

All the experiments conducted so far are all for the preparation of ocean field tests. In the next chapter, a detailed system structure and technique explanation will be given, as well as the ocean field test results for both OFDM system and FSK system.

CHAPTER 5

PARTICLE VELOCITY DATA MULTIPPLEXING VIA ONE VECTOR TRANSMITTER FOR UNDERWATER COMMUNICATION

5.1 Acoustic Particle Velocity Channel and Vector Transmitter

To modulate data on a specific acoustic particle velocity component, e.g., *x* axis component, we propose to acoustically induce data into water at the transmit side such that from the viewpoint of the receive end, spatial gradient of the acoustic pressure along the *x* axis becomes convolved with the data. This means modulating the data on the *x* component of acoustic particle velocity. To explain the proposed particle velocity modulation method, we use dipoles.

Consider two dipoles along *x* and *y* axes (Figure 5.1a), each composed of two closely spaced scalar transmitters. To modulate a signal or data stream s_1 on the *x*-dipole, we propose the poles A and B (Figure 5.1a) to transmit s_1 and $-s_1$, respectively. To understand why this proposed method modulates s_1 on the *x* particle velocity component, let h_{Aq} and h_{Bq} represent the acoustic pressure channel impulse responses between A and B and a scalar receiver q, respectively (Figure 5.1a). Therefore, the received signal can be written as superposition of convolution of s_1 and $-s_1$ with h_{Aq} and h_{Bq}, respectively, i.e., $r = h_{\mathrm{Aq}} \oplus s_1 + h_{\mathrm{Bq}} \oplus (-s_1) = (h_{\mathrm{Aq}} - h_{\mathrm{Bq}}) \oplus s_1$, where $\oplus$ is the convolution. On the other hand, $h_{\mathrm{q}}^{x} = \partial h_{\mathrm{oq}} / \partial x$ is the *x* particle velocity, i.e., the spatial gradient of h_{oq}, where h_{oq} is acoustic pressure channel impulse response between the point "o" (Figure 5.1a) and the scalar receiver q. Given the small spacing d_{AB} between A and B, finite difference

representation of the spatial gradient results in $h_{\mathrm{q}}^{x} = \partial h_{\mathrm{oq}} / \partial x \approx (h_{\mathrm{Aq}} - h_{\mathrm{Bq}}) / d_{\mathrm{AB}}$, i.e., h_{q}^{x} is proportional to $h_{\mathrm{Aq}} - h_{\mathrm{Bq}}$. By substituting this into the received signal equation we obtain $r = h_{\mathrm{q}}^{x} \oplus s_1$. This is a key result which demonstrates that upon using the proposed method, the signal or data stream s_1 is indeed modulated on the *x* particle velocity channel h_{q}^{x}. Similarly, a second signal or data stream s_2 can be simultaneously modulated on the *y* particle velocity channel h_{q}^{y}. As two examples of such underwater communication channels, h_5^{x} represents impulse response of an *x* particle velocity channel between a transmitting *x*-dipole and hydrophone number 5 of a receiving scalar array (Figure 5.1c), whereas h_1^{y} represents impulse response of a *y* particle velocity channel between a transmitting *y*-dipole and hydrophone number 1 of the same receiving scalar array (Figure 5.1c). Overall, the proposed idea means particle velocity multiplexing of two data streams, to double the data rate. Since the transmitter (Figure 5.1a) modulates data on *x* and *y* components of a vector quantity, i.e., the acoustic particle velocity, we call it a vector transmitter. In principle, a third dipole can be added along the *z* axis, to modulate a third signal or data stream s_3 on the *z* particle velocity, to triple the data rate. However, as explained later, we triple the data rate by devising a specific method that still uses the vector transmitter as is (Figure 5.1a), without adding a third dipole.

With the proposed vector transmitter composed of two dipoles (Figure 5.1a), we propose two-dipole and three-dipole vector receivers (Figure 5.1b), and an array of five spatially-separated hydrophone scalar receivers (Figure 5.1c) for comparison purposes (practical implementation of the vector transmitter using a ring device and the vector receivers using ring and sphere devices is discussed in the next paragraph). There are 10

particle velocity-based communication channels in each system (Figure 5.1b, 5.1c). To name all these channels originating from the vector transmitter, we use superscripts to indicate the transmitting dipoles, and subscripts to identify the receiving dipoles and scalar hydrophones (Figure 5.1b, 5.1c). For example, $h^{y}_{z,\text{sphere}}$ is the communication channel when a *y*-dipole transmits, and *z*-dipole of a sphere receives (Figure 5.1b).

To implement the proposed vector transmitter, we note that a dipole can be built using a ring with two electrodes [32]. To build the proposed vector transmitter having two dipoles (Figure 5.1a, 5.1b, 5.1c), we use a ring with four electrodes. Receivers include a similar ring (Figure 5.1d, right), which measures *x* and *y* particle velocity components, as well as a sphere [33] (Figure 5.1d, right), acting as a three-dipole receiver, measuring *x*, *y* and *z* particle velocity components. These two are our proposed and custom-made vector receivers. As a reference for comparison, we also use an array of spatially separated scalar receivers (Figure 5.1e, right), which are regular hydrophones that measure the acoustic pressure. Since the ring and sphere vector receivers (Figure 5.1d) provide 5 receiving channels, 5 hydrophones are considered in the scalar array receiver accordingly (Figure 5.1e). We use our custom-made vector and scalar devices (Figure 5.2) to implement Figure 5.1d and 5.1e system configurations in underwater experiments. An important advantage of a vector receiver such as a sphere (Figure 5.2) over an array of spatially separated scalar receivers is its compact size, as it measures multiple particle velocity components at a single point in space. This is particularly important for modern medium and small underwater platforms and modems.

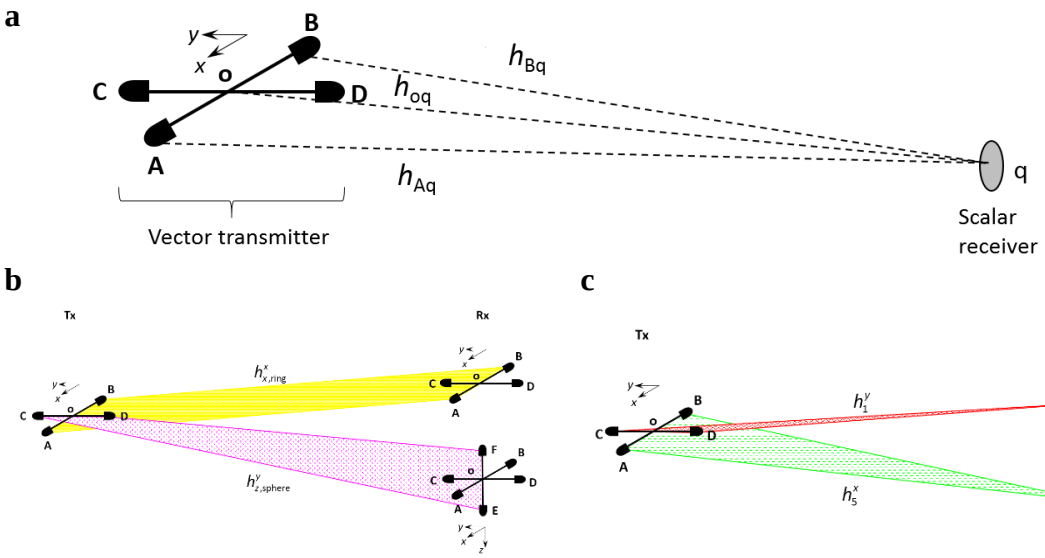

Figure 5.1 The proposed particle velocity double data multiplexing system for underwater acoustic communication via one vector transmitter and various number of vector or scalar receivers. **a,** Schematic representation of the proposed vector transmitter for particle velocity data multiplexing. There are two dipoles along the *x* and *y* axes. Since using the two dipoles and the method proposed in the main text, the transmitter modulates two data streams s_1 and s_2 on the *x* and *y* components of the acoustic particle velocity, a vector quantity, we call it a vector transmitter. This new transmitter doubles the transmission rate via data multiplexing. As demonstrated later, it can multiplex a third data stream s_3 to triple the transmission rate. **b,** Illustration of two out of ten vector particle velocity-related communication channels in the proposed fully-vector system. The system is composed of two transmitting dipoles (implemented using a ring device explained later), two receiving dipoles (implemented using another ring device) and three receiving dipoles (implemented using a sphere device explained later). This is a 2×5 system. As two out of ten fully-vector communication channels in the system, $h^x_{x,\mathrm{ring}}$ in yellow is the communication channel utilized when the *x*-dipole transmits and the *x*-dipole of the ring receives, whereas $h^y_{z,\mathrm{sphere}}$ in purple is the communication channel used when the *y*-dipole transmits and the *z*-dipole of the sphere receives. We have measured impulse responses of all these ten channels (Extended Data Figure 5.2). **c,** Illustration of two out of ten semi-vector particle velocity-related communication channels in the proposed semi-vector system. The system is composed of two transmitting dipoles (implemented using a ring device explained later), and five receiving scalar hydrophones. This is a 2×5 system. As two out of ten semi-vector communication channels in the system, h^x_5 in green is the communication channel used when the *x*-dipole transmits and hydrophone number 5 receives, whereas h^y_1 in red is the communication channel utilized when the *y*-dipole transmits and hydrophone number 1 receives. We have measured impulse responses of all these ten channels as well.

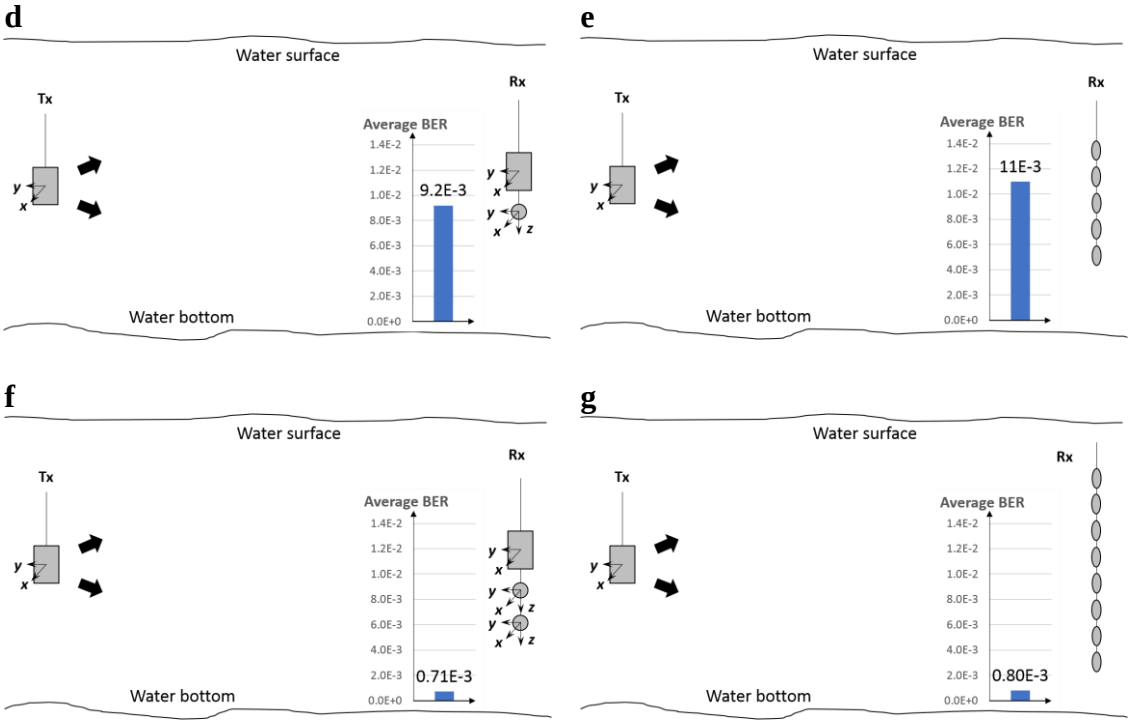

Figure 5.1 (continued) d, The proposed fully-vector underwater communication system implemented with one ring vector transmitter acting as two dipoles (Figure 5.1b, left), one ring vector receiver (two dipoles, Figure 5.1b, right) and one sphere vector receiver (three dipoles, Figure 5.1b, right), providing five receive channels in total. Two bold arrows represent simultaneous transmission of two data streams, therefore, this is a 2×5 system. The average bit error rate (BER) is obtained by averaging over five trials, and each trial includes transmission of fifty OFDM blocks per each data stream. **e,** The proposed semi-vector underwater communication system implemented with one ring vector transmitter acting as two dipoles (Figure 5.1c, left) and five hydrophone scalar receivers, a 2×5 system, considered for comparison. **f,** A fully-vector system with one ring vector transmitter, one ring vector receiver and two sphere vector receivers, providing eight receive channels (a 2×8 system). **g,** A semi-vector system with one ring vector transmitter and eight hydrophone scalar receivers, a 2×8 system, considered for comparison.

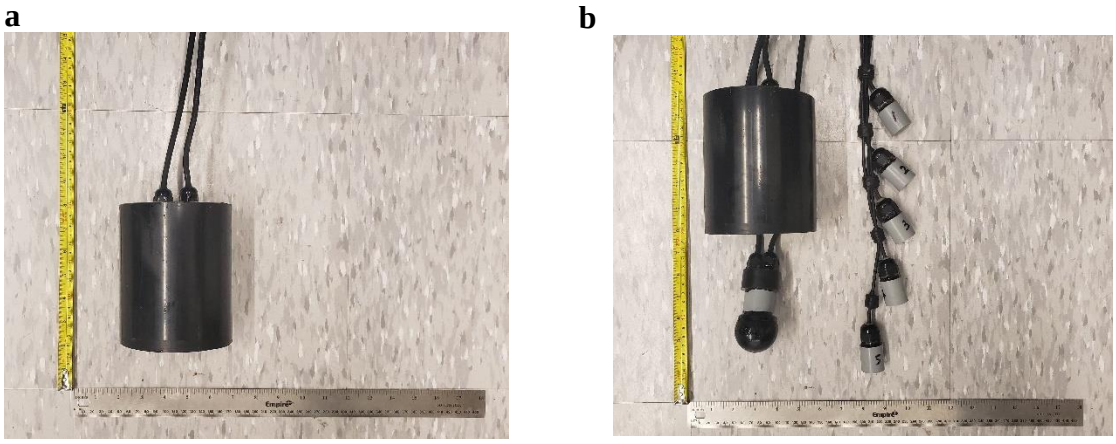

Figure 5.2 Custom-made vector and scalar devices to implement Figure 5.1d and 5.1e system configurations in underwater communication experiments. **a,** The ring vector transmitter to multiplex two or three data streams. **b,** A similar ring device used as the ring vector receiver, the sphere vector receiver, and the scalar array receiver composed of five hydrophones. By adding or removing some devices on the receive side, we implement other system configurations (Figure 5.1f, 5.1g, 5.7a, 5.7b, and 5.9) for various other underwater communication experiments.

5.2 Vector OFDM and FSK Systems Implementation

5.2.1 Vector OFDM System Implementation and Methods

The vector OFDM system implemented in sea experiments has several functional blocks (Figure 5.3). After coding each source binary data stream using a convolutional encoder, they are mapped to quadrature phase shift keying (QPSK) constellation points (other coding techniques and constellations can be used as well). Then pilot tones are added for channel estimation, followed by inverse fast Fourier transform (IFFT). The multi-channel digital-to-analog converter (DAC) converts the data to the analog OFDM signals $s_1(t)$ and $s_2(t)$ for double data multiplexing, or $s_1(t), s_2(t)$ and $s_3(t)$ for triple data multiplexing. Using the proposed particle velocity modulation methods presented earlier in this chapter, the OFDM signals are applied to the vector transmitter as follows: for double data multiplexing, $s_1(t)$ and $-s_1(t)$ are applied to the poles A and B (Extended Data Fig. 6, the

Vector Transmitter block), respectively, whereas $s_2(t)$ and $-s_2(t)$ are applied to the poles C and D, respectively; and for triple data multiplexing, $s_1(t)+s_3(t)$ and $-s_1(t)-s_3(t)$ are applied to the poles A and B, respectively, while $s_2(t)+s_3(t)$ and $-s_2(t)-s_3(t)$ are applied to the poles C and D, respectively.

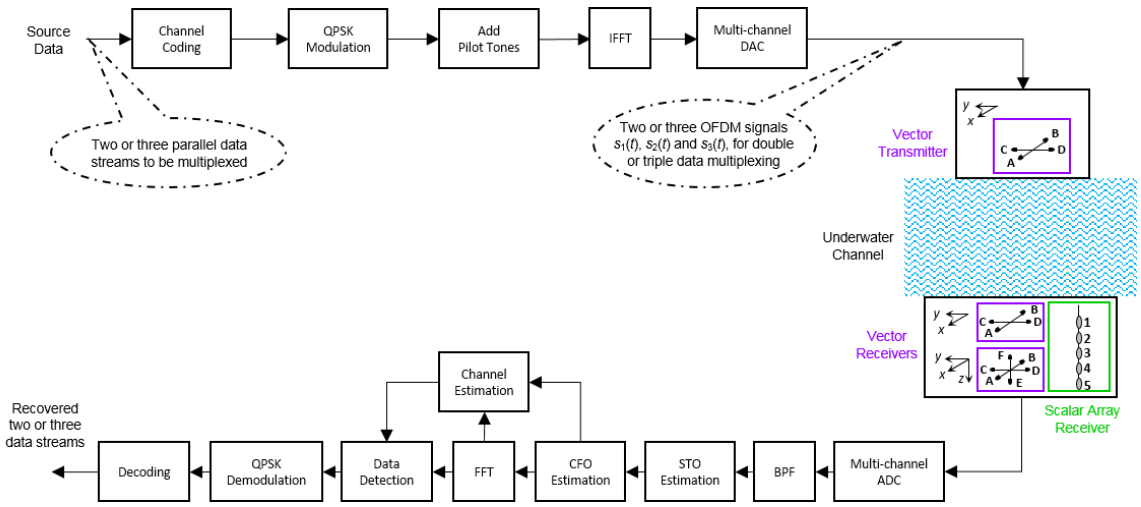

Figure 5.3 Block diagram of the implemented vector orthogonal frequency division multiplexing (OFDM) system in underwater communication experiments, for double or triple data multiplexing over a given bandwidth, using one vector transmitter. Abbreviations in some blocks are: QPSK (quadrature phase shift keying), IFFT (inverse fast Fourier transform), DAC (digital-to-analog converter), ADC (analog-to-digital converter), BPF (bandpass filter), STO (symbol timing offset), and CFO (carrier frequency offset). The vector transmitter and receivers and the scalar array receiver correspond to Figure 5.1b and 5.1c.

The signals received by vector receivers and a scalar array of one wavelength λ-spaced hydrophones are collected by a multi-channel analog-to-digital converter (ADC), followed by bandpass filter (BPF) to remove out-of-band noise. To estimate symbol timing offset (STO), we use a filter matched to the chirp signal included at the beginning of each transmitted frame that consists of fifty OFDM blocks. Carrier frequency offset (CFO) and channel responses are estimated using null and pilot tones, respectively [6]. After

performing fast Fourier transform (FFT), data on OFDM tones are detected using the minimum mean square error (MMSE) method [34], and then converted back to binary data streams using the QPSK demodulator, followed by the Viterbi decoding algorithm.

OFDM parameters of the system are 1024 tones (subcarriers) over the bandwidth from 18.4 kHz to 22.4 kHz, which include 256 pilot tones for channel estimation and 96 null tones for noise power estimation and CFO estimation. Each transmission trial (frame) contains 50 OFDM blocks, each OFDM block length is 256 ms, with 25 ms guard time intervals between each two consecutive OFDM blocks in one frame.

5.2.2 Vector Non-Coherent FSK System Implementation and Methods

To demonstrate the feasibility of particle velocity data multiplexing using one vector transmitter and FSK signaling, we transmit two 4FSK-modulated data streams $s_1(t)$ and $s_2(t)$, one transmitted from the A-B dipole and the other from the C-D dipole (Figure 5.4). To implement this two-channel vector transmitter, we use a ring device. Using another ring device as a two-channel vector receiver, we obtain two signals $r_x(t)$ and $r_y(t)$ (Figure 5.4). To benefit from this multi-channel signal reception, we use non-coherent equal gain combing [26]. To address channel frequency selectivity, we use frequency hopping, by dividing our 18.4 - 22.4 kHz bandwidth to several hopping groups.

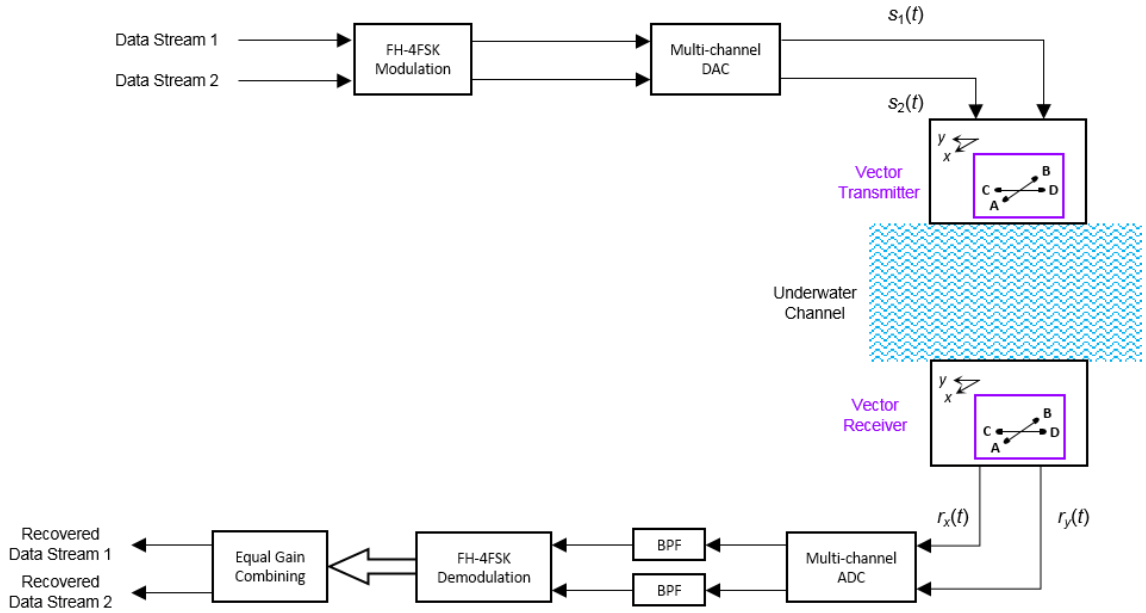

Figure 5.4 Block diagram of one implemented vector frequency shift keying (FSK) system in underwater communication experiments, for double data multiplexing over a given bandwidth, using one vector transmitter. Abbreviations in some blocks are: FH (frequency hopping), DAC (digital-to-analog converter), ADC (analog-to-digital converter), and BPF (bandpass filter). The vector transmitter and receiver are two transmit dipoles and two receive dipoles, respectively.

5.3 Vector OFDM and FSK Systems Ocean Test Results

5.3.1 Vector OFDM System Ocean Test Results

Using orthogonal frequency division multiplexing (OFDM) pilot tones and a least squares technique (see Section 5.2.1), we measured impulse responses (Figure 5.5) of all the ten vector particle velocity-based communication channels in the proposed fully-vector system (Figure 5.1d), from 18.4 kHz to 22.4 kHz. Experiments were conducted in late September of 2018, in shallow waters off Woods Hole, MA. The single vector transmitter and the receivers were placed 15 m below the water surface, with the receivers maintained at one location. For the transmitter location we examined various distances from the receivers. Since our power amplifiers were not strong enough, the longest range for coherent

communication turned out to be about 26 m. At this range, average signal-to-noise ratios (SNRs) were below 9 dB, and sometimes were as low as about 6 dB. However, still we could demodulate the data, to demonstrate the feasibility of particle velocity data multiplexing using one vector transmitter. Later in this chapter we show that at a longer range of 65 m and with about 1 dB SNR, particle velocity data multiplexing is feasible using power-efficient non-coherent frequency shift keying (FSK) modulation.

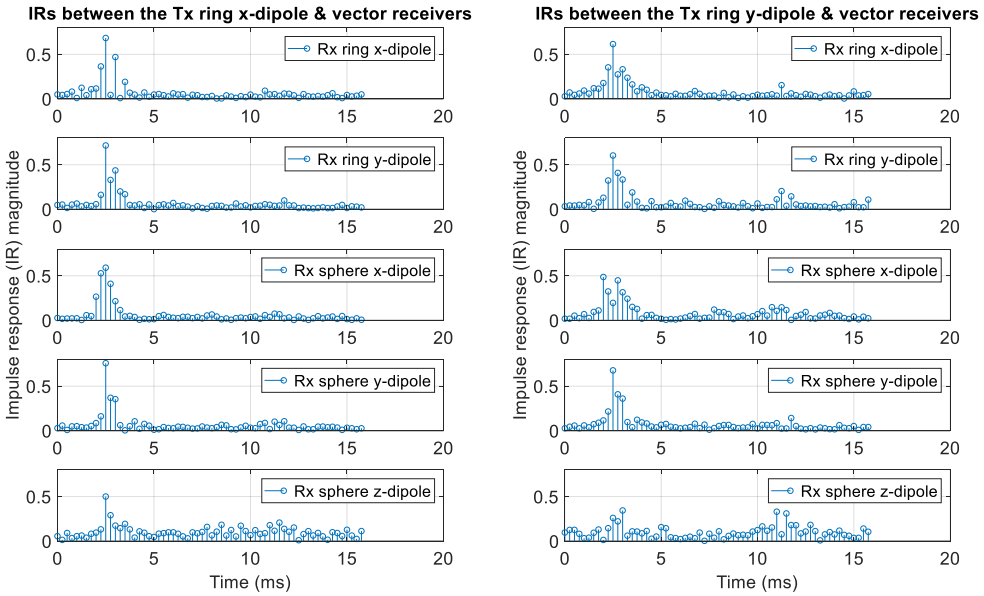

Figure 5.5 Magnitudes of measured impulse responses of all the ten vector particle velocity-related communication channels in the proposed fully-vector system (Figure 5.1d), over one OFDM block. In the system we have one ring vector transmitter, one ring vector receiver and one sphere vector receiver. Tx and Rx in the above figures stand for transmitter and receiver, respectively. The Tx ring has two dipoles, *x*-dipole and *y*-dipole, the Rx ring similarly has two dipoles, *x*-dipole and *y*-dipole, and the Rx sphere has three dipoles, *x*-dipole, *y*-dipole and *z*-dipole. Figures in the left column are measured impulse response (IR) magnitudes of the channels between the Tx ring *x*-dipole and the dipoles of the Rx ring and Rx sphere, whereas figures in the right column are measured IR magnitudes of the channels between the Tx ring *y*-dipole and the dipoles of the Rx ring and Rx sphere.

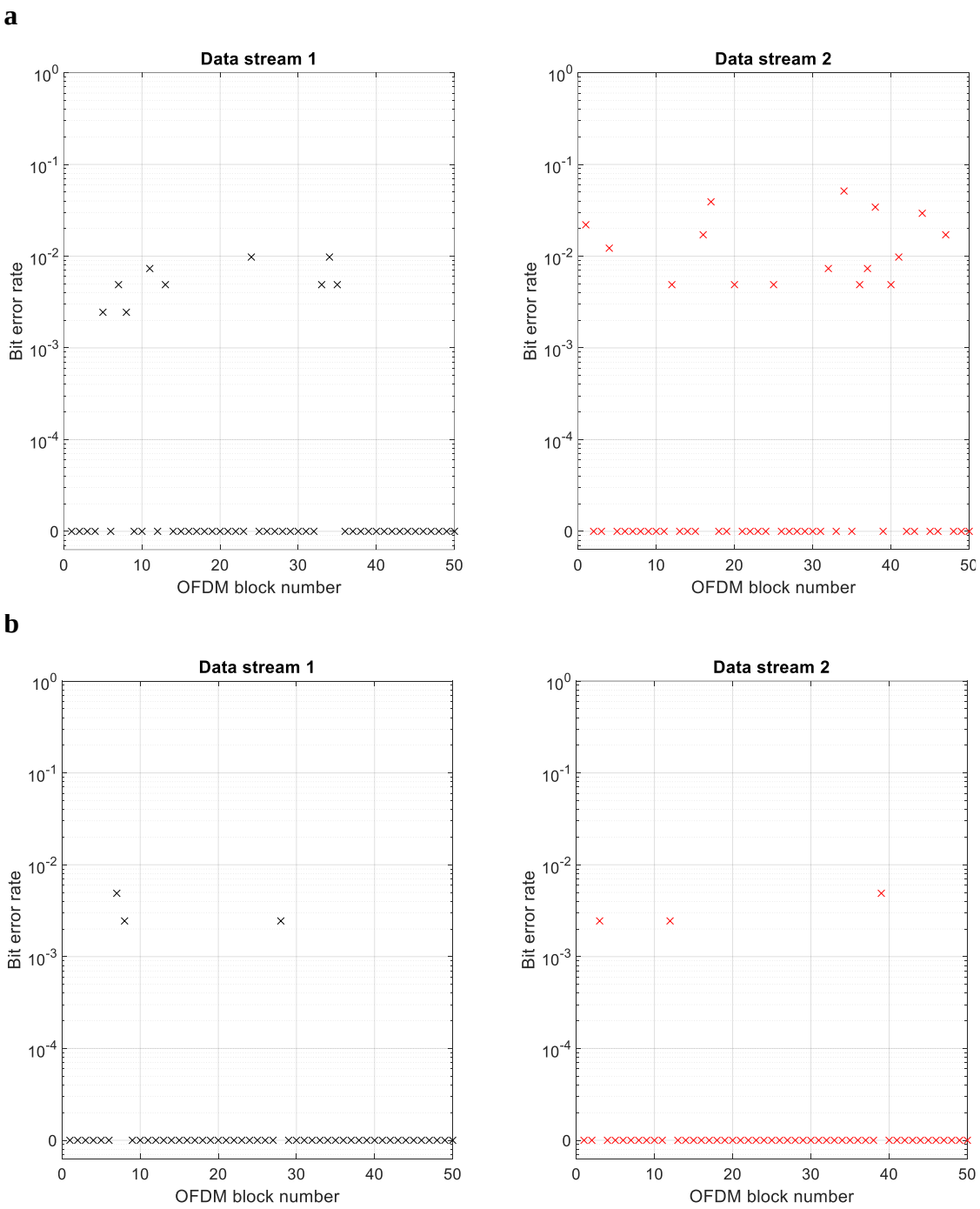

Figure 5.6 Bit error rates (BERs) of OFDM blocks in two data streams multiplexed by the vector transmitter in the proposed fully-vector system with different number of vector receivers (Figure 5.1d and Figure 5.1f). a, BERs with one ring vector receiver and one sphere vector receiver, providing five receive channels (the 2×5 system in Figure 5.1d). b, BERs with one ring vector receiver and two sphere vector receivers, providing eight receive channels (the 2×8 system in Figure 5.1f). We observe that by using one additional vector receiver, many more OFDM blocks are demodulated with zero BER.

The implemented system utilizes OFDM with minimum mean square error (MMSE) detection (see Section 5.2.1). Average bit error rate (BER) of the 2×5 fully-vector system is 9.2E-3 (Figure 5.1d), obtained by averaging over five trials, and each trial includes transmission of fifty OFDM blocks per each of the two data streams. The average SNR is 7.5 dB. As a reference, average BER of the 2×5 semi-vector system is 11E-3 (Figure 5.1e), with an average SNR of 8.9 dB. With slightly better performance, key advantage of the vector receiver is its compact size, as it does not use an array of spatially separated scalar receivers. Nevertheless, both systems demonstrate the feasibility of demodulating two data streams, multiplexed and transmitted by one vector transmitter over the same bandwidth. Since typically more receivers are needed to decrease BER [6, 35], we add a three-channel sphere vector receiver (Figure 5.1f), which reduces the average BER by about an order of magnitude, from 9.2E-3 to 0.71E-3. This comes from having more OFDM blocks demodulated with zero BER (Figure 5.6). Similarly, by adding three hydrophone scalar receivers (Figure 5.1g), the average BER decreases by about an order of magnitude, from 11E-3 to 0.8E-3. This BER reduction again shows the developed vector transmitter can work with both vector and scalar receivers. To study the effect of higher SNRs, and since our power amplifiers were not strong enough, we had to reduce the range in some experiments, to increase SNR. In the 2×5 fully-vector system (Figure 5.1d), average SNR is increased from 7.5 dB at the original longer range to 18 dB at 9 m, resulting in a two order of magnitude BER reduction from 9.2E-3 to 0.07E-3.

With the increased SNR at the shorter range, now we can examine the system performance with smaller number of receive channels. With a three-channel sphere vector receiver, the 2×3 system (Figure 5.7a) exhibits an average BER of 0.039E-3. This is

obtained using a maximum likelihood (ML) detector, as the MMSE detector provides a higher BER due to the small number of receive channels, which is three here. A sphere decoder can be used instead, which offers near ML performance, with less computational complexity [36]. To see how far we can go in terms of reducing the number of receive channels, now we use a ring receiver. With a two-channel ring vector receiver, the 2×2 system (Figure 5.7b) provides an average BER of 0.23E-3. Comparison of some typically observed OFDM blocks BERs for the 2×3 and 2×2 fully-vector systems (Figure 5.8) reveals that the ring vector receiver exhibits few more OFDM blocks with non-zero BERs than the sphere vector receiver.

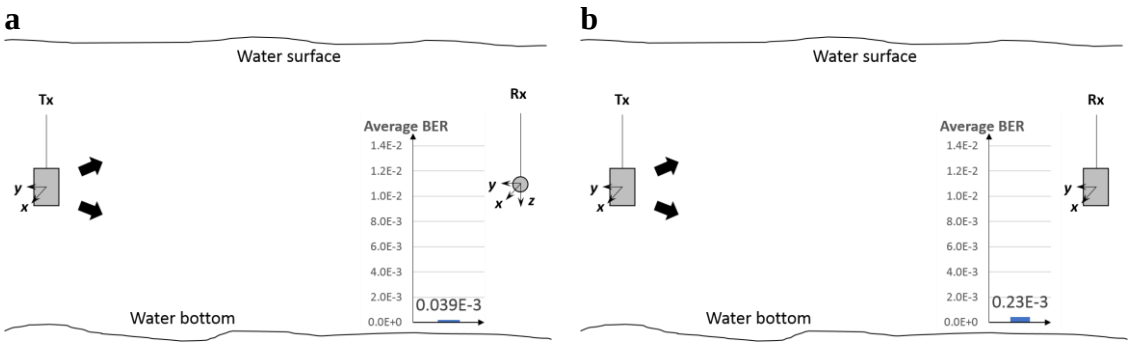

Figure 5.7 The proposed particle velocity *double* data multiplexing system for underwater acoustic communication via one vector transmitter and a three-channel or two-channel vector receiver. **a**, A fully-vector underwater communication system with one ring vector transmitter and one sphere vector receiver, providing three receive channels. Two bold arrows represent simultaneous transmission of two data streams; therefore, this is a 2×3 system. The average bit error rate (BER) is obtained by averaging over five trials, and each trial includes transmission of fifty OFDM blocks per each data stream. **b**, A fully-vector underwater communication system with one ring vector transmitter and one ring vector receiver, providing two receive channels, a 2×2 system.

To multiplex and transmit three signals or data streams s_1, s_2 and s_3 from the same vector transmitter (Figure 5.1a), to triple the data rate, we propose to modulate them on the *x* and *y* components of acoustic particle velocity as follows: the poles A and B (Figure 5.1a) transmit $s_1 + s_3$ and $-s_1 - s_3$, respectively, and the poles C and D (Figure 5.1a) transmit

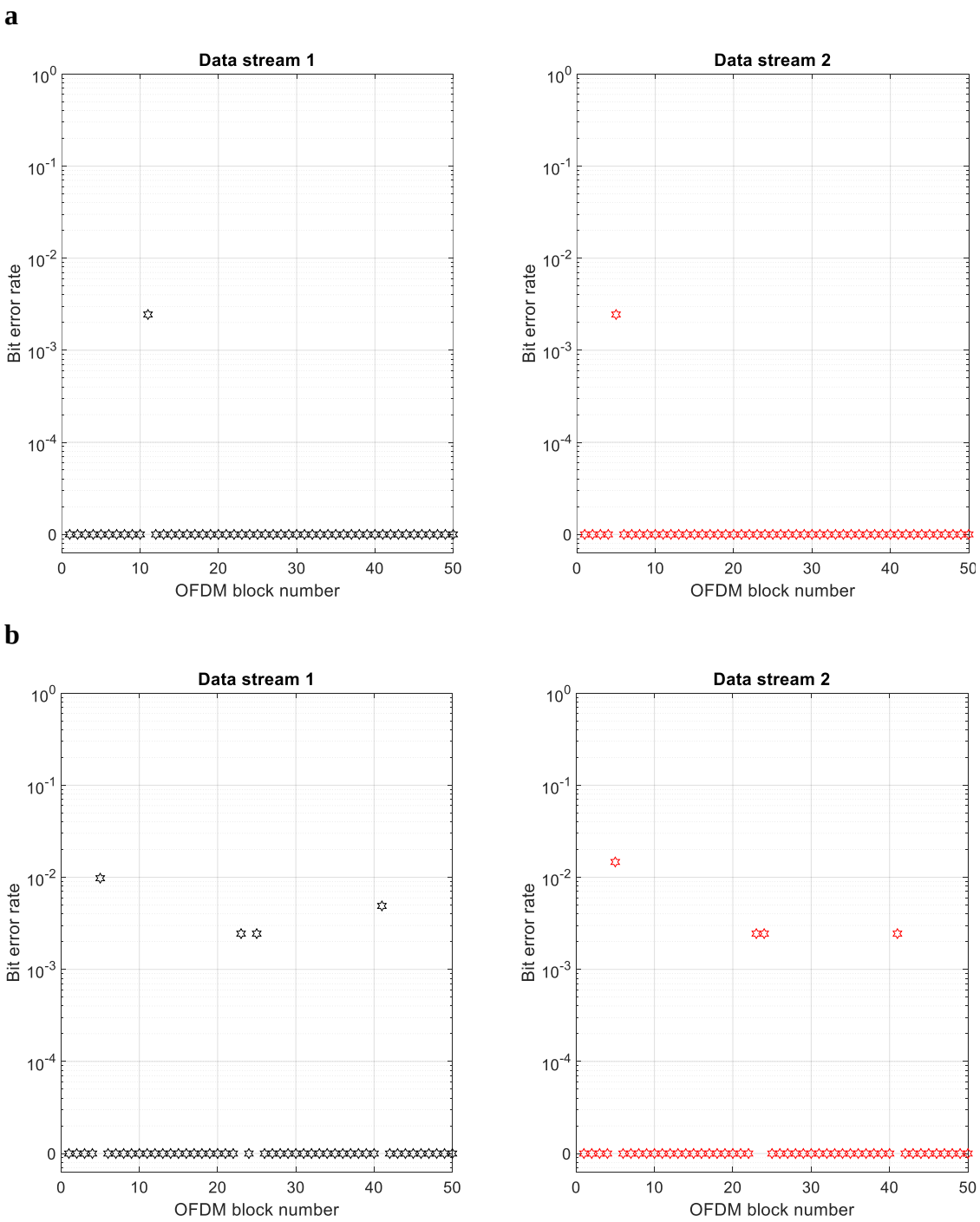

Figure5.8 Bit error rates (BERs) of OFDM blocks in two data streams multiplexed by the vector transmitter in the proposed fully-vector system with a three-channel or two-channel vector receiver (Figure 5.7a and Figure 5.7b). **a,** BERs with one sphere vector receiver, providing three receive channels (the 2×3 system in Figure 5.7a). **b,** BERs with one ring vector receiver, providing two receive channels (the 2×2 system in Figure 5.7b). We observe few more OFDM blocks with non-zero BERs, when using a vector receiver with a smaller number of channels.

$s_2 + s_3$ and $-s_2 - s_3$, respectively. The rationale behind this modulation method is that we envision a third dipole whose first pole is composed of A and C, and its second pole consists of B and D. This third dipole allows to modulate the extra signal or data stream s_3, in addition to s_1 and s_2. To implement the method, we present a system (Figure 5.9) which consists of one vector transmitter and three vector receivers. The average BER of this system is 0.2E-3, obtained using an ML detector. Examination of some typically observed OFDM blocks BERs for the three multiplexed data streams (Figure 5.10) demonstrates that most of the OFDM blocks are demodulated with no error. Motivated by the specific way we modulate s_3 together with s_1 and s_2, we have also developed a computationally inexpensive successive interference cancellation algorithm combined with MMSE detection, which offers a trade-off between system performance and complexity (data not shown), a matter of interest in some applications. Another option is a computationally inexpensive near-ML sphere decoding detection algorithm [36].

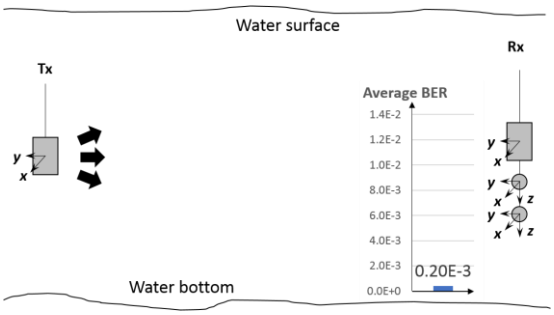

Figure 5.9 The proposed particle velocity *triple* data multiplexing system for underwater acoustic communication via one vector transmitter and an eight-channel vector receiver. A fully-vector underwater communication system with one ring vector transmitter, one ring vector receiver and two sphere vector receivers, providing eight receive channels. Three bold arrows represent simultaneous transmission of three data streams (triple data multiplexing), therefore, this is a 3×8 system. The average bit error rate (BER) is obtained by averaging over five trials, and each trial includes transmission of fifty OFDM blocks per each data stream.

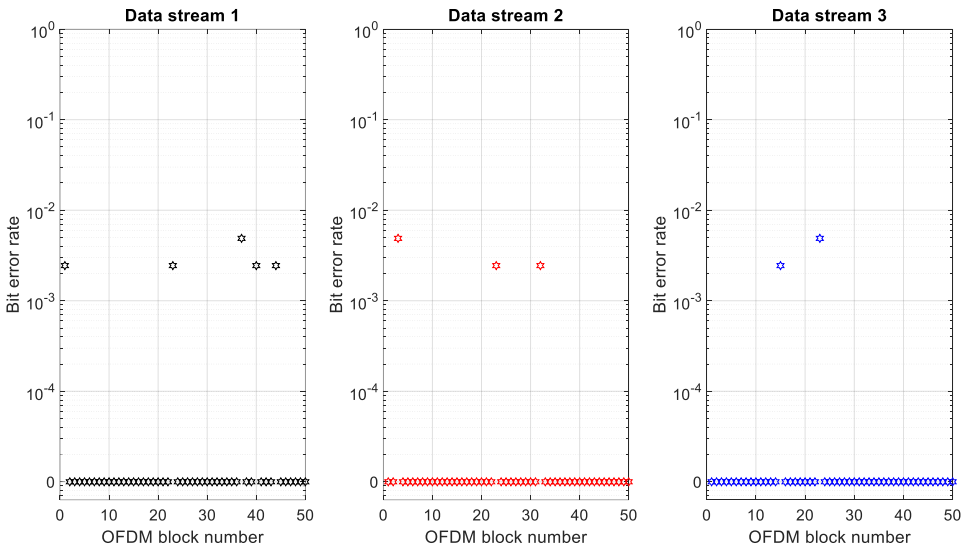

Figure 5.10 Bit error rates (BERs) of OFDM blocks in three data streams multiplexed by the proposed vector transmitter and demodulated by an eight-channel vector receiver (Figure 5.9). BERs with one ring vector transmitter, one ring vector receiver and two sphere vector receivers, providing eight receive channels (the 3×8 system in Figure 5.9). Most of the OFDM blocks are demodulated with zero BER.

5.3.2 Vector FSK System Ocean Test Results

The experimental results provided in previous subsection are obtained using coherent OFDM signaling and demodulation. This subsection presents experimental results that demonstrate the feasibility of particle velocity data multiplexing using one vector transmitter, together with non-coherent FSK signaling and demodulation. The implemented vector non-coherent FSK system (see Section 5.2.2) includes one ring vector transmitter to multiplex two data streams, and a similar two-channel ring vector receiver. With no channel coding in the feasibility study, average BER is 1.65E-02, obtained by averaging over five trials, and each trial includes transmission of 900 bits per each of the two data streams. The average SNR is 1.2 dB.

5.4 Conclusion

In summary, physics-based communication concepts for multiplexing multiple data streams over the same bandwidth to increase data rates, using underwater acoustic particle velocity field components, are introduced and verified through experiments.

CHAPTER 6

DATA MULTIPPLEXING IN DRILL STRINGS OF OIL AND GAS WELLS USING MULTIPLE ACTUATORS

Other than underwater communication, acoustic transmission is a viable and useful in applications such as oil and gas wells operations. In this chapter, using multiple actuators is proposed, to transmit several data streams simultaneously over the same bandwidth, and then separate and demodulate them at the receive side. This allows for data rate increase and optimal utilization of the small available bandwidth. In fact, using two actuators on a drill string testbed, it can be shown that data rate can doubled, by transmitting two data streams simultaneously, without increasing the bandwidth. While two piezoelectric actuators are used here, one can use magnetostrictive actuators [23, 24, 37] as well.

The rest of this chapter is organized as follows. The experimental testbed is explained in Section 6.1. Channel measurements and communication test results are presented in Sections 6.2 and 6.3, respectively. Section 6.4 provides some concluding remarks.

6.1 The Experimental Testbed

The drill string testbed shown in Figure 6.1a is composed of two steel pipes connected using a coupling. Length and diameter of each pipe are about 1.5 m and 10 cm, respectively, whereas length of the coupling is about 9 cm. The two transmitters are piezoelectric transducers shown in Figure 6.1a. Receivers are shown in Figure 6.1b and include one strain sensor, PCB model 740B02, and one triaxial accelerometer, PCB model 356B21. These two sensors are needed to separate and demodulate the two data streams sent out

simultaneously by the two transmitters, to double the transmission rate. The strain sensor measures fractional particle displacement along the drill pipe x axis [23], whereas the triaxial accelerometer measures particle accelerations along x, y and z axes [23]. The strain sensor is used because of the smaller delay spread and therefore less frequency selective behavior of strain channels [24], which can improve data detection and reduce bit error rate. The triaxial accelerometer is used to explore performance of the three orthogonal acceleration channels for data detection. Frequency responses and impulse responses of all these channels are measured and studied in the next section. A schematic drawing of the entire testbed is provided in Figure 6.1c.

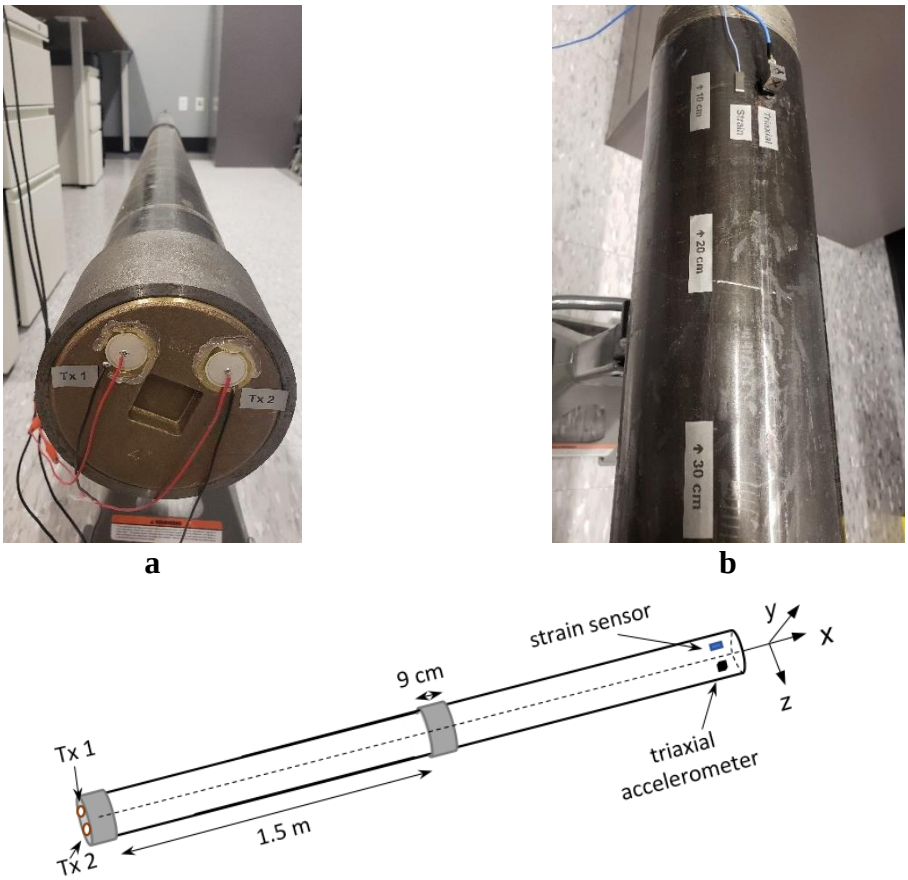

Figure 6.1 The drill string testbed: **a**, Two piezoelectric transmitters labeled as Tx 1 and Tx 2; **b**, Two receiver sensors, including one strain sensor labeled as Strain, and one triaxial accelerometer labeled as Triaxial; **c**, Schematic drawing of the testbed.

6.2 Experimental Results on Channel Measurements

Orthogonal frequency division multiplexing (OFDM) is used for signal transmission. Each actuator has transmitted from 2 to 6 kHz, using 1024 subcarriers, including 128 pilot tones for channel estimation and 96 null tones for noise power estimation. Each OFDM symbol duration is 256 ms, with 25 ms guard time interval in between. A least squares method is used for channel estimation [31], whereas for data detection a hard minimum mean squared error (MMSE) algorithm is used (see the Appendix B). The used modulation and coding are quadrature phase shift keying (QPSK) and convolutional coding.

Magnitudes of frequency responses of the channels measured by the receiving sensors in Figure 6.1b are presented in Figure 6.2. One can observe that the strain channel has a nearly flat frequency response, whereas the acceleration channels frequency responses exhibit more frequency selectivity. The unequal strain and acceleration magnitudes in Figure 6.2 can be attributed to different sensor sensitivities: 50 milliVolt/με for the strain sensor and 10 milliVolt/*g* for each channel of the triaxial accelerometer [23]. Here με represents the strain magnitude unit in micro fractional particle displacement, whereas g = 9.8 m/sec^2 is the gravity acceleration, used as the unit for particle acceleration magnitude. A method is discussed in [23] to scale readouts of the strain and acceleration sensors according to their sensor sensitivities, such that strain and acceleration signals magnitudes can be compared using the same unit. Here, for simplicity we use sensors readouts as they are, for demodulating and detecting the transmitted data.

To better understand the less frequency selective behavior of the strain channel compared to the acceleration channels, these channels are examined in time domain as well, by looking at their inverse Fourier transforms. Magnitudes of impulse responses of

the channels measured by the receiving sensors in Figure 6.1b are presented in Figure 6.3. It is noteworthy that the strain channel impulse response has a shorter duration, compared to the acceleration channels which have longer durations, behaviors that are also observed in [23, 24]. Given the properties of Fourier transform, the short duration of the strain impulse response corroborates the relatively flat strain frequency response.

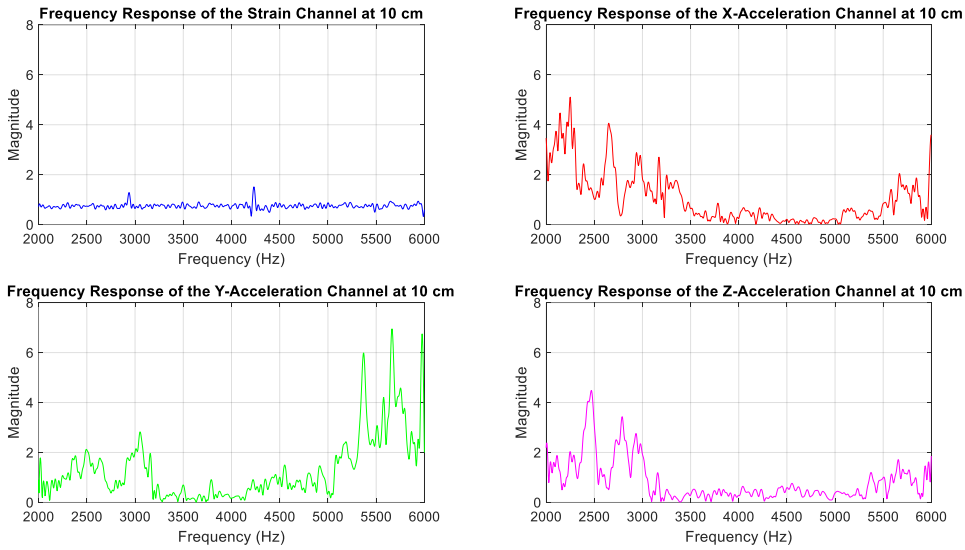

Figure 6.2 Magnitudes of frequency responses of channels measured by the receiving sensors in Figure 6.1b.

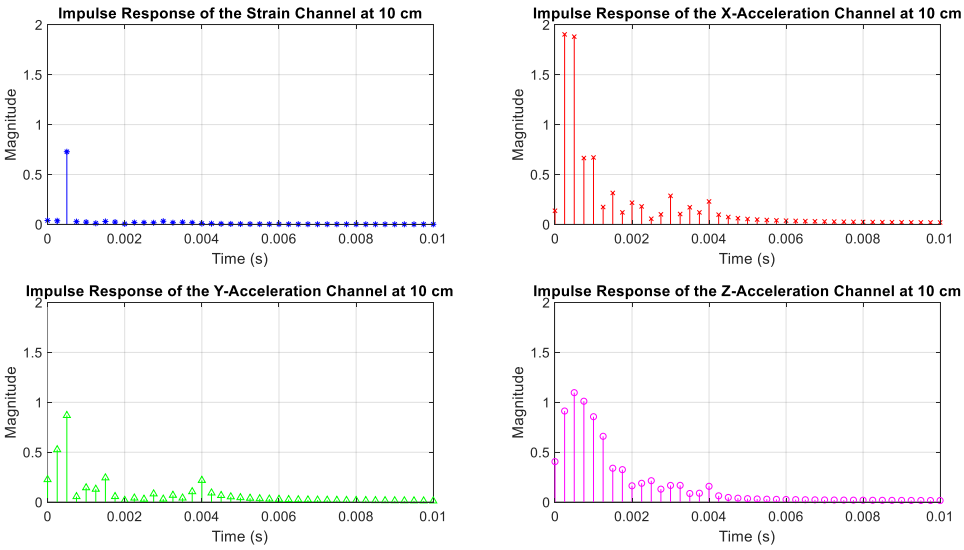

Figure 6.3 Magnitudes of impulse responses of the channels measured by the receiving sensors in Figure 6.1b.

6.3 Experimental Results on Communication and Data Detection

In this section, first we present communication results on one actuator transmitting one data stream. These will serve as some benchmarks. Then we provide communication results on two actuators transmitting two data streams simultaneously, to double the transmission rate over the same bandwidth.

6.3.1 One Actuator Transmitting One Data Stream

In this section, we consider experiments where Tx 1 in Figure 6.1a has transmitted, over the bandwidth of 2 to 6 kHz, fifty OFDM symbols in a row, repeated five times to have multiple trials. With the same transmit power per actuator throughout the entire chapter and in all the experiments, measured bit error rates (BERs), i.e., bit error probabilities, for various receiving sensors at different positions identified in Figure 6.1b are presented in Figure 6.4. For each sensor at each position, five BERs and their average are provided, obtained from five trails. We observe that quite often BERs of the strain sensor receiver are smaller than BERs of the accelerometer receivers.

The signal-to-noise ratio (SNR) for each BER data point of Figure 6.4 and their average over five trials are provide in Figure 6.5. The SNR reported throughout this chapter is obtained by calculating the ratio of the power of pilot sub-carriers to the power of null sub-carriers [31]. In most cases, we observe that SNRs of the strain sensor receiver are smaller than SNRs of the accelerometer receivers. This can be attributed to the sensitivity of the particular strain sensor we have used, which produces weaker signals compared to the accelerometer signals, as discussed in the previous section.

Smaller BERs of the strain sensor receiver, while having smaller SNRs, can be related to the relatively flat strain channel frequency response in Figure 6.2. This makes

equalization and data detection simpler and more accurate, compared to the non-flat and frequency selective behavior of the acceleration channels frequency responses in Figure 6.2.

To better understand the data presented in Figures 6.4 and 6.5, their measurement results averaged over five different receiver positions are listed in Table 6.1. It is observed that the BER of the strain sensor receiver is smaller than the BERs of the accelerometer receivers. This can be attributed to the relatively flat strain channel frequency response in Figure 6.2, which renders equalization and data detection more accurate, compared to the frequency selective and non-flat acceleration channels frequency responses in Figure 6.2. Smaller SNR of the strain sensor receiver can be related to the sensitivity of the specific strain sensor used in the experiments, which produces signals weaker than the accelerometer signals, as mentioned in Section 6.2.

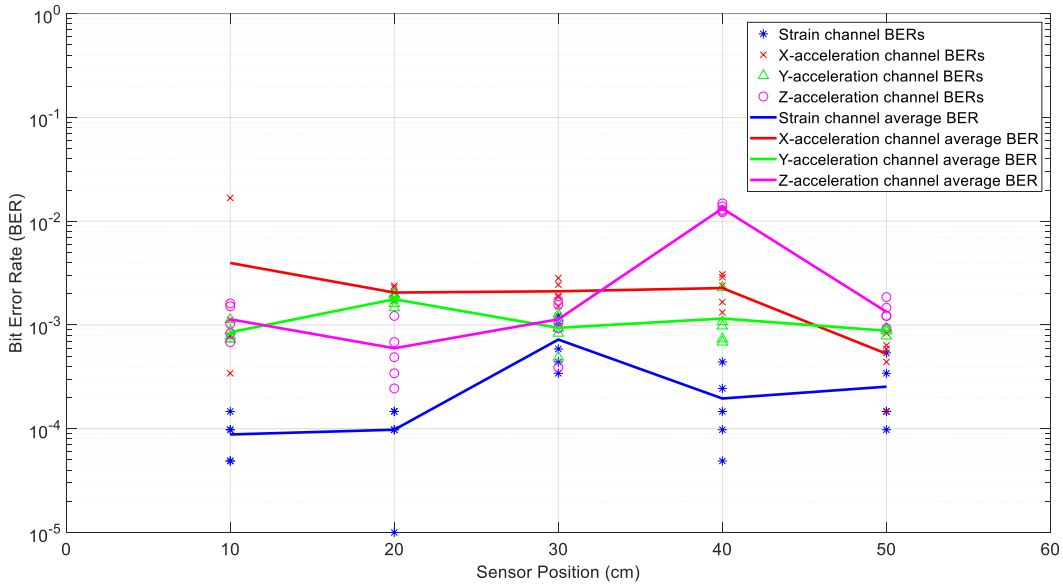

Figure 6.4 Bit error rates of various receiving sensors at different positions, with one actuator transmitting one data stream. The receivers are a strain sensor and a triaxial accelerometer with x, y and z channels. The piecewise linear graphs represent average BERs of each sensor versus the sensor position.

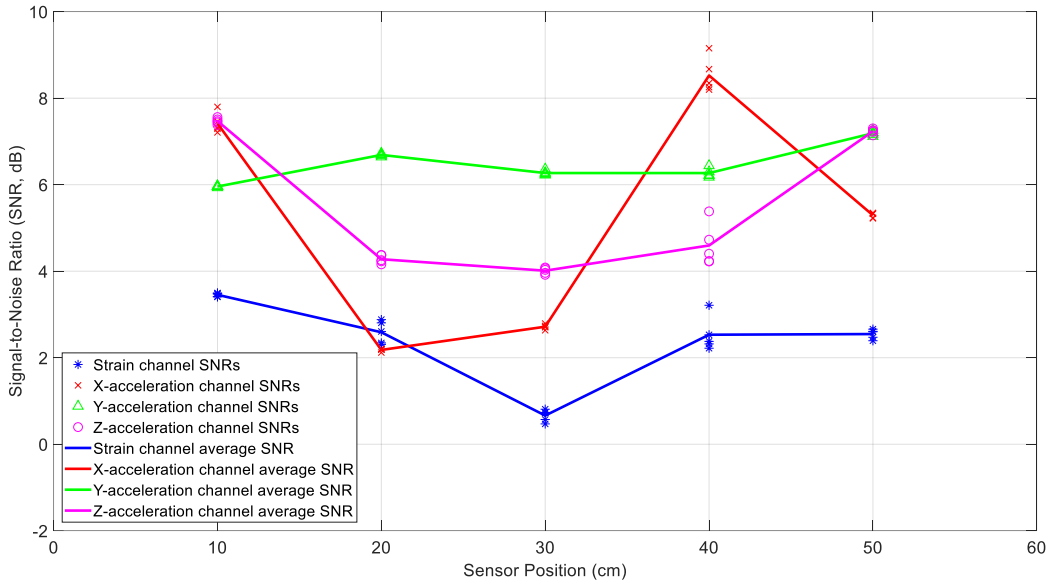

Figure 6.5 Signal-to-noise ratios of various receiving sensors at different positions, with one actuator transmitting one data stream. The receivers are a strain sensor and a triaxial accelerometer with x, y and z channels. The piecewise linear graphs represent average SNRs of each sensor versus the sensor position.

Table 6.1 Average BERs and SNRs of Various Receiving Sensors, with One Actuator Transmitting One Data Stream

Receiving Sensor	BER	SNR (dB)
Strain	2.7E-04	2.4
X-Acceleration	2.2E-03	5.2
Y-Acceleration	1.1E-03	6.5
Z-Acceleration	3.5E-03	5.5

6.3.2 Two Actuators Simultaneously Transmitting Two Data Streams

Here we consider experiments where Tx 1 and Tx 2 in Figure 6.1a have both transmitted simultaneously and with the same power, two different sets of data, over the same bandwidth of 2 to 6 kHz. More specifically, each actuator has transmitted fifty OFDM symbols in a row, repeated five times to have multiple trials. This simultaneous transmission of two data streams doubles the transmission rate, without any bandwidth increase. To separate and demodulate the two data streams at the receive side, we use two

receiving sensors: the strain sensor and the triaxial accelerometer. Since the latter has the three x, y and z acceleration channels, there are six possible receiver configurations using two channels: strain and x-acceleration, strain and y-acceleration, strain and z-acceleration, x-acceleration and y-acceleration, x-acceleration and z-acceleration, and y-acceleration and z-acceleration. Details of the data separation and detection method are discussed in the Appendix B. Measured BERs and SNRs for these six receivers at different positions identified in Figure 6.1b are presented in Figures 6.6 to 6.11, respectively. For each receiver at each position, five BERs, five SNRs and their averages for each of the first and the second data streams are provided, obtained from five trails.

To compare performance of these six 2×2 systems with two transmitting actuators and a two-channel receiver, we consider the best performance of the one actuator system of the previous subsection as a benchmark. According to Figure 6.4, lowest average BERs are below 10^{-3} for the system with the strain receiver, for average SNRs less than 4 dB at various receiver positions. Based on Figure 6.7 and compared to this benchmark, the two-actuator system using the strain and the y - acceleration receivers offers the best performance among the six two-actuator systems. This is because in all the receiver positions its average BERs are less than 10^{-3}, with average SNRs close to or less than 4 dB. The second best two-actuator system appears to be the one which utilizes the strain and the x - acceleration receivers, whose BERs and SNRs are shown in Figure 6.6.

It is noteworthy that average BERs of the two-actuator systems that do not use the strain sensor receiver are all greater than 10^{-3} at all positions, for average SNRs ranging from 1.5 to 9 dB (see Figures 6.9 to 6.11). As discussed in the previous section, this can be related to the relatively flat strain channel frequency response, which makes equalization

and data detection simpler and more accurate, compared to the non-flat and frequency-selective behavior of the acceleration channels.

To better comprehend the data presented in Figures 6.6 to Figure 6.11, their measurement results averaged over five different receiver positions and over two data streams are provided in Table 6.2. It was observed that when the strain sensor was one of the receivers, the BER tended to be smaller. This held true even for strain and z-acceleration in Table 6.2, if the abnormally high BERs in Figure 6.8 for this receiver pair at 40 cm were not included in the average, which updated the BER and SNR for this receiver pair in Table 6.2 to 2.6E-04 and 3.4 dB, respectively. Overall, these smaller BERs can be attributed to the relatively flat strain channel frequency response, which made data recovery and equalization simpler and more effective, compared to the acceleration channels which were non-flat and more frequency selective.

Table 6.2 Average BERs and SNRs of Various Receiving Sensor Pairs, with Two Actuators Simultaneously Transmitting Two Data Streams

Receiving Sensor Pair	BER	SNR (dB)
Strain and X-Acceleration	7.1E-04	3.0
Strain and Y-Acceleration	2.9E-04	3.1
Strain and Z-Acceleration	1.3E-02	3.6
X- and Y-Acceleration	3.1E-02	4.3
X- and Z-Acceleration	4.5E-02	4.7
Y- and Z-Acceleration	3.6E-02	4.9

6.4 Conclusions

In this chapter it is demonstrated that using two actuators, one can transmit two data sets simultaneously through drill strings and pipes, to double the transmission rate in such communication media. Experimental bit error probability performance of the proposed two-actuator new system on a testbed is shown to be about the same as a system that uses

only one actuator, which therefore can offer only half of the data rate of the new system. Upon using more actuators, one can increase the data rate further. For example, three actuators can triple the data rate.

Although only a two-channel receiver is proposed and used in this chapter to separate and demodulate data of the two actuators, one can use more receiving channels and sensors to improve the system performance. The benefit of having a multi-channel receiver with one actuator is discussed in [23, 37].

In this chapter, various combinations of strain and acceleration sensors are considered at the receive side. Due to some properties of strain channels such as smaller delay spreads [24] and their less frequency-selective behavior presented here, it appears that a strain sensor receiver and an accelerometer receiver together can offer a good performance, when separating and demodulating the two data streams transmitted simultaneously by the two actuators.

While not discussed here, one can use the additional actuators to induce redundancy at the transmit side to reduce bit error probability, using space-time codes, space-frequency codes, etc.

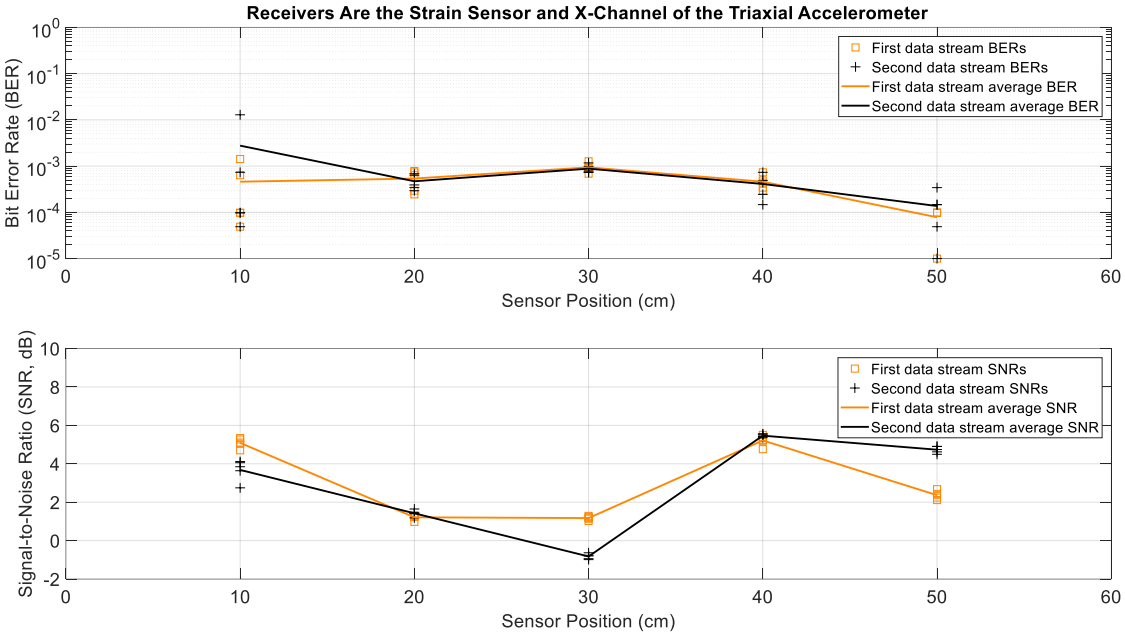

Figure 6.6 BERs (top) and SNRs (bottom) at different receiver positions, with two actuators transmitting two data streams simultaneously. The receivers are a strain sensor and x-channel of a triaxial accelerometer. The piecewise linear graphs represent average BERs and SNRs for each of the two data streams versus the receiver position.

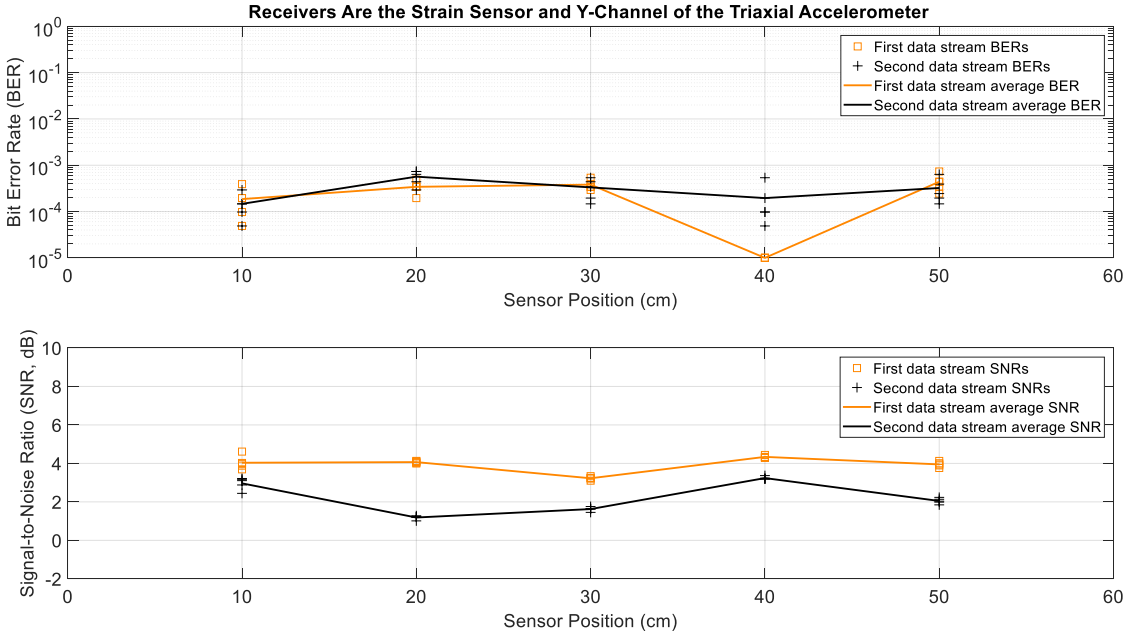

Figure 6.7 BERs (top) and SNRs (bottom) at different receiver positions, with two actuators transmitting two data streams simultaneously. The receivers are a strain sensor and y-channel of a triaxial accelerometer. The piecewise linear graphs represent average BERs and SNRs for each of the two data streams versus the receiver position.

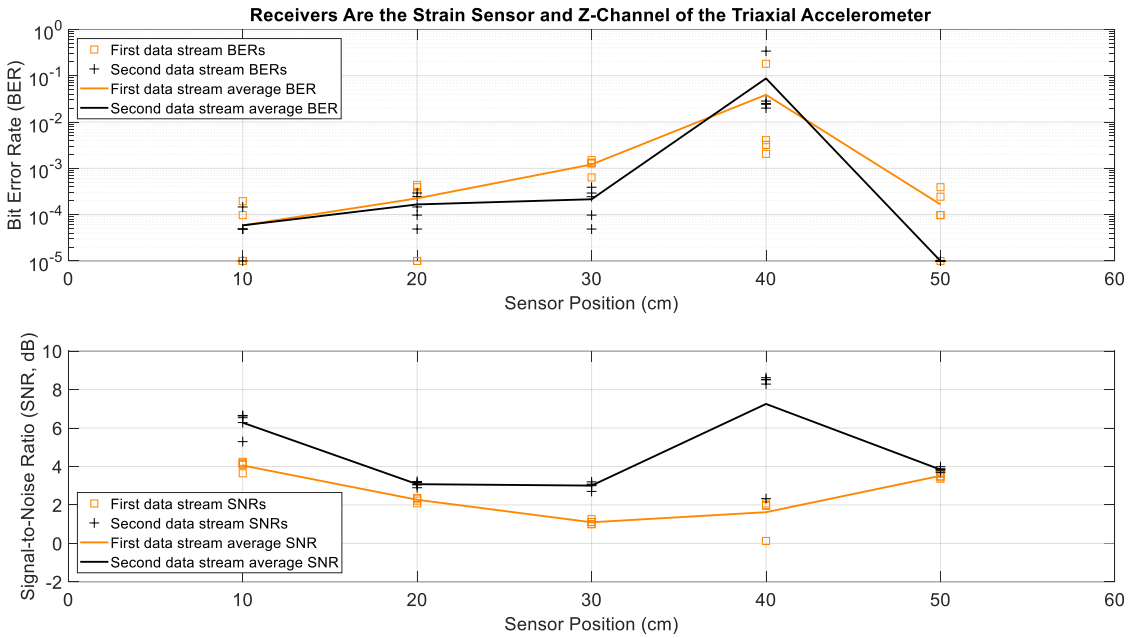

Figure 6.8 BERs (top) and SNRs (bottom) at different receiver positions, with two actuators transmitting two data streams simultaneously. The receivers are a strain sensor and z-channel of a triaxial accelerometer. The piecewise linear graphs represent average BERs and SNRs for each of the two data streams versus the receiver position.

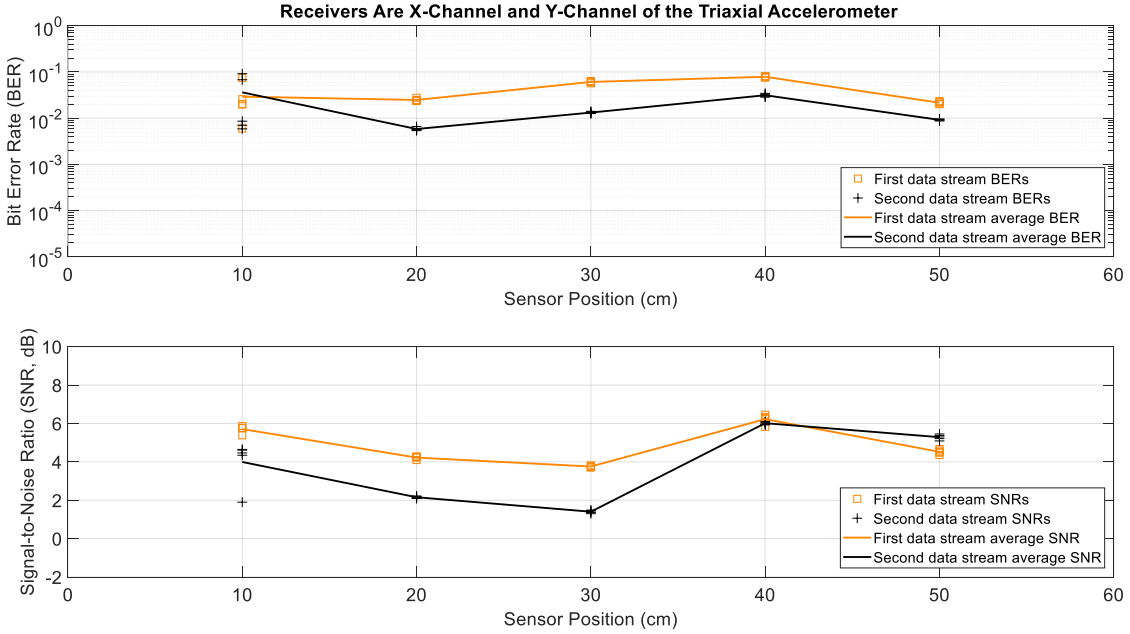

Figure 6.9 BERs (top) and SNRs (bottom) at different receiver positions, with two actuators transmitting two data streams simultaneously. The receivers are x-channel and y-channel of a triaxial accelerometer. The piecewise linear graphs represent average BERs and SNRs for each of the two data streams versus the receiver position.

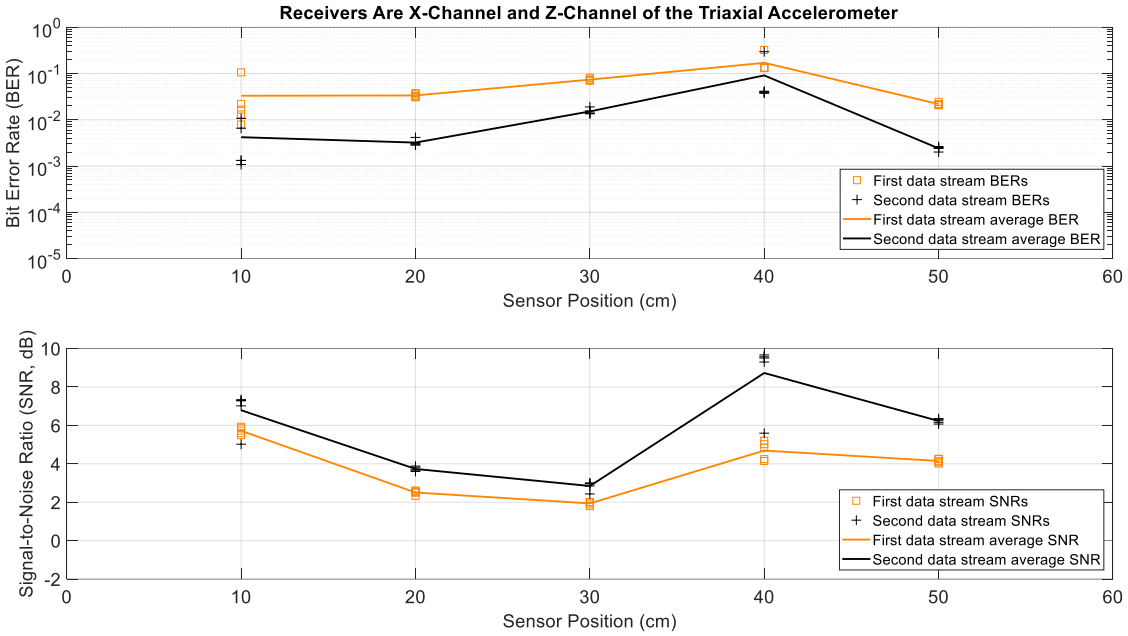

Figure 6.10 BERs (top) and SNRs (bottom) at different receiver positions, with two actuators transmitting two data streams simultaneously. The receivers are x-channel and z-channel of a triaxial accelerometer. The piecewise linear graphs represent average BERs and SNRs for each of the two data streams versus the receiver position.

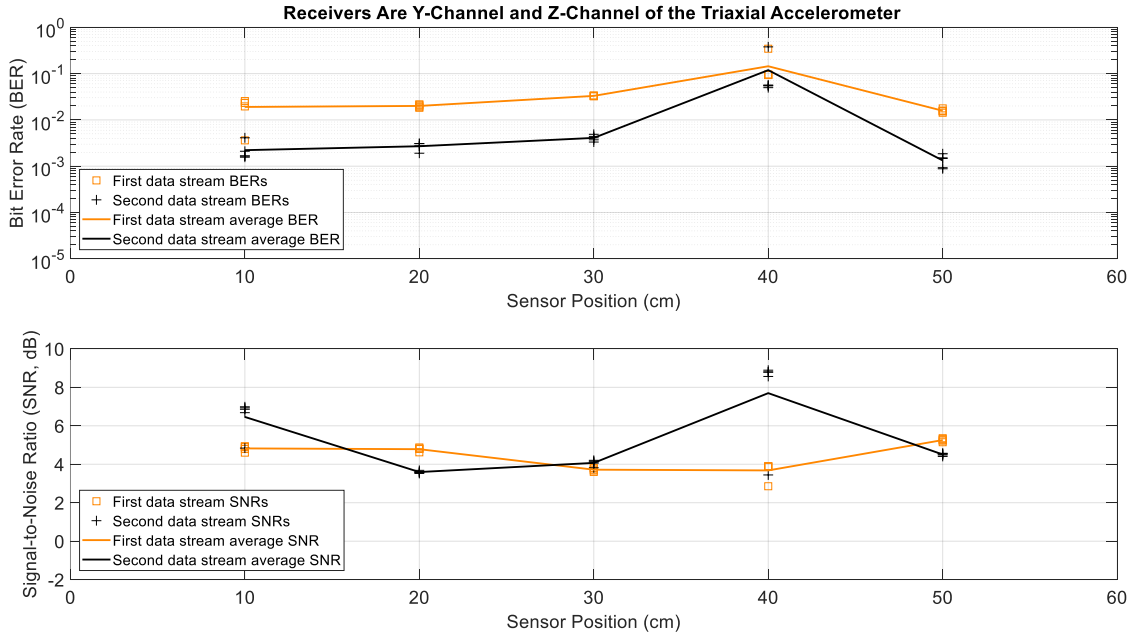

Figure 6.11 BERs (top) and SNRs (bottom) at different receiver positions, with two actuators transmitting two data streams simultaneously. The receivers are y-channel and z-channel of a triaxial accelerometer. The piecewise linear graphs represent average BERs and SNRs for each of the two data streams versus the receiver position.

CHAPTER 7

CONCLUSIONS AND FUTURE WORKS

In this dissertation, new idea regarding acoustic communications is introduced and developed by using the acoustic vector transmitter and vector receivers. Both FSK and OFDM communication systems has been designed and implemented for different applications. Signal and noise power characteristics, doppler spread and BER performance of such systems are also investigated. Via extensive experimental work under different scenarios, the performance of a MIMO vector system is studied and compared with single and multiple pressure sensor receivers.

In Chapters 2 and 3, the feasibility of using a vector transmitter and a vector receiver for underwater communication is studied respectively via FSK modulation in controlled environments, such as water tank and pool. The BER comparisons between a scalar transmitter and a vector transmitter shows that one can utilize vector transmitter for data multiplexing without physically adding more devices and any performance penalty. It also shows hydrophone array can be replace by a vector receiver with no performance issue, while vector occupies less space.

To further increase the data rate and effectively utilize the limited bandwidth in underwater environment, a MIMO OFDM system benefitting vector transmitter and receivers is designed and implemented. The BER performance is investigated under controlled environments. Using multiple setup, the potential of a vector MIMO OFDM system is explored.

In Chapter 5, the field test results are shown. By being tested under real ocean environment, the idea of data multiplexing via underwater acoustic particle velocity field components for underwater communication is verified.

Later in Chapter 6, based on the successful experience with the underwater communication system, the attempt of data multiplexing using vector receivers shows encouraging results.

For future work, more effective channel coding can be implemented to further improve the system proposed in this dissertation. Also. the potential of using multiple vector transmitters can be an interesting direction to explore. The implementation of the current system is still preliminary. More integration can be done to achieve real-time demodulation.

APPENDIX A

EXPERIMENTAL RESULTS ON SYNCHRONIZATION WITH CHIRP SIGNALS USING A VECTOR SENSOR RECEIVER

Chirp signals, also known as linear frequency modulated signals, are widely used for synchronization, signal acquisition, and frame detection in underwater communication systems. This is due to the peak at the output of the chirp matched filter at the receive side. In low signal-to-noise ratio (SNR) scenarios, however, this peak can be buried in noise, which results in major synchronization errors and system performance loss. While a scalar array of spatially separated hydrophones can increase SNR to improve synchronization, the size of the array may not be suitable for small platforms. Acoustic vector sensors, on the other hand, are small-size devices that can serve as multichannel communication receivers. In this appendix, performance of a vector sensor receiver for synchronization using a chirp signal is studied.

The experimental setup is as follows: A scalar omni projector used for transmission; One receiver is a three-channel vector sensor; Another receiver is a three-hydrophone scalar vertical array with λ element spacing (used as a scalar receiver benchmark). Transmitter and receivers are 20 m apart, as shown in Figure A.1. Linear frequency modulated chirp signal s(t) is used. Chirp duration, bandwidth, amplitude: 200 ms, 2 kHz (19-21 kHz), 1 V. 100 chirps transmitted, with 200 ms gap between each two subsequent chirps, as shown in Figure A.2.

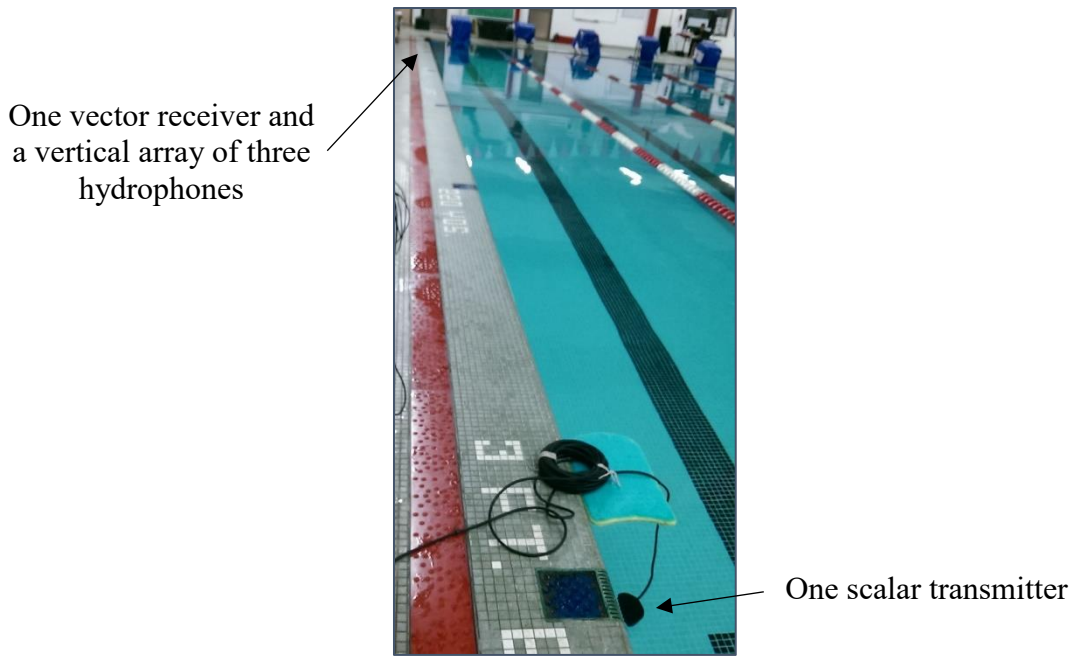

Figure A.1 Transmitter and receiver positions.

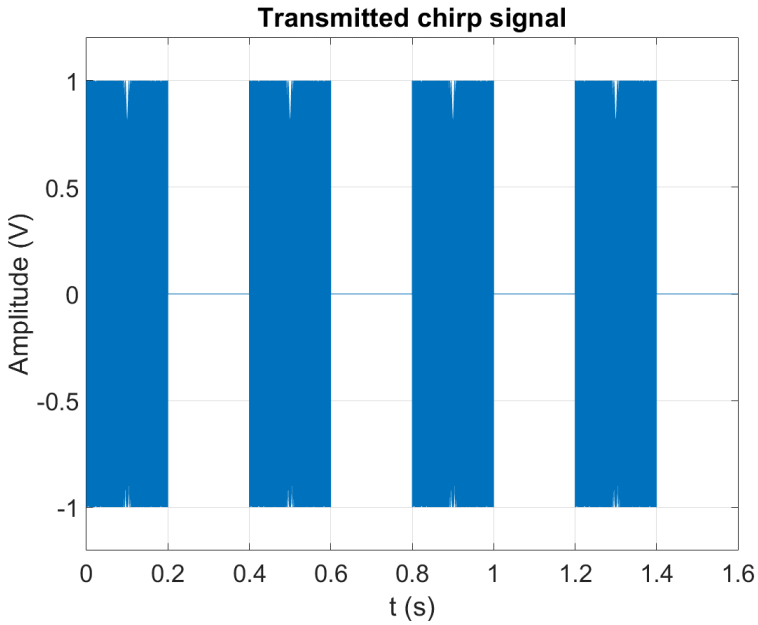

Figure A.2 First four out of one hundred transmitted chirp signals.

For the 1x3 vector system, received signals can be written as

$$\begin{bmatrix} r_x(t) \\ r_y(t) \\ r(t) \end{bmatrix} = \begin{bmatrix} h_x(t) \\ h_y(t) \\ h(t) \end{bmatrix} \oplus s(t) + \begin{bmatrix} n_x(t) \\ n_y(t) \\ n(t) \end{bmatrix}, \tag{A.1}$$

where h's and n's represent channel impulse responses and noise terms, respectively, and $\oplus$ represents convolution. Similarly, for the 1x3 scalar system, the received hydrophone signals can be written as

$$\begin{bmatrix} r_1(t) \\ r_2(t) \\ r_3(t) \end{bmatrix} = \begin{bmatrix} p_1(t) \\ p_2(t) \\ p_3(t) \end{bmatrix} \otimes s(t) + \begin{bmatrix} n_1(t) \\ n_2(t) \\ n_3(t) \end{bmatrix}. \tag{A.2}$$

Since multiple signals are received, a combining method can be helpful for processing the signals. Selection combining [35] and normalized combining are both deployed separately at the receiver, to study the performance of the 1x3 system with a vector sensor receiver, as well as the 1x3 system with three scalar receivers (hydrophones).

For selection combining, the received signal power is first calculated at each receiver according to

$$P_i = \frac{1}{T}\int_T |r_i(t)|^2 dt, \tag{A.3}$$

where T is the signal duration.

The receiver that has the maximum power is selected and then applied to the filter matched to the chirp signal $s(t)$. The output of the matched filter can be written as

$$\zeta(t) = r_{\max P}(t) \otimes s^*(-t), \tag{A.4}$$

where $r_{\max P}(t)$ has the maximum power. The matched filter output using selection combining is shown in Figure A.3.

For normalized combining, each received signal is first normalized and then combined, as follows:

$$r_{\text{vector,nc}}(t) = \frac{1}{3}\left(\frac{r_x(t)}{\max\left(r_x(t)\right)} + \frac{r_y(t)}{\max\left(r_y(t)\right)} + \frac{r(t)}{\max\left(r(t)\right)} \right), \tag{A.5}$$

$$r_{\text{scalar,nc}}(t)=\frac{1}{3}\left(\frac{r_1(t)}{\max\left(r_1(t)\right)}+\frac{r_2(t)}{\max\left(r_2(t)\right)}+\frac{r_3(t)}{\max\left(r_3(t)\right)}\right). \tag{A.6}$$

Afterwards, the combined signal is applied to the matched filter.

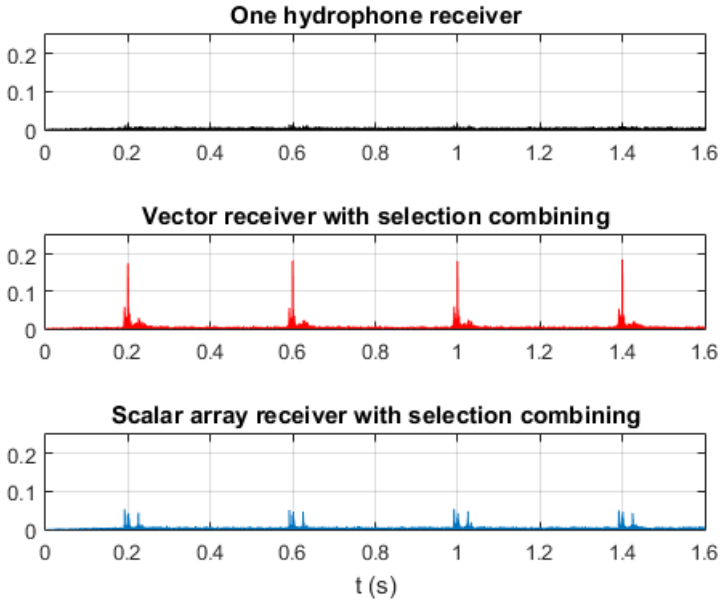

Figure A.3 The matched filter output using selection combining with one hydrophone output as benchmark shown on top panel.

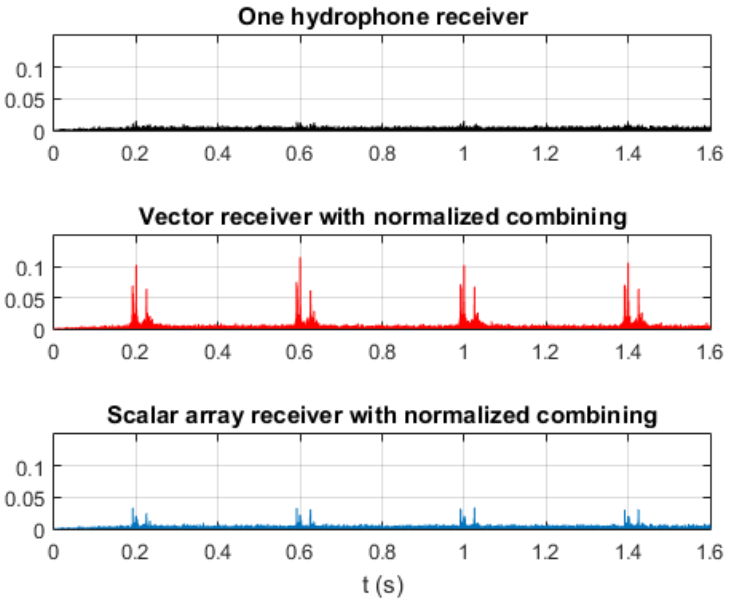

Figure A.4 The matched filter output using normalized combining with one hydrophone output as benchmark shown on top panel.

By measuring covariance matrices of the vector and scalar array receivers, we observe the vector receiver channels are less correlated than the vertically-separated acoustic pressure channels. This can explain the vector receiver better performance, which provides three nearly uncorrelated signals.

$$\mathbf{C}_{\text{vector}} = E\left\{\begin{bmatrix} r_x \\ r_y \\ r \end{bmatrix}\begin{bmatrix} r_x & r_y & r \end{bmatrix}\right\} = \begin{bmatrix} 1 & -0.16 & -0.2 \\ -0.16 & 1 & 0.1 \\ -0.2 & 0.1 & 1 \end{bmatrix}, \tag{A.7}$$

$$\mathbf{C}_{\text{scalar}} = E\left\{\begin{bmatrix} r_1 \\ r_2 \\ r_3 \end{bmatrix}\begin{bmatrix} r_1 & r_2 & r_3 \end{bmatrix}\right\} = \begin{bmatrix} 1 & 0.42 & 0.4 \\ 0.42 & 1 & 0.44 \\ 0.4 & 0.44 & 1 \end{bmatrix}. \tag{A.8}$$

The experimental results indicate that a compact vector sensor receiver can significantly enhance the output of the filter matched to the chirp signal. This is because the proposed vector matched filter significantly suppresses the noise and provides a sharp peak at the output. This is particularly important for synchronization and signal acquisition in underwater communication systems operating in low SNR environments.

APPENDIX B

MMSE MIMO DETECTION METHOD USED IN OFDM SYSTEM

Here it is shown how in the experiments the two data streams transmitted via OFDM by the two actuators are separated and detected using two received signals and an MMSE algorithm. The system model with N_{rx} receivers and N_{tx} transmitters can be written as

$$\mathbf{r} = \mathbf{H}\boldsymbol{\gamma} + \mathbf{n} \,. \tag{B.1}$$

In the above equation for the κ-th OFDM data sub-carrier, $\mathbf{r} = [r_1(f_\kappa) \cdots r_{N_{rx}}(f_\kappa)]^T$ is the received signal vector, ^{T} is the transpose, $\boldsymbol{\gamma} = [\gamma_1(f_\kappa) \cdots \gamma_{N_{tx}}(f_\kappa)]^T$ is the transmitted symbol vector, $\mathbf{n} = [n_1(f_\kappa) \cdots n_{N_{rx}}(f_\kappa)]^T$ is the noise vector and $\mathbf{H}$ is the $N_{rx} \times N_{tx}$ channel matrix

$$\mathbf{H} = \begin{bmatrix} H_{11}(f_\kappa) & \cdots & H_{1N_{tx}}(f_\kappa) \\ \vdots & \ddots & \vdots \\ H_{N_{rx}1}(f_\kappa) & \cdots & H_{N_{rx}N_{tx}}(f_\kappa) \end{bmatrix}. \tag{B.2}$$

In the experiments, elements of $\boldsymbol{\gamma}$ are independent QPSK symbols, $N_{tx} = 2$ corresponds to the two transmitting actuators, and $N_{rx} = 2$ refers to any of these two receivers: strain and *x*-acceleration, strain and *y*-acceleration, strain and *z*-acceleration, *x*-acceleration and *y*-acceleration, *x*-acceleration and *z*-acceleration, and *y*-acceleration and *z*-acceleration. To recover the two transmitted symbols in $\boldsymbol{\gamma}$ at each sub-carrier from the corresponding 2×1 received signal vector $\mathbf{r}$ in (B.1), an MMSE detector [38] is used in the experiments

$$\hat{\boldsymbol{\gamma}} = \hat{\mathbf{H}}^{H}\left(\hat{\mathbf{H}}\hat{\mathbf{H}}^{H} + \hat{\boldsymbol{\Sigma}}\right)^{-1}\mathbf{r}, \tag{B.3}$$

$$\hat{\boldsymbol{\Sigma}} = \begin{bmatrix} \hat{\sigma}_1^2 & \cdots & 0 \\ \vdots & \ddots & \vdots \\ 0 & \cdots & \hat{\sigma}_{N_{rx}}^2 \end{bmatrix}. \tag{B.4}$$

In equation (B.3), $\hat{\boldsymbol{\gamma}}$ includes the MMSE-based symbol estimates, $\hat{\mathbf{H}}$ is the estimated channel matrix $\mathbf{H}$ in (B.2), obtained using a least squares method [31], ^{H} is the transpose conjugate, and $\hat{\boldsymbol{\Sigma}}$ in equations (B.3) and (B.4) is the estimated $N_{rx} \times N_{rx}$ diagonal receiver noise covariance matrix., in which the noise variances are obtained using the null sub-carriers received by the receivers [31].

The above MMSE detector is a linear method, so, highly desirable in practice due to its low computational complexity. Upon using a nonlinear method such as a maximum likelihood method, detection performance and BERs can be improved, at the cost of higher computational complexity [38].

REFERENCES

[1] "The underwater acoustic communication market is expected to grow from USD 1.31 billion in 2017 to USD 2.86 billion by 2023, at a CAGR of 13.8% between 2017 and 2023," in *PRNewswire*, New York, NY, USA, Jan 25, 2018.

[2] P. J. Gendron, "Shallow Water Acoustic Response and Platform Motion Modeling via a Hierarchical Gaussian Mixture Model," *The Journal of the Acoustical Society of America*, vol. 139, no. 4, pp. 1923-1937, 2016.

[3] A. L. Moustakas, H. U. Baranger, L. Balents, A. M. Sengupta, and S. H. Simon, "Communication Through a Diffusive Medium: Coherence and Capacity," *Science*, vol. 287, no. 5451, p. 287, 2000.

[4] M. R. Andrews, P. P. Mitra, and R. deCarvalho, "Tripling the Capacity of Wireless Communications Using Electromagnetic Polarization," *Nature*, vol. 409, no. 6818, pp. 316-318, 2001.

[5] Y. Yan *et al.*, "High-Capacity Millimetre-Wave Communications With Orbital Angular Momentum Multiplexing," *Nature Communications*, vol. 5, p. 4876, 2014.

[6] S. Zhou and Z. Wang, *OFDM for Underwater Acoustic Communications*. Chichester, West Sussex, UK: Wiley, 2014.

[7] R. Kastner, A. Lin, C. Schurgers, J. Jaffe, P. Franks, and B. S. Stewart, "Sensor Platforms for Multimodal Underwater Monitoring," in *International Green Computing Conference (IGCC)*, 2012, pp. 1-7.

[8] A. D. Pierce and R. T. Beyer, "Acoustics: An Introduction to Its Physical Principles and Applications. 1989 Edition," *The Journal of the Acoustical Society of America*, vol. 87, no. 4, pp. 1826-1827, 1990.

[9] C. Chen and A. Abdi, "Signal Transmission Using Underwater Acoustic Vector Transducers," *IEEE Transactions on Signal Processing*, vol. 61, no. 14, pp. 3683-3698, 2013.

[10] D. B. Kilfoyle and A. B. Baggeroer, "The State of the Art in Underwater Acoustic Telemetry," *IEEE Journal of Oceanic Engineering*, vol. 25, no. 1, pp. 4-27, 2000.

[11] M. Stojanovic, "High Speed Underwater Acoustic Communications," in *Underwater Acoustic Digital Signal Processing and Communication Systems*, R. S. H. Istepanian and M. Stojanovic, Eds. Boston, MA, USA: Kluwer, 2002, pp. 1-35.

[12] A. Abdi and H. Guo, "A New Compact Multichannel Receiver for Underwater Wireless Communication Networks," *IEEE Transactions on Wireless Communications,* vol. 8, no. 7, pp. 3326-3329, 2009.

[13] A. Abdi, H. Guo, A. Song, and M. Badiey, "An Overview of Underwater Acoustic Communication via Particle Velocity Channels: Channel Modeling and Transceiver Design," *Proceedings of Meetings on Acoustics,* vol. 9, no. 1, p. 070002, 2010.

[14] A. Abdi, H. Guo, and P. Sutthiwan, "A New Vector Sensor Receiver for Underwater Acoustic Communication," in *OCEANS 2007*, 2007, pp. 1-10.

[15] H. Guo, C. Chen, A. Abdi, A. Song, M. Badiey, and P. Hursky, "Capacity and Statistics of Measured Underwater Acoustic Particle Velocity Channels," *Proceedings of Meetings on Acoustics,* vol. 14, no. 1, p. 030006, 2011.

[16] H. Guo and A. Abdi, "On the Capacity of Underwater Acoustic Particle Velocity Communication Channels," in *2012 Oceans*, 2012, pp. 1-4.

[17] H. Guo, A. Abdi, A. Song, and M. Badiey, "Delay and Doppler Spreads in Underwater Acoustic Particle Velocity Channels," *The Journal of the Acoustical Society of America*, vol. 129, no. 4, pp. 2015-2025, 2011.

[18] C. Chen, S. Wang, and A. Abdi, "Second-Order Statistics of the Instantaneous Mutual Information in Time-Varying Underwater Particle Velocity Channels," *Proceedings of Meetings on Acoustics,* vol. 23, no. 1, p. 070001, 2015.

[19] A. Abdi and H. Guo, "Signal Correlation Modeling in Acoustic Vector Sensor Arrays," *IEEE Transactions on Signal Processing,* vol. 57, no. 3, pp. 892-903, 2009.

[20] F. B. Poletto and F. Miranda, *Seismic While Drilling: Fundamentals of Drill-Bit Seismic for Exploration*. Boston, MA, USA: Elsevier, 2004.

[21] N. G. Franconi, A. P. Bunger, E. Sejdić, and M. H. Mickle, "Wireless Communication in Oil and Gas Wells," *Energy Technology*, vol. 2, no. 12, pp. 996-1005, 2014.

[22] T. G. Barnes and B. R. Kirkwood, "Passbands for Acoustic Transmission in an Idealized Drill String," *The Journal of the Acoustical Society of America,* vol. 51, no. 5B, pp. 1606-1608, 1972.

[23] A. H. Alenezi and A. Abdi, "On Multiple Wireless Channels in Oil Wells Drill Strings," *IEEE Wireless Communications Letters,* vol. 6, no. 6, pp. 738-741, 2017.

[24] A. Alenezi and A. Abdi, "Strain Sensor and Accelerometer Communication Channels in Drill Pipes of Oil Wells: Delay Spreads and Eigenvalues," *International Journal of Sensor Networks and Data Communications,* vol. 7, no. 3, 2018.

[25] C. Chen and A. Abdi, "Channel Models for Underwater Vector Transducer Communication Systems," in *Oceans,* 2012, pp. 1-12.

[26] M. K. Simon, S. M. Hinedi, and W. C. Lindsey, *Digital Communication Techniques: Signal Design and Detection*. Englewood Cliffs, NJ, USA: Prentice-Hall PTR, 1994.

[27] B. S. Borowski, "Application of Channel Estimation to Underwater, Acoustic Communication," Ph.D. Dissertation, Stevens Institute of Technology, 2011.

[28] C. H. Sherman and J. L. Butler, *Transducers and Arrays for Underwater Sound*. New York, NY, USA: Springer, 2007.

[29] Q. T. Zhang, "Exact Analysis of Postdetection Combining for DPSK and NFSK Systems Over Arbitrarily Correlated Nakagami Channels," *IEEE Transactions on Communications,* vol. 46, no. 11, pp. 1459-1467, 1998.

[30] E. Kinsler and A. R. Frey, *Fundamentals of Acoustics*, 2nd ed. New York, NY, USA: Wiley, 1962.

[31] B. Li *et al.*, "MIMO-OFDM for High-Rate Underwater Acoustic Communications," *IEEE Journal of Oceanic Engineering,* vol. 34, no. 4, pp. 634-644, 2009.

[32] R. S. Gordon, L. Parad, and J. L. Butler, "Equivalent Circuit of a Ceramic Ring Transducer Operated in the Dipole Mode," *The Journal of the Acoustical Society of America,* vol. 58, no. 6, pp. 1311-1314, 1975.

[33] S. H. Ko and H. L. Pond, "Improved Design of Spherical Multimode Hydrophone," *The Journal of the Acoustical Society of America,* vol. 64, no. 5, pp. 1270-1277, 1978.

[34] E. Zhang and A. Abdi, "Communication Rate Increase in Drill Strings of Oil and Gas Wells Using Multiple Actuators," *Sensors*, vol. 19, no. 6, p. 1337, 2019.

[35] M. K. Simon and M.-S. Alouini, *Digital Communication over Fading Channels*, 2nd ed. Hoboken, NJ, USA: Wiley, 2004.

[36] M. O. Damen, H. E. Gamal, and G. Caire, "On Maximum-Likelihood Detection and the Search for the Closest Lattice Point," *IEEE Transactions on Information Theory*, vol. 49, no. 10, pp. 2389-2402, 2003.

[37] A. H. Alenezi and A. Abdi, "A Comparative Study of Multichannel and Single Channel Accelerometer Sensors for Communication in Oil Wells," in *International Conference on Communication and Signal Processing (ICCSP)*, 2017, pp. 0153-0153.

[38] T.-D. Chiueh and P.-Y. Tsai, *OFDM Baseband Receiver Design for Wireless Communications*. Hoboken, NJ, USA: Wiley, 2007.